

Failure and Delamination in Microelectronic Packages

Proefschrift

Ter verkrijging van de graad van doctor
aan de Technische Universiteit Delft,
op gezag van de Rector Magnificus prof. ir. K.C.A.M. Luyben,
voorzitter van het College voor Promoties,
in het openbaar te verdedigen op 26 februari 2013 om 15:00 uur

door

Mahdi SADEGHINIA

Master of Science in Mechanical Engineering, Khaje Nasir Toosi University of
Technology, Iran

geboren te Chaloos, Iran

Dit proefschrift is goedgekeurd door de promotor:

Prof. dr. ir. L.J. Ernst

Copromotor: Dr.ir. K.M.B. Jansen

Samenstelling promotiecommissie:

Rector Magnificus,	voorzitter
Prof. dr. ir. L.J. Ernst,	Technische Universiteit Delft, promotor
Dr. ir. K.M.B. Jansen,	Technische Universiteit Delft, copromotor
Prof. dr. D.G. Yang,	Guilin University of Electronic Technology
Prof. dr. A.A.O. Tay,	National University of Singapore
Prof. dr. ir. R. Akkerman,	University of Twente
Prof. dr. L.K. Nanver,	Technische Universiteit Delft
Dr. ir. H. Pape,	Infineon Technologies AG
Prof. dr. U. Staufer,	Technische Universiteit Delft, reservelid

ISBN/EAN: 978-94-6186-116-0

Copyright © 2013 by M. Sadeghinia

All rights reserved. No part of the material protected by this copyright notice may be reproduced or utilized in any form or by any means, electronic or mechanical, including photocopying, recording or by any information storage and retrieval system, without the prior permission of the author.

Author e-mail: Mahdi.Sadeghinia@gmail.com

To my beloved wife, Elaheh
To my Parents, Behrooz and Shahrbanoo

Table of contents

1. Introduction	1
1.1 Failure in microelectronics	1
1.2 Delamination in microelectronic packages	3
1.3 Objective of this thesis and Nano-Interface project	6
1.4 Outline of the thesis	8
2. Basic Theory on Fracture Mechanics and Viscoelasticity	15
2.1 Fracture Mechanics	15
2.2 Delamination in microelectronic packages	16
2.2.1 Energy release rate	17
2.2.2 The mode mixity of fracture	19
2.2.3 Numerical methods for interface fracture	22
2.3 Packaging materials	24
2.3.1 Viscoelasticity of epoxy molding compound	24
2.3.2 Factors affecting viscoelasticity	28
3. Thermo-mechanical properties of fully cured molding compound	33
3.1 Introduction	33
3.2 Experiments	34

3.2.1	Materials and sample preparation	34
3.2.2	PVT Measurement	35
3.2.2.1	Coefficient of Thermal Expansion (CTE)	35
3.2.2.2	Bulk Modulus	38
3.2.3	Dynamic Mechanical Analyzer (DMA)	39
3.3	Conclusions	45
4.	Cure dependent parameters of an epoxy molding compound	49
4.1	Introduction	49
4.2	Experimental	50
4.2.1	DSC experiment	51
4.2.1.1	Cure kinetics	51
4.2.1.2	Glass transition	55
4.2.2	PVT experiment (cure shrinkage)	57
4.2.3	DMA experiment	60
4.2.3.1	Test setup	60
4.2.3.2	Deriving the modulus	62
4.2.3.3	Construction of time-cure mastercurve	65
4.2.3.4	Cure dependency of elastic parts	71
4.3	Conclusion	72
5.	Developing the harsh environment testing setup	75
5.1	Introduction	75
5.2	Design of the setup	77
5.3	Experiments	81
5.3.1	Material	81
5.3.2	Mechanical properties in dry environment	81

5.3.3 Creep under high pressure steam condition	84
5.4 Conclusions	89
6. Interfacial fracture properties in pressurized steam condition	91
6.1 Introduction	91
6.2 Materials characterization	92
6.2.1 Dry condition	93
6.2.1.1 CTE and bulk modulus	93
6.2.1.2 Relaxation tensile and shear modulus	94
6.2.2 Creep under high pressure steam condition	97
6.3 Delamination in interfaces	99
6.3.1 Sample preparation	99
6.3.2 Mixed Mode Bending setup	99
6.3.3 Delamination experiment	101
6.4 Finite Element Model for energy release rate calculation	106
6.5 Conclusions	112
7. Conclusion	115
7.1 Conclusion concerning the establishment of fully cured material model	115
7.2 conclusion concerning the characterization of the cure dependent material properties	116
7.3 Conclusion concerning the development of the pressure vessel apparatus	117
7.4 Conclusion concerning the interfacial fracture properties	118

Abbreviations

CTE	Coefficient of Thermal Expansion
CSDEM	Crack Surface Displacement Extrapolation Method
DMA	Dynamic Mechanical Analyzer
DSC	Differential Scanning Calorimeter
EMC	Epoxy Molding Compound
FEM	Finite Element Method
LEFM	Linear Elastic Fracture Mechanics
LF	Lead Frame
MMB	Mixed Mode Bending
PV	Pressure Vessel
RH	Relative Humidity
T_g	Glass Transition Temperature

Chapter **1**

Introduction

1.1 Failure in microelectronics

Electronic devices have increasingly become an integral part of countless products in the industrial, consumer and military market. Hence, the failure of these devices in critical applications, such as aviation and automotive applications may have detrimental consequences in term of safety or productivity. These failures are mainly related to reliability of electronics packaging.

Electronic packaging is the technology relating to the establishment of electrical interconnections and appropriate housing for Integrated Circuits (ICs). Electronic packages provide a few major functions: interconnection of electrical signals, mechanical protection of the device from mechanical and chemical hazards, providing support for circuits, distribution of electrical power, and dissipation of heat generated by the circuits. The ability of a package to adequately perform these functions depends on the properties of the device as well as the properties of the package.

Therefore, thermo-mechanical reliability of the electronic packages and assemblies is one of the major concerns in the electronics industry. Currently, thermo-mechanical related failures account for about 65% of total failures in microelectronics [1]. Examples of these failures are interfacial delamination, cracking of the silicon die, package

cracking and thermal cooling down-induced warpage [2-5]. This is expected to become even more critical in future products, due to further miniaturization and function integration, which causes increased power dissipation density, higher interconnection density and higher reliability demands.

To understand interfacial delamination related failure in IC packages, that is caused by thermal-mechanical loading, the extension of fracture mechanics application from cracking in homogenous material to bi-material interface delamination problems has become of great interests [6]. The bi-material interface delamination theory is widely used experimentally and numerically. It enables the prediction of interfacial delamination related failures of IC packages in qualification tests to enable a designer to design more reliable IC packages. On the other hand, the experimental methodologies are still underdeveloped due to lack in quality and poor reproducibility. More reliable test methods with quantitatively and qualitatively reproducible results are needed.

For the pre-moisturized microelectronic packages the interface delamination failure often initiates during the heating up process, likewise soldering reflow, in production steps. Here temperatures can reach far above the 100°C limit. Due to the presence of trapped water in EMC and interface, steam will be generated in the packages which will initiate pop-corning and damage in the interfaces [7-9]. However So far, interface reliability predictions for this temperature/ humidity regime (temperature above 100°C and 100%RH) could not well be performed as the critical fracture data were missing.

In this study an interfacial characterization methodology for establishing the critical delamination parameters in microelectronic packages under pressure cooker condition is developed. The designed and developed setup and procedure is capable of testing a sample at different temperature and moisture condition as well as at different loading mixities. The interface between epoxy molding compound (EMC) and copper (-oxide) lead frame is used as a case study to investigate the feasibility of the experimental setup and verifying the characterization procedure.

1.2 Delamination in microelectronic packages

Thin layers of dissimilar materials are used in most microelectronic assemblies in order to achieve specialized functional requirements. Generally, the interface between two different materials is a weak link due to the mismatch in thermo-mechanical properties, such as Young's modules, coefficients of thermal expansion, hydro-swelling, and vapor pressure induced expansion. Furthermore, the residual stresses from the production processes and the changing thermal and humidity conditions are acting as additional crack driving factors for interface delamination. Failure of an interface induces decreased reliability of microelectronic packages. Therefore, quantified delamination properties of interfaces under various environmental conditions are desirable.

In order to explore the risk of interface damage, FE simulations of the fabrication steps as well as the testing conditions are generally performed during the design stage. In order to be able to assess the risk for interface fracture, the critical fracture properties of the interfaces being applied should be available and should include their dependency on the occurring combinations of temperature and moisture preconditioning [10-13]. As a consequence, there is an urgent need to establish these critical interface fracture parameters. For brittle interfaces such as between epoxy molding compound (EMC) and metal (-oxide) substrates or Si-EMC, the critical energy release rate (or delamination toughness, G_c) can be considered as the suitable material parameter. This material parameter is strongly dependent on the temperature, the moisture content of the materials involved and on the so-called mode mixity of the stress state near the crack tip.

Recently, in the Mechanics of Materials group at Delft University of Technology several research projects have been conducted for establishing the critical interfacial fracture properties of electronic packages. Xiao [14] developed a mixed mode bending test method for establishing the delamination toughness of interfaces between epoxy molding compound and copper lead frame. Furthermore, Schlottig [15] designed a modified mixed mode Chisel setup and described the interfacial delamination in silicon

die from molding compound. Moreover, Ma [16] provided a framework in developing a knowledge based fast qualification method which shortens the qualification time and design cycles for different electronic packages during the operational condition. Moisture sensitivity level analysis and thermal cycling were chosen as the fast qualification methods in his work.

Since during the studies on the EMC-Cu/Si interfacial delamination no inelastic deformation prior to fracture were observed [14-16], Linear Elastic Fracture Mechanics (LEFM) theory was considered for these interfaces. In LEFM a criterion is built on the assumption that for crack growth to occur, a critical load level has to be reached independently from time and inelastic phenomena. Loads below such critical levels would not lead to fracture. In fracture reality the critical load often depends on aspects involving such phenomena. This problem opened own areas of research, such as dynamic and creep fracture mechanics [17]. Fracture might also appear at load levels that are lower than the ones deemed necessary for a critical stress state, because not all influences on the stress state have been considered. Such influences can be for instance residual stresses, thermo-mechanical cycling loads or the presence of moisture [18-25]. This happens also if the materials involved show nearly linear elastic behavior [26]. To consider all mechanisms in the analysis is difficult, and some researches termed such fracture characteristics sub-critical fracture [27], which contradicts the very definition of the criterion and downplays the importance of residual stresses.

Characteristic for the procedure of establishing the fracture toughness from fracture test results is that adequate FE simulations of the fracture test are required. Since delamination in IC packages is essentially a 3D problem, using a 2D analysis will obscure some of the information (for example, the effect of the initial delamination shape) pertaining to the problem, although it is still useful in predicting trends. Although several researchers have recently extended the analysis from 2D to 3D [28-31], currently there still seems to be more challenges on better understanding of the influence of the initial delamination shape on the mechanics of interfacial crack propagation [32].

Cohesive zone (CZ) methods have also been extensively used for the homogeneous body fracture of well described materials such as silicon [33] but although many studies report its use for delamination problems [34-37], and although CZ methods offer the advantage that no local crack spot has to be assumed in the model, the results have limited fracture mode details and the CZ methods need substantial computational time.

A non-trivial problem in interface delamination testing and the interpretation of fracture properties via FEM-simulation is the choice of the relative sample width. Some researchers used a relatively wide sample, as it was thought that then the FE model could be reduced to a 2D model with plane strain assumption. However, this assumption appears to be erroneous for Cu-EMC or Si-EMC interfaces because of the high level of residual stresses in the lateral direction. Instead, Schlottig and Xiao [14,15] proposed that a narrow sample with the 2D FE plane stress assumption could be a better approximation of reality. Since their proposed samples had a quite narrow width, the effect of the specimens' cutting edge damages on the delamination force levels should also be considered in more details.

In case that moisture sensitivity was included in delamination researches the highest temperature was limited to below 85°C. This limitation is quite restrictive for the application of the obtained critical fracture data in reliability studies of microelectronic packages. This is because of the fact that for pre-moisturized microelectronic packages the interface delamination failure often occurs not below this temperature limit. Contrarily in many cases the damage is initiated during heating up in subsequent production steps. Here temperatures can reach even far above the 100°C which will initiate pop-corning and delamination in interfaces, Figure 1-1. So far, interface reliability predictions for this temperature/ humidity regime could not well be performed as the critical fracture data were missing.

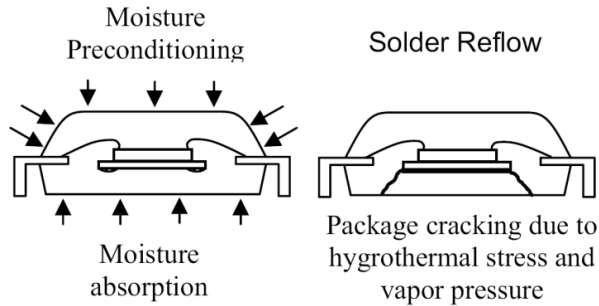


Figure 1-1 Mechanism of pop-corning failure in soldering reflow process

This thesis concentrates on the interface delamination measurements in microelectronic packages, especially interested in pressure cooker environment (humidity combined with temperatures above the 100°C). For the humid state with $T > 100^\circ\text{C}$, the effect of (trapped) steam at the interface during the delamination measurements should be compensated by performing the measurements in a pressure chamber. Therefore a pressure vessel with highly accurate tensile setup for force and displacement measurements, surrounding the delamination test setup, is designed and developed. The characterization procedure is verified via investigating the interfacial toughness of epoxy molding compound (EMC) and copper (-oxide) lead frame, as a case study.

1.3 Objective of this thesis and Nano-Interface project

The overall objective of this thesis is to develop a common framework of experimental and modeling methodologies for predicting the interface reliability for lead frame based packages in pressure cooker environment, ie. temperature above 100 °C and 100%RH. Due to the financing the research, the work was imbedded in the european research project “Nano-Interface-FP7”.

The overall scientific objective of the Nano-Interface project was to establish an experimentally verified software tool based on a multi-scale and multi-physics approach in which molecular interfacial models at atomic level will be explicitly coupled to finite

element models at macroscopic (product) level in order to quantitatively predict the reliability of the electronic devices. The project focus was on the material and interface behavior of metal-oxide-polymer systems which cover approximately 95% of all material systems in current and future electronic devices.

The developed software is assessed establishing the interfacial toughness of the EMC-Cu lead frame interfaces and comparing that with the experimental established toughness which were performed by different partners of the Nano-interface project. The main concern of our part in this project was the establishment of the interfacial properties of EMC- Cu lead frame interfaces for the humid condition with temperature above 100°C.

Since commercial materials often have complicated mixtures of ingredients with unknown chemistry which makes modeling in atomic scale difficult (for other partners of the project), we chose to use a model epoxy system consisting of similar components as used in commercial molding compounds on copper substrates. The system consists of epoxy Novolac (EPN 1180) as a matrix material, Bisphenol-A as hardener and fused silica spheres as filler. Two hand-made EMCs were labeled in this thesis as DF and DU, which corresponded to the filled and unfilled samples, respectively.

Because of the foreseen interpretation of the delamination measurement results via FEM modeling, a complete thermo-mechanical property of the DF and DU EMCs was required. Therefore, Chapter 3 and 4 of this thesis focus on viscoelastic characterization of DU and DF EMCs. Later, it was found out that the interfacial bonding of the hand-made DF and DU EMCs on copper lead frames appeared to be weak, such that the effect of temperature and moisture on the inter-laminar adhesion couldn't be well established. Moreover, the singulation of the samples seemed to be hardly possible. Therefore, due to the severe delay in the interface delamination characterization (because of lacking of the inter-laminar samples) it was decided to change the samples to factory-made interface samples, using commercial EMC (labeled in this thesis as IF) on copper lead frames, fabricated in a standard production process. Since the thermo-mechanical

properties of the IF samples were also required as the input for the ABAQUS model, the viscoelastic characterizations were repeated for this EMC and reported in Chapter 6.

1.4 Outline of the thesis

To make this thesis self-contained, in Chapter 2 a brief description of the linear elastic fracture mechanics theory is given. In Chapter 3, an investigation on the thermo-mechanical properties of the hand-made DU and DF is discussed. The coefficient of thermal expansion, the bulk and the storage modulus are measured through various experiments and the results are fitted to appropriate models. Also the effect of the filler on the mechanical properties of the cured materials is considered. These properties are required for the interpretation of the delamination measurement results via FEM modeling.

Chapter 4 describes the changes in the viscoelastic properties of DU EMC during the curing period. The changes in the shear modulus are monitored during cure and based on the time-temperature superposition principle the viscoelastic master curves and the related shift factors are extracted.

Chapter 5 focuses on developing a special steam chamber (temperature above 100°C and relative humidity equal to 100%) with a highly accurate tensile setup for force and displacement measurements. This vessel is required for establishing the interfacial toughness of IF EMC-Cu interfaces in harsh environment, which will be discussed in Chapter 6. The pressurized steam environment surrounding the inter-laminar sample will compensate the effect of the tapped steam in the interface, during the delamination measurement in harsh environment.

The functionality and performance of the setup is assessed measuring the viscoelastic creep compliance of an EMC in dry condition and comparing that with creep measurements using a commercial instrument. The commercial EMC studied in Chapter 5 had a T_g around 160 °C in dry environment and labeled in this thesis as NX. This material was selected such that it remains in its viscoelastic range under the pressurized steam conditions, studied here. As the next step in Chapter 5, the mechanical properties

of the NX are determined for the pressurized steam environment and the effect of the moisture is quantified.

Chapter 6 presents the establishment of the critical fracture properties of the IF EMC-Cu lead frame interfaces at pressure cooker conditions, temperature above 100°C and 100%RH. The effect of the trapped steam in the interface is removed by performing the delamination test in pressurized steam environment. The interfacial properties are obtained by interpreting the experimental results through dedicated finite element modeling. As input parameters, the material properties of the IF EMC are both experimentally and numerically characterized in dried and pressure cooker condition. In order to establish the interfacial toughness accurately, the influence of the residual stress in the sample is considered. Furthermore, the effect of the moisture, mode mixity and temperature level are also investigated.

Finally, in Chapter 7, the thesis is concluded with highlighting the main results from the research work. Recommendations for further work are proposed.

References

- [1] G.Q. Zhang, W.D. van Driel, X.J. Fan, *Mechanics of Microelectronics*, Springer, Dordrecht, 2006.
- [2] W.D. van Driel J.H.J. Janssen, G.Q. Zhang, D.G. Yang, L.J. Ernst, Packaging induced die stresses- Effect of chip anisotropy and time-dependent behavior of molding compound, *J. Electron. Packag.* 125 (2003) 520-525
- [3] D.G. Yang, K.M.B. Jansen, L.J. Ernst, G.Q. Zhang, W.D. van Driel, H.J.L. Bressers, J.H.J. Janssen, Numerical modelling of warpage induced in QFN array modeling process, *J. Microelectron. Reliab.* 47(2007) 310-318.
- [4] D. Lu, C.P. Wang, *Materials for advanced packaging*, Springer, New York, 2009.
- [5] J. de Vreugd, *The effect of aging on molding compound properties*, PhD thesis, Delft, 2011.
- [6] J. W. Hutchinson and Z. Suo, Mixed mode cracking in layered materials, *J. Adv. in Appl. Mech.* 29 (1991), 63-191.
- [7] A.A.O. Tay, *Mechanics of interfacial delamination in IC packages undergo solder reflow*, IEEE High density microsystem design and packaging and component failure analysis conference (Shanghai, June 2005), pp. 1-7.
- [8] I. Fukuzawa, S. Ishiguro, S. Nanbu, . Tay, *Moisture resistance degradation of plastics LST's by reflow soldering*, IEEE 23rd International reliability physics symposium (Orlando, March 1985), pp. 192-1977.
- [9] A.A.O. Tay, T.Y. Lin, *Effects of moisture and delamination on cracking of plastic IC packages during solder reflow*, IEEE 46th ECTC conference (Orlando, May 1996), pp. 777-782.
- [10] Hu Guojun, *A Theoretical and Numerical Study of Crack Propagation Along a Bimaterial Interface With Applications to IC Packaging*, PhD thesis, National University of Singapore, 2006.
- [11] A.A.O. Tay, T.Y. Lin, *Influence of temperature, humidity and defect location on delamination in plastic IC packages*, IEEE Transaction on components and packaging technologies, 22(4) (1994) 512-518.

-
- [12] B. Wunderle, M. Schuls, J. Keller, G. Schlottig, I. Maus, D. May, O. Holck, H. Pape, B. Michel, fracture-mechanical interface characterization for thermo-mechanical co-design- an efficient and comprehensive method for critical mixed mode data extraction, IEEE 61st ECTC conference (Lake Buena Vista, June 2011), pp. 1459-1467.
- [13] B. Wunderle, M. Schuls, J. Keller, D. May, I. Maus, H. Pape, B. Michel, Advanced mixed- mode bending test: A rapid, inexpensive and accurate method for fracture-mechanical interface characterization, IEEE 13th EuroSimE conference (Cascais, April 2012), pp. 1-11.
- [14] A. Xiao, Interface characterization and failure modeling for semiconductor application, PhD thesis, Delft, 2012.
- [15] G. Schlottig, Reliability at chip interfaces: Delaminating the silicon die from molding compound, PhD thesis, Delft, 2012.
- [16] X. Ma, Fast qualification methods for microelectronic packages, PhD thesis, Delft, 2011.
- [17] D. Gross, T. Seelig, Fracture mechanics, with introduction to micromechanics, 1st edition, Springer, Berlin, 2006.
- [18] A. Xiao, H. Pape, B. Wunderle, K.M.B. Jansen, J. de Vreugd, L.J. Ernst, Interfacial fracture properties and failure modeling for microelectronics, IEEE 58th ECTC conference (Lake Buena Vista, May 2008), pp. 1724-1730.
- [19] G. Schlottig, H. Pape, B. Wunderle, L.J. Ernst, Establishing the critical fracture properties of the die backside to molding compound interface, IEEE 61st ECTC conference (Lake Buena Vista, June 2011), pp. 1090-1096.
- [20] G. Hu, A.A.O. Tay, Y. Zhang, W. Zhu, S. Chew, Characterization of viscoelastic behaviour of a molding compound with application to delamination analysis in IC packages, IEEE 8th EPTC conference (Singapore, December 2006), pp. 53-59.
- [21] G. Hu, A.A.O. Tay, Y. Zhang, W. Zhu, S. Chew, Experimental and numerical study of the effect of viscoelasticity on delamination in a plastic IC package, IEEE 57th ECTC conference (Reno, May 2007), pp. 1062-1068.

- [22] A.A.O. Tay, Modeling of interfacial delamination in plastic IC packages under hygrothermal loading, *J. Electron. Packag.* 127 (3) 268-275.
- [23] A.A.O. Tay, Y. Ma, T. Nakamura, S. H. Ong, A Numerical and Experimental Study of Delamination of Polymer-Metal Interfaces in Plastic Packages at Solder Reflow Temperatures, In Proceedings of the 9th Intersociety Conference on Thermal and Thermomechanical Phenomena in Electronic Systems, ITherm 2004 (Las Vegas, June 2004), pp. 245-252.
- [24] S.P.M. Noijen, O. Van der Sluis, P.H.M. Timmermans, An extensive investigation of the four point bending test for the interface characterization, IEEE 13th EuroSimE conference (Cascais, April 2012), pp. 1/9-9/9.
- [25] J. Thijssen, O. van der Sluis, J.A.W. van Dommelen, W.D. van Driel, M.G.D. Geers, Characterization of semiconductor interfaces using a modified mixed mode bending apparatus, *J. Microelectron. Reliab.* 48(3) (2008) 401-407.
- [26] J.E. Ritter, T.J. Lardner, W. Grayeski, G.C. Prakash, J. Lawrence, Fatigue crack propagation at polymer adhesives interfaces, *J. Adhes.* 63(4) (1997) 265-268.
- [27] H.K. Singh, K.T. Wan, J.G. Drillard, D.A. Dillard, P. Reboa, J. Smith, E. Chappell, A. Sharan, Subcritical delamination in epoxy bonds to silicon and glass adherends: effect of temperature and preconditioning, *J. Adhes.* 84(7) (2008) 619-637.
- [28] A.A.O. Tay, Y.Y. Ma, G.J. Hu, The effect of moisture on the critical defect size for delamination failure at the pad/encapsulate interface of plastic IC packages undergoing solder reflow, IEEE 6th ICEPT conference (Shenzhen, September 2005), pp. 657-662.
- [29] G. Kravchenko, C. Bohm, A study of chip top delamination in plastic encapsulated packages under temperature loadings, IEEE 9th EPTC conference (Singapore, December 2007), pp. 675-679.
- [30] Z. Zhen, C.J. Zhai, R.N. Master, 3D fracture mechanics analysis of underfill delamination for flip chip packages, In Proceedings of the 11th Intersociety Conference on Thermal and Thermomechanical Phenomena in Electronic Systems, ITherm 2008 (Orlando, May 2008), pp. 751-755.

-
- [31] Y.R. Chen, G.S. Shen, H.C. Yang, Three dimensional corner delamination analysis for fan-out chip scale package, IEEE 9th ICEPT-HDP conference (Shanghai, July 2008), pp. 1-5.
- [32] S.L. Ho, A.A.O. Tay, Effect of shapes of crack front on the mechanics of 3D interfacial delamination in IC packages, IEEE 59th ECTC conference (San Diego, May 2009), pp. 1397-1403.
- [33] S Mariani, A. Ghici, R. Martini, A. Corigliano, B. Simoni, Two- Scale Vs three-scale FE analyses of shock-induced failure in poly silicon MEMS, IEEE 11th EuroSimE conference (Bordeaux, April 2010), pp. 1-7.
- [34] A. Needleman, An analysis of decohesion along an imperfect interface, *Int. J. Fract.* 42 (1990) 21-40.
- [35] M. Ortiz, A. Pandolfi, Finite deformation irreversible cohesive elements for three-dimensional crack propagation analysis, *Int. J. Numer. Methods in Eng.* 44(9) (1999) 1267-1282.
- [36] N. Chandra, Evaluation of interfacial fracture toughness using cohesive zone model, *J. Compos. Part A.* 33(10) (2002) 1433-1447.
- [37] Z.N. Jin, C.T. Sun, A comparison of cohesive zone modeling and classical fracture mechanics based on near tip stress field, *Int. J. Solids and Struct.* 43(5) (2006) 1047-1060.

Chapter 2

Basic Theory on Fracture Mechanics and Viscoelasticity

2.1 Fracture Mechanics

In the nineteenth century the industrial revolution resulted in an enormous increase in the use of metals (mainly steel) for structural applications. Unfortunately, there also occurred many accidents, with loss of life, owing to failure of these structures. Some of these accidents were due to the poor design, but it was also gradually discovered that material deficiencies in the form of pre-existing flaws could initiate cracking and fracture.

The object of fracture mechanics is to provide quantitative answers to specific problems concerning cracks in the structures. The commonly accepted first successful analysis of a fracture problem was that of Griffith in 1920 [1], who considered the propagation of brittle cracks in glass. Griffith assumed that there is a simple energy balance consisting of a decrease in elastic strain energy within the stressed body as the crack extends, counteracted by the energy needed to create the new crack surfaces.

Irwin [2] pointed out that the Griffith-type energy balance must be between (i) the stored strain energy and (ii) the surface energy plus the work done in plastic

deformation. Irwin defined the 'energy release rate' or 'crack driving force', G , as the total energy that is released during cracking per unit increase in crack size. He also recognized that for relatively ductile materials the energy required to form new crack surfaces is generally insignificant compared to the work done in plastic deformation.

In the middle 1950s Irwin [3-5] contributed another major advance by showing that the energy approach is equivalent to a stress intensity (K) approach, according to which fracture occurs when a critical stress distribution ahead of the crack tip is reached. The material property governing fracture may therefore be stated as a critical stress intensity, K_c , or in terms of energy as a critical value G_c .

2.2 Delamination in microelectronic packages

In nowadays engineering problems, fracture covers a broad range in which there are more interface crack problems beside homogenous crack problems. Microelectronic packages are typical examples that are made of composite structures. Due to the mismatch in thermo-mechanical properties, such as Young's modules and Poisson's ratio, the coefficients of thermal expansion, the hydro-swelling, and vapor pressure induced expansion [6], the interface between two dissimilar materials is where fracture most likely will occur.

It is generally agreed that a brittle interfacial crack will propagate when the load at the crack tip exceeds critical strength values. The success of predicting delamination in IC packaging strongly depends on accurate characterization of the critical interface strength. In general, for dissimilar materials due to material mismatch, the interface cracks propagate under a mixed mode combined condition. This means that mode I, mode II and even mode III (3D case) may co-exist together.

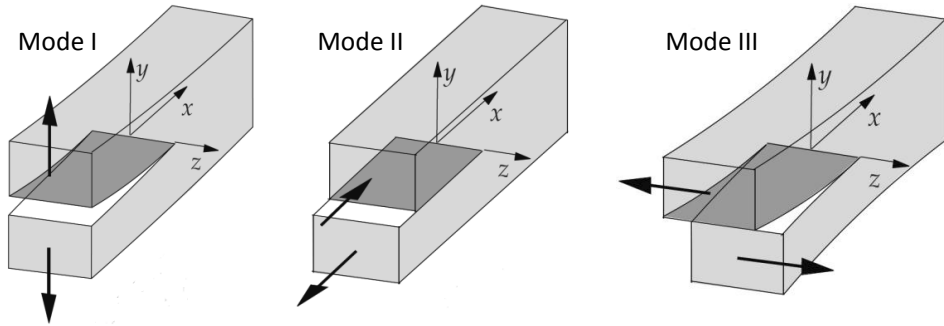


Figure 2-1 Different fracture modes in materials.

The crack propagation under pure mode I (opening mode) and pure mode II (sliding mode) have been extensively studied in many literatures. However, more and more attention must be paid to mixed mode loading because it is the most realistic situation. Usually, for the interface delamination, crack propagates under mixed mode I and mode II combined conditions [7,8]. Thus two fracture parameters, namely the fracture toughness and mode mixity are needed to effectively characterize the propagation of interfacial cracks. The contribution of mode III (tearing mode) is often neglected because as the effect on fracture is rather small in comparison with mode I and II. In this section, some basic theory of linear elastic interface fracture mechanics for interfaces is given. Some more details are described in [9-11].

2.2.1 Energy release rate

Linear elastic interface fracture mechanics theory describes if and how a crack will grow under given loading conditions when assuming an initial crack with given length and location. It assumes the existence of some detectable cracks and predicts the probability of crack propagation during processing and operational cycles. It applies when the nonlinear deformation of the material is confined to a small region near the crack tip compared to the size of the crack. For brittle materials, it accurately establishes the criteria for the failure analysis. In this theory, it first assumes that the material is isotropic and linear elastic. Based on the assumption, the stresses and/or the energy near the crack tip are calculated. In linear elastic fracture mechanics, to predict interface

delamination, fracture quantities are needed for comparison to the critical data such as fracture toughness. In general, stress intensity factors (*SIF*) and/or energy release rate are used to define the loading state near the crack tip. For linear and homogeneous material, both the stress intensity factors and energy release rate can be used.

The energy approach states that the energy added to an object in order to fracture an infinitesimally small area, dA , equals the energy that is required to create this area, with Griffith's assumptions the surface energy. A criterion for crack growth can be obtained regarding the energy balance of the material.

$$dU_e = dU_i + dU_a + dU_d + dU_k \quad 2-1$$

Whereas dU_e is the change of external mechanical energy that is supplied to the system, dU_i is the change in elastic energy that is stored in the material, dU_a is the change in energy dissipated by crack growth, dU_d is the change in energy dissipation caused by other mechanisms and dU_k is the change in kinetic energy.

For brittle materials it is assumed that dU_d is zero, implying that the crack growth is the only cause of energy dissipation. dU_k is also zero, means that the crack growth is that slow that the kinetic energy change is negligible. The remaining energy balance is known as the Griffith's energy balance, which regards energy per unit of newly created fracture surface:

$$dU_a = dU_e - dU_i \quad 2-2$$

The energy release rate will be extracted by dividing equation 2-2 with the newly created fracture surface, assuming $dA=da \times B$, where B is the sample thickness and da is the newly created crack length:

$$G = \frac{1}{B} \left| \frac{dU_a}{da} \right| = \frac{1}{B} \left| \frac{dU_e}{da} - \frac{dU_i}{da} \right| \equiv \frac{d|U_P|}{da} \quad 2-3$$

So the energy release rate is the absolute change in potential energy per unit of crack area. This energy release rate is then compared to the so-called critical energy release rate G_c . The initial crack will propagate if the energy release rate is larger or equals its critical value.

$$G \geq G_c \quad 2-4$$

2.2.2 The mode mixity of fracture

The critical energy release rate G_c is generally considered as a material property of the material under consideration. However, its value is not really unique. Temperature and moisture have a major effect on the critical energy release. Furthermore, the G_c is highly dependent to the stress state or mode mixity in front of the crack tip. The latter depends: how much shear there is compared to the tensile stress, equation 2-5.

$$\Psi = \tan^{-1} \left(\frac{\sigma_{12}}{\sigma_{22}} \right) \quad 2-5$$

Where Ψ is the defined mode mixity. σ_{22} and σ_{12} are the tensile and shear stresses in crack tip respectively.

For an isotropic homogeneous material, a mode angle of 0° describes pure mode I loading, and mode angles of -90° or 90° describes pure mode II loading. The criterion for fracture will be expressed as:

$$G(T, C, \Psi) \geq G_c(T, C, \Psi) \quad 2-6$$

Where T , C and Ψ are the temperature, moisture level and mode mixity in front of the crack tip, respectively.

For a bi-material interface the fracture criteria (equation 2-6) appears to be well applicable. However the calculation of the mode mixity needs some more attention. Consider a semi-infinite traction-free crack at the interface between two homogeneous, isotropic and linear elastic materials, with material 1 above the interface and material 2 below as shown in Figure 2-2.

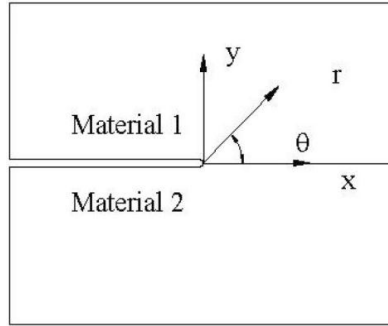


Figure 2-2 A crack along a bi-material interface and basic material properties.

The stress solution in the neighborhood of the crack tip typically has the following form [9-11]:

$$\sigma_{ij} = \text{Re} \left[\frac{\bar{K}}{\sqrt{2\pi r}} \cdot r^{i\varepsilon} \cdot \bar{f}_{ij}(\theta, \varepsilon) \right] \quad 2-7$$

Where $\bar{f}_{ij}(\theta, \varepsilon)$ is a complex function and \bar{K} is the complex stress intensity factor. r is the distance from the crack tip. Here ε represents the so-called oscillatory index defined as:

$$\varepsilon = \frac{1}{2\pi} \ln \left(\frac{1 - \beta_D}{1 + \beta_D} \right) \quad 2-8$$

Where, β_D represents the Dundur's parameter:

$$\beta_D = \frac{\mu_1(K_2 - 1) - \mu_2(K_1 - 1)}{\mu_1(K_2 + 1) + \mu_2(K_1 + 1)} \quad 2-9$$

With $K_i = (3 - \nu_i)/(1 + \nu_i)$ for plain strain and $K_i = (3 - 4\nu_i)$ for plain stress conditions. μ_i , E_i and ν_i ($i=1,2$) are the shear modulus, Young's modulus and Poisson's ratio of the respective materials.

On the interface at $\theta=0$, the solution of equation 2-7 will have a simple form and the traction ahead of the crack tip can be given as:

$$\sigma_{22} + \sigma_{12} = \bar{K} \cdot \sqrt{2\pi r} \cdot r^{i\varepsilon} \quad 2-10$$

Where $\bar{K} = K_I + iK_{II}$ is the complex stress intensity factor at the crack tip. Here K_I and K_{II} represent intensities of mode I (traction) and mode II (shear) stress states, respectively. $r^{i\varepsilon}$ is defined as:

$$r^{i\varepsilon} = \cos(\varepsilon \cdot \ln r) + i \cdot \sin(\varepsilon \cdot \ln r) \quad 2-11$$

When $\beta_D = 0$ (homogenous material) the mode mixity is specified by:

$$\psi = \tan^{-1} \left(\frac{\sigma_{12}}{\sigma_{22}} \right)_{\theta=0} \quad \text{as } r \rightarrow 0 \quad 2-12$$

There are also various alternative mode mixity definitions possible that can be well established through FEM simulations. Ryoji and Cho [12,13] proposed a crack surface displacement extrapolation method (CSDEM) to calculate the mode mixity.

$$\psi = \lim_{r \rightarrow 0} \left[\tan^{-1} \left(\frac{\delta u_x + 2\varepsilon \delta u_y}{\delta u_y - 2\varepsilon \delta u_x} \right) - \varepsilon \ln \left(\frac{r}{2a} \right) \right] \quad 2-13$$

Here δu_x and δu_y are the components of the crack surface opening displacement, parallel and perpendicular to the crack tip, respectively (see Figure 2-3). ε is the so-called oscillatory index which depends on the material incompatibility according to [9], r is the distance from the crack tip and $2a$ is a chosen reference length which is selected as the current crack length in this report.

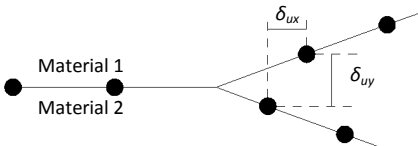


Figure 2-3 Schematic diagram of crack tip opening displacements method.

In FEM approximations the limit for $r \rightarrow 0$ in equation 2-13 is obtained using fit functions for the differential nodal point displacements δu_x^n and δu_y^n (n is the node number). Depending on the fit function used, different mode mixity values are obtained. In our present work a linear fit functions is chosen [14].

2.2.3 Numerical methods for interface fracture

Numerically, there are several methods available for calculation of the energy release rate and stress intensity factors, e.g. J -integral, virtual crack closure, cohesive zone, etc. In this study, the J -integral method is used for calculation of the critical energy release rate. The J -integral concept was first introduced by Rice and Cherpanov [15,16]. Based on an energy approach Rice formulated J as a path-independent line integral with a value equal to the decrease in potential energy per increment of crack extension in linear or nonlinear elastic materials. its path independence implies that J can be seen as a measure for the intensity of stresses and strains at the tips of the notches and cracks. Therefore the J -integral can be viewed both as an energy parameter, comparable to G , and as a stress intensity parameter comparable to K . For two dimensional problems, the J -integral equation is written as:

$$J = \int_{\Gamma} (W dy - T_i \frac{\partial u_i}{\partial x_i}) ds \quad 2-14$$

$$W = \int_0^{\varepsilon} \sigma_{ij} d\varepsilon_{ij} \quad 2-15$$

Where W is the strain energy density per unit volume, ds is an infinitesimal element of the contour arc length, Γ denotes any contour path surrounding the crack tip, here T denotes traction vectors and u is the displacement vector along the contour Γ . W can be further written in equation 2-15, with σ_{ij} and ε_{ij} denoting the stress and strain tensors, respectively. According to the definition, J -integral is the decrease of strain energy in the field per unit crack growth. As previously stated, for a linear elastic material, the J -value is equal to the energy release rate G ($J = G$).

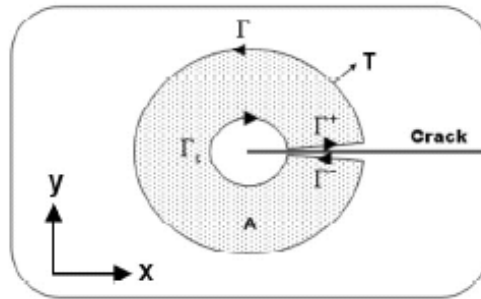


Figure 2-4 The path contour of a two dimensional crack in an elastic-plastic material [17].

Thus for a crack with the tip pointing in the positive X direction, this expression enables J or the decrease in potential energy per increment of crack growth, to be evaluated as a line integral along an arbitrary path surrounding the crack tip, starting somewhere on the lower crack flank and ending somewhere on the upper crack flank. This is a standard definition for the J -integral function. More information related to the J -integral in interface problems can be founded in literatures [18-22]. For interface problems the J -integral function is accounted in ABAQUS software [23].

2.3 Packaging materials

2.3.1 Viscoelasticity of epoxy molding compound

The behavior of materials is usually discussed in terms of two particular types of ideal material: the elastic solid and the viscous liquid. The elastic solid has a definite shape and is deformed by external forces into a new equilibrium shape. On removal of the external forces the elastic solid reverts back to its original form. The elastic solid stores all the energy that it obtains from the external forces during the deformation. This energy is available to restore the original shape when the forces are removed. By contrast a viscous liquid has no definite shape and flows irreversibly under the action of external forces. Molding compounds can display both elastic solid and viscous liquid properties depending on the temperature and experimentally chosen time-scale. This form of response which combines both liquid-like and solid-like features is termed “Viscoelasticity”. The term “Viscoelastic” pertains to those substances which exhibit both viscous and elastic properties. Epoxy molding compounds are viscoelastic materials and their mechanical properties change with time and temperature.

When an instantaneous strain is applied to a linear viscoelastic solid material, an instantaneous stress that subsequently will decay with time (Figure 2-5), will be recorded. This behavior is referred to as stress relaxation.

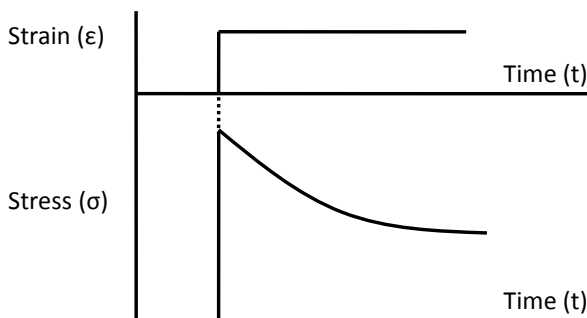


Figure 2-5 Stress relaxation of a viscoelastic material versus time.

Making the assumption of linear viscoelastic behavior we can define the stress relaxation modulus $E(t)$ as [24]:

$$E(t) = \sigma(t) / \varepsilon \quad 2-16$$

If $E(t)$ is measured over a number of decades of time, and is plotted against $\log t$, it exhibits a curve of the form as shown in Figure 2-6. It can be observed that at very short times $E(t)$ is in glassy region, while at very long times $E(t)$ is in the rubbery region. The region in between the glassy and rubbery region is the viscoelastic transition region. In the glassy region as well as in the rubbery region the molding compound is elastic i.e., $E(t)$ is independent of time. In the viscoelastic region, $E(t)$ is dependent on the time.

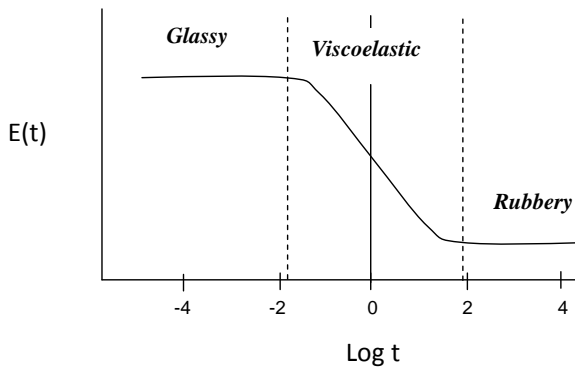


Figure 2-6 The stress relaxation modulus $E(t)$ as a function of time for a viscoelastic material.

A well-known characterization technique for understanding the effects of both time and temperature on the stress relaxation of molding compound is by conducting dynamic measurements using a Dynamic Mechanical Analyzer, TA instrument Q800. In this experimental method a sinusoidal displacement (strain ε) is applied to a sample and the resulting force (stress σ) is measured [25]. The experiment usually covers the frequency and temperature range of 0.32-60 Hertz and 20-200°C, respectively. For a perfectly elastic material, the resulting stress and the strain will be completely in-phase. For a purely viscous material, there will be a 90 degree phase lag of stress with respect

to strain. Viscoelastic materials have the characteristics in between, where some phase lag will occur during DMA tests.

$$\varepsilon = \varepsilon_0 \sin(\omega t) \quad 2-17$$

$$\sigma = \sigma_0 \sin(\omega t + \delta) \quad 2-18$$

In which ω is the applied angular frequency and δ the measured phase lag. By expanding equation 2-18, the stress can be considered to consist of two components:

$$\sigma = \sigma_0 \sin(\omega t) \cos \delta + \sigma_0 \cos(\omega t) \sin \delta \quad 2-19$$

The relation between the applied strain and the measured stress can be defined by two parameters: E' and E'' where:

$$E' = \frac{\sigma_0}{\varepsilon_0} \cos \delta \quad \text{and} \quad E'' = \frac{\sigma_0}{\varepsilon_0} \sin \delta \quad 2-20$$

$$\frac{E''}{E'} = \tan \delta \quad 2-21$$

The complex modulus E^* can be used to express the moduli E as follows:

$$E^* = E' + iE'' \quad 2-22$$

E' is called the storage modulus, since it is proportional to the stored energy in the test sample and representing the elastic portion. E'' on the other hand is called the loss modulus since it is proportional to the dissipated energy. Figure 2-7 shows a typical viscoelastic curve of the storage modulus with respect to the temperature.

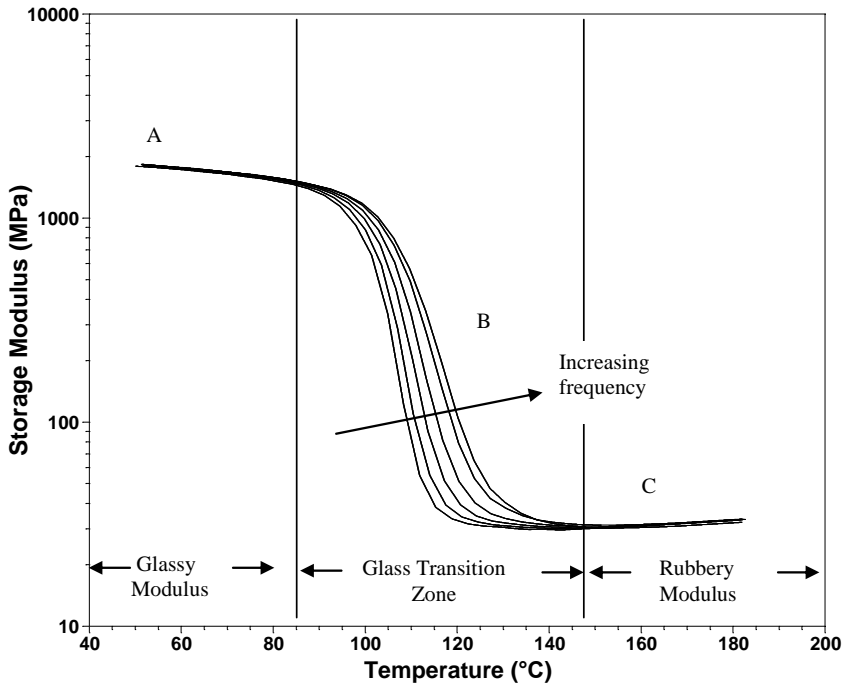


Figure 2-7 Plot of storage modulus $E'(\omega)$ versus temperature. Each line corresponds to the modulus response with respect to temperature for different frequencies.

The viscoelastic curve as shown in Figure 2-7 can be divided into three distinct regions. In the glassy region the material has the highest modulus and is almost independent of frequency and temperature. It can be seen that in this region the modulus remains constant for all applied frequencies and appears as a plateau conventionally termed as the glassy plateau or glassy state.

In the glass transition zone, the storage modulus is temperature and frequency dependent and drops by the increase of temperature. The drop in the storage modulus is due to the large scale molecular motion of the polymeric chains until it reaches the equilibrium rubbery modulus.

In the rubbery region the material exhibits its lowest storage modulus and is again largely independent of the applied frequency i.e., purely elastic. The modulus remains

constant and appears as a plateau region and hence is termed as the rubbery plateau or state.

2.3.2 Factors affecting viscoelasticity

The viscoelastic properties of the encapsulation material depend highly on different parameters which include:

1) The curing process

The curing process is one of the major packaging processes for electronic packages. During the curing process, the molding compound transfers from a liquid into a viscoelastic solid with a relatively high glassy modulus and glass transition temperature, accompanied with chemical shrinkage. Because of the cross-linking reaction and thermal shrinkage, stress will arise in areas where shrinkage is (partly) prevented by geometrical constraints. Furthermore, subsequent cooling or thermal cycling will produce additional stress contribution and deformation due to the mismatches in the thermal expansion among the materials in the package.

2) Time and temperature

It is well known that epoxy molding compounds show strong temperature and time dependent behavior. Generally the behavior is viscoelastic, such that the creep or relaxation phenomenon occurs in packages at various levels. Such behavior has significant influence on the thermo-mechanical behavior of plastic IC packages.

3) The filler effect

Epoxy molding compounds are usually filled with fillers to improve mechanical, physical, optical and electrical properties. It is very common in electronic packaging to use silica fillers in conjunction with polymers to increase the elastic modulus and thermal conductivity and decrease the coefficient of thermal expansion (CTE), and cure shrinkage to meet the requirements for electronic packaging. Also addition of silica fillers can reduce the cost.

4) Moisture uptake

It is known that the process of moisture absorption in polymers and molding compounds is accompanied by swelling which is always associated with changes in the mechanical properties. The absorbed water decreases the glassy and rubbery elastic moduli of the EMC. In addition water absorption speeds up the relaxation process by reducing the glass transition temperature.

Reference

- [1] A.A. Griffith, The phenomena of rupture and flow in solids, *Philosophical Transactions of the Royal Society*, 221 (1920) A 163–198.
- [2] G.R. Irwin, Onset of fast crack propagation in high strength steel and aluminum alloys, In *Sagamore Research Conference Proceedings*, 2 (1956) 289-305.
- [3] G.R. Irwin, Analysis of stresses and strains near the end of a crack traversing a plate, *J. Appl. Mech.* 24 (1957) 361-372.
- [4] G.R. Irwin. Linear fracture mechanics, fracture transition and fracture control, *Eng. Fractu. Mech.* 1(2) (1968) 241–257.
- [5] G.R. Irwin, J.M. Krafft, P.C. Paris, and A.A. Wells, Basic aspects of crack growth and fracture, *NRL Report 6598*, Naval Research Laboratory, Washington D.C., 1967.
- [6] W. D. van Driel, H.K.L. Bressers, J.H.J. Janssen, J.A. Bielen, X. Yan, M.A.J. van Gils, P.M.P. Stevens, P.J.J.H.A. Habets, G.Q. Zhang, L.J. Ernst, Driving mechanisms of delamination related reliability problems in exposed pad packages, *IEEE 6th EuroSimE conference* (Berlin, April 2005), PP 183-189.
- [7] A. Xiao, H. Pape, B. Wunderle, K.M.B. Jansen, J. de Vreugd, L.J. Ernst, Interfacial fracture properties and failure modeling for microelectronics, *IEEE 58th ECTC conference* (Lake Buena Vista, May 2008), pp. 1724-1730.
- [8] G.Q. Zhang, W.D. van Driel, X.J. Fan, *Mechanics of Microelectronics*, Springer, Dordrecht, Netherlands, 2006.
- [9] J. W. Hutchinson and Z. Suo, Mixed mode cracking in layered materials, *J. Adv. in Appl. Mech.* 29 (1991), 63-191.
- [10] A. A. O. Tay, Modeling of Interfacial Delamination in Plastic IC Packages Under Hydrothermal Loading, *ASME J. Electron. Packag.* 127 (3) (Sept 2005) 268-275.
- [11] A. A. O. Tay, Y. Ma, T. Nakamura, S. H. Ong, A Numerical and Experimental Study of Delamination of Polymer-Metal Interfaces in Plastic Packages at Solder Reflow Temperatures, In *Proceedings of the 9th Intersociety Conference on Thermal and Thermomechanical Phenomena in Electronic Systems*, IThERM 2004 (Las Vegas, June 2004), pp. 245-252

- [12] Y. Ryoji, S.B. Cho, Efficient Boundary Element Analysis of Stress Intensity Factors for Interface Cracks in Dissimilar Materials, *J. Eng. Fractu. Mech.* 34 (1989) 179–188.
- [13] S.B. Cho, K.R. Lee, Y.S. Choy, Y. Ryoji, Determination of Stress Intensity Factors and Boundary Element Analysis for Interface Cracks in Dissimilar Anisotropic Media, *Eng. Fractu. Mech.* 43(4) (1992) 603–614.
- [14] Hu Guojun, A Theoretical and Numerical Study of Crack Propagation Along a Bimaterial Interface With Applications to IC Packaging, PhD thesis, National University of Singapore, 2006.
- [15] G. P. Cherepanov, *Methods of Fracture Mechanics: Solid Matter Physics (Solid Mechanics and Its Applications)*, Springer, Dordrecht, Netherlands, 1997.
- [16] J. R. Rice, A Path Independent Integral and Approximate Analysis of Strain Concentration by Notch and Cracks, *J. Appl. Mech.*, 35 (1968) 379-386.
- [17] C. C. Lee, C. C. Chiu, K. N. Chiang, Stability of J -Integral Calculation in the Crack Growth of Copper/Low- k Stacked Structures, IEEE 56th ECTC conference (San Diego, June 2006), pp. 885-891.
- [18] R.E. Smelser, On the J -integral for bi-material bodies, *Int. J. Fractu.* 13 (1977) 382–384.
- [19] L.G. Zhao, Y.H. Chen, The J -integral analysis of an interface main crack interacting with near tip subinterface microcracks, *Int. J. Fractu.* 80 (1996) 25–30.
- [20] W.Y. Tian, K.T. Chau, Y.H. Chen, J -integral analysis of the interaction between an interface crack and parallel subinterface cracks in dissimilar anisotropic materials, *Int. J. Fractu.* 111 (2001) 305–325.
- [21] S.I. Chou, Note on path-independent integral for bi-material bodies, *Int. J. Fractu.* 45 (1990) 49–53.
- [22] N. Sukumar, Z.Y. Huang, J.H. Prevost, Z. Sou, Partition of unity enrichment for biomaterial interface cracks, *Int. J. Numer. Meth. Eng.* 59 (2004) 1075–1102.
- [23] A. Xiao, Interface characterization and failure modeling for semiconductor application, PhD thesis, Delft, 2012.
- [24] J.D. Ferry, *Viscoelastic properties of polymers*, third ed., Wiley, New York, 1980.

[25] I.M. Ward, J. Sweeney, an introduction to the mechanical properties of solid polymers, Second edition, John Wiley & Sons, Chichester, West Sussex, 2004.

Thermo-mechanical properties of fully cured molding compound

3.1 Introduction

Thermosetting polymers are widely used in the electronics industries as packaging materials. Typical examples are electrical insulators, conductive adhesives, molding compounds and underfill materials. The reliability of these materials is of great importance, because their failure may lead to the malfunctionality of the whole product.

Failure in microelectronics packaging mostly happens through polymer cracking, interface delamination and thermal fatigue, caused mainly by thermo-mechanical loadings [1]. Temperature changes occurring during operation may result in mechanical stresses in the individual components of microelectronic packages often through mismatches in the coefficients of thermal expansion. Moreover, shrinkage of the resin material during cure will introduce additional internal stresses. These stresses are generally considered to have a negative influence on the reliability of the product [2]. This is expected to become an even greater problem in the future as a result of on-going miniaturization accompanied with higher power dissipation densities and greater temperature gradients [3].

Based on:

M. Sadeghinia, K.M.B. Jansen and L.J. Ernst. Characterization and modeling the thermo-mechanical cure-dependent properties of epoxy molding compound. International Journal of Adhesion & Adhesives. 32:82-88, 2012.

For reliable prediction of the stresses and deformation in microelectronic packages, viscoelastic properties of the molding compound have to be taken into account [4,5]. De Vreugd et al. [6,7] showed that an accurate estimation on the stress distribution and warpage in the copper-molding compounds map molds is highly dependent on how well the thermo-mechanical properties of the molding compounds are characterized. Therefore, nowadays investigating the thermo-mechanical properties of thermosetting polymers has become one of the concern issues in electronic packaging [8–16].

This Chapter concentrates on the thermo-mechanical properties of two hand-made epoxy molding compounds, labeled here as DU and DF. They were prepared for fabricating the EMC-Cu interface samples for delamination measurement. However, due to the weak interface bonding and as an emergency situation a commercial EMC-Cu from Infineon Technologies AG was replaced which is labeled in this thesis as IF EMC (See section 1-3). The thermo-mechanical properties of IF EMC will be discussed in Chapter 6. The latter will be implemented as the input of FEM ABAQUS model for establishing the delamination toughness of IF EMC-Cu lead frame interfaces in Chapter 6.

3.2 Experiments

3.2.1 Materials and sample preparation

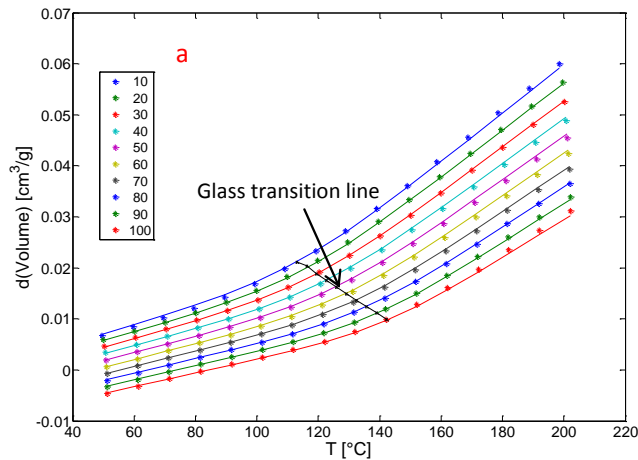
Two types of epoxy molding compounds are used in this study. The hand-made filled and unfilled samples, which named as DF and DU, are particulate-filled composite containing similar components as used in commercial molding compounds. Their systems consist of epoxy Novolac (EPN 1180, Huntsman Advanced Materials, equivalent weight 175–182 g/eq) as a matrix material, Bisphenol-A (equivalent weight 114 g/eq) as hardener and fused silica spheres (FB-940, ex Denka, median diameter 15 μm , density 2.20 g/cm^3) as filler. Triphenylphosphine (TPP, 0.5 g/100 g epoxy) is used as a catalyst. The epoxy Novolac and Bisphenol-A were mixed in a stoichiometric ratio. The unfilled sample has 0% filler, while the filled one contains 64.5 wt% (50 vol%) filler.

The coefficient of thermal expansion, bulk and storage modulus of the EMCs are measured through different experiments and the results were fitted to appropriate models. The thermo-mechanical properties of the DF and DU EMCs will be used for extracting the cure dependent parameters in Chapter 4.

3.2.2 PVT Measurement

3.2.2.1 COEFFICIENT OF THERMAL EXPANSION (CTE)

A GNOMIX high pressure dilatometer (PVT apparatus) was used to determine the coefficient of thermal expansion (CTE) and bulk modulus of the fully cured EMC samples. For these measurements the sample pressure and temperature were stepwise increased and the corresponding volume changes were recorded. Typical temperature and pressure ranges were 40-200°C (in steps of 10°C) and 10 to 100 MPa (in steps of 10MPa). The volume changes of the fully cured molding compounds are shown in Figure 3-1.



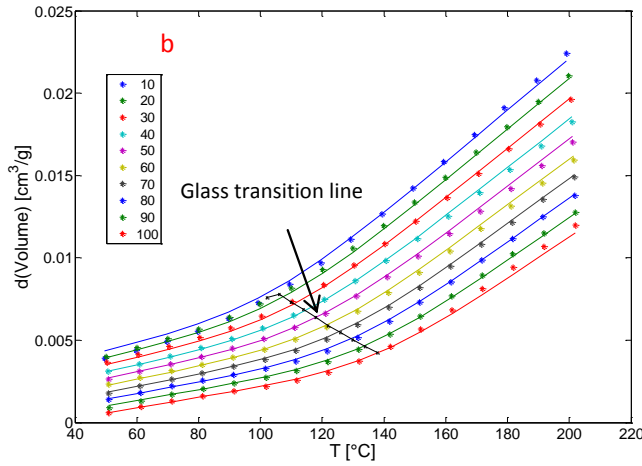


Figure 3-1 Volume changes of the samples in different temperature and pressure from PVT measurement, symbols: experimental data, full lines: fit to equation 3-2, the legend refers to the applied pressures, a: DU, b: DF.

The results clearly show a linear volume increase in the glassy region and a second linear region above the glass transition temperature. With respect to the data analysis it is more convenient to fit the volume changes first to a model and then obtain the coefficients of thermal expansion and the compressibility by differentiating this model with respect to temperature and pressure, respectively. As a model we use the well-known Tait equation [17].

$$v(T,P) = v''(T) \left[1 - C \times \ln \left(1 + \frac{P}{b_1 \exp(-b_2 T)} \right) \right] \quad 3-1$$

where $C = 0.0894$, b_1 and b_2 are fitting parameters. In order to allow for a smooth transition between glassy and rubbery behavior we modified the thermal part $v''(T)$ as:

$$v''(T) = v_0 \left(1 + k_1(T - T_{gp}) + \frac{1}{2} k_2 \left[(T - T_{gp}) + \frac{\ln(\cosh[A_1(T - T_{gp})])}{A_1} \right] \right) \quad 3-2$$

in which A_1 is a fitting parameter related to the width of the transition regime and T_{gp} is the pressure dependent glass transition temperature, $T_{gp} = T_g^{pvt} + s_0 P$.

Here T_g^{pvt} is the fully cured T_g at atmospheric pressure and s_0 is the pressure dependency of the glass transition. The fit parameters were determined by non-linear curve fitting (using MatLab) and are summarized in Table 3-1. As mentioned before, the volumetric CTE then follows by differentiating with respect to temperature, resulting in

$$CTE_v(T,0) = k_1 + \frac{1}{2}k_2 \left(1 + \tanh[A_1(T - T_g^{pvt})]\right) \quad 3-3$$

Since the tanh function varies between -1 and +1, the k_1 and $(k_1 + k_2)$ represent the volumetric thermal expansion in the rubbery and glassy state respectively.

Material	Properties							s_0 (°C/MPa)
	u_0 (cm ³ /g)	k_1 (1/°C)	k_2 (1/°C)	A_1 (1/°C)	b_1 (MPa)	b_2 (1/°C)	T_g^{pvt} (°C)	
DU	0.846	2.1 E-4	3.63 E-4	0.035	1370.9	6.4E-3	109.7	0.324
DF	0.609	7.9 E-5	1.88 E-4	0.033	5633.8	9.1 E-3	98	0.445

Table 3-1 T_g and fit parameters corresponding to equation 3-1 and equation 3-2; $C=0.0894$.

Since it is more customary to work with the linear coefficients of thermal expansion we defined those as 1/3 of the volumetric ones. The linear coefficients of thermal expansion are presented in Figure 3-2.

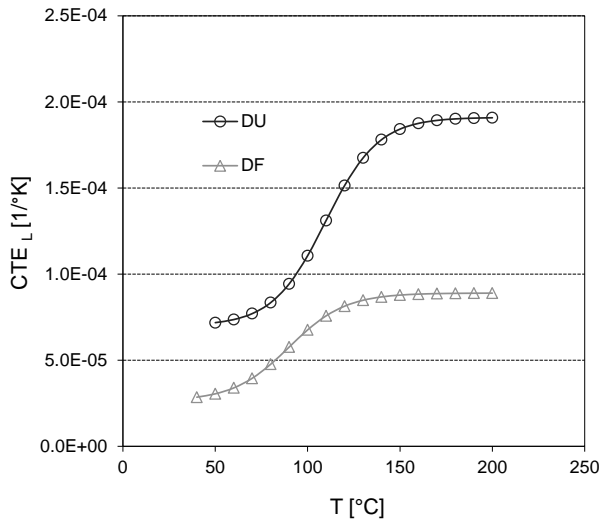


Figure 3-2 Linear CTE of the EMCs vs. temperature, extracted from the PVT measurement.

It shows that the calculated CTE increases by temperature with a clear change around T_g . The glassy and rubbery CTE of the DF samples is almost 45% of that of the unfilled one (i.e. DU), which matches quite well with expectation since the expansion is mostly due to the resin which is almost 50 vol% of the DF materials' contents.

3.2.2.2 BULK MODULUS

The compressibility is a fundamental material property that relates the volume changes in a material to the imposed hydrostatic stress. This property can be determined in a similar way as for the CTE but now by differentiating with respect to volume.

$$\beta(T) = k_1 s_0 + \frac{1}{2} k_2 s_0 \left\{ 1 + \tanh \left[A_1 (T - T_g^{pvt}) \right] \right\} + \frac{C}{b_1 \exp(-b_2 T)} \quad 3-4$$

The bulk modulus is a material property which is often needed as input in most thermal-mechanical simulation software and is obtained here as the inverse of the bulk compressibility:

$$K = \frac{1}{\beta(T)} \quad 3-5$$

Figure 3-3 shows that, with respect to the DF and DU samples, as expected both the glassy and rubbery bulk modulus increase with filler content. Due to filler the glassy and rubbery bulk modulus of the filled sample (DF) becomes 2.4 and 2 times higher than the unfilled one (DU).

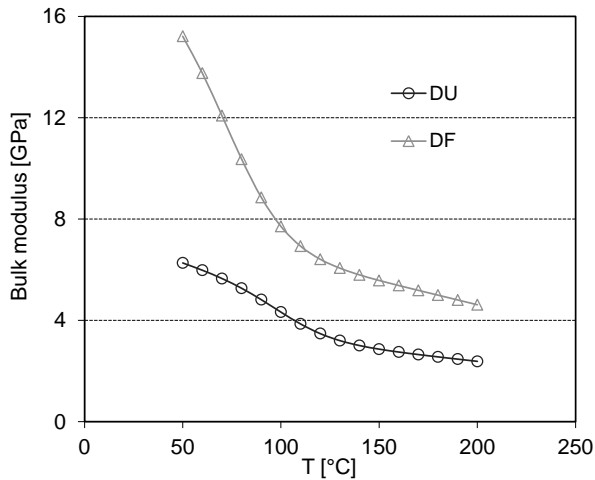


Figure 3-3 Bulk modulus of the materials in different temperatures, data are extracted from the PVT measurement.

3.2.3 Dynamic Mechanical Analyzer (DMA)

The viscoelastic tensile properties of the fully cured DU and DF materials as a function of the excitation frequency and temperature are studied by a Dynamic Mechanical Analyzer, TA instrument Q800. A sinusoidal displacement (strain ϵ) is applied to a sample and the resulting force (stress σ) is measured [18]. The experiment covered the frequency and temperature range of 0.32-32 Hertz and 20-200°C respectively. For a

perfectly elastic material, the resulting stress and the strain will be completely in phase. For a purely viscous material, there will be a 90 degree phase lag of stress with respect to strain. Viscoelastic materials have the characteristics in between where some phase lag will occur during DMA tests.

$$\varepsilon = \varepsilon_0 \sin(\omega t) \quad 3-6$$

$$\sigma = \sigma_0 \sin(\omega t + \delta) \quad 3-7$$

In which ω is the applied frequency and δ the measured phase lag. By expanding equation 3-7, the stress can be considered to consist of two components:

$$\sigma = \sigma_0 \sin(\omega t) \cos \delta + \sigma_0 \cos(\omega t) \sin \delta \quad 3-8$$

The relation between the applied strain and the measured stress can be defined by two parameters: E' and E'' where:

$$E' = \frac{\sigma_0}{\varepsilon_0} \cos \delta \quad \text{and} \quad E'' = \frac{\sigma_0}{\varepsilon_0} \sin \delta \quad 3-9$$

$$\frac{E''}{E'} = \tan \delta \quad 3-10$$

The complex modulus E^* can be used to express the modulus E as follows:

$$E^* = E' + iE'' \quad 3-11$$

E' is called the storage modulus, since it is proportional to the stored energy in the test sample. E'' on the other hand is called the loss modulus since it is proportional to the dissipated energy. Similarly the shear storage and loss moduli, G' and G'' , are defined.

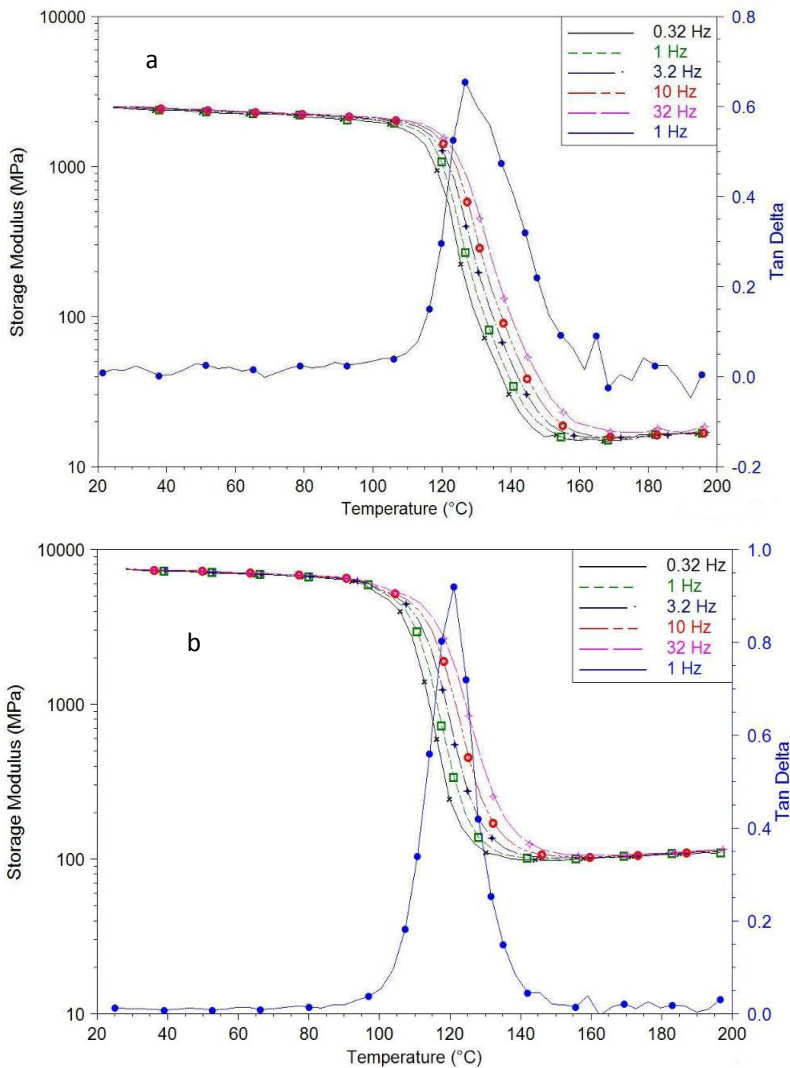


Figure 3-4 Storage modulus (E') vs. temperature measured by the DMA experiment. a): DU sample. b): DF sample. The $\tan \delta$ curve is only shown for 1 Hz frequency.

Figure 3-4 clearly shows that for each material, the E_g (Elongation glassy modulus) and E_r (Elongation rubbery modulus) are independent of the frequency. However in the glass transition regime clear frequency dependent effects can be seen. If we take the

peak position of the 1 Hz $\tan \delta$ curves as the DMA glass transition temperature, we obtain values of 128°C and 121°C for the DU and DF material respectively.

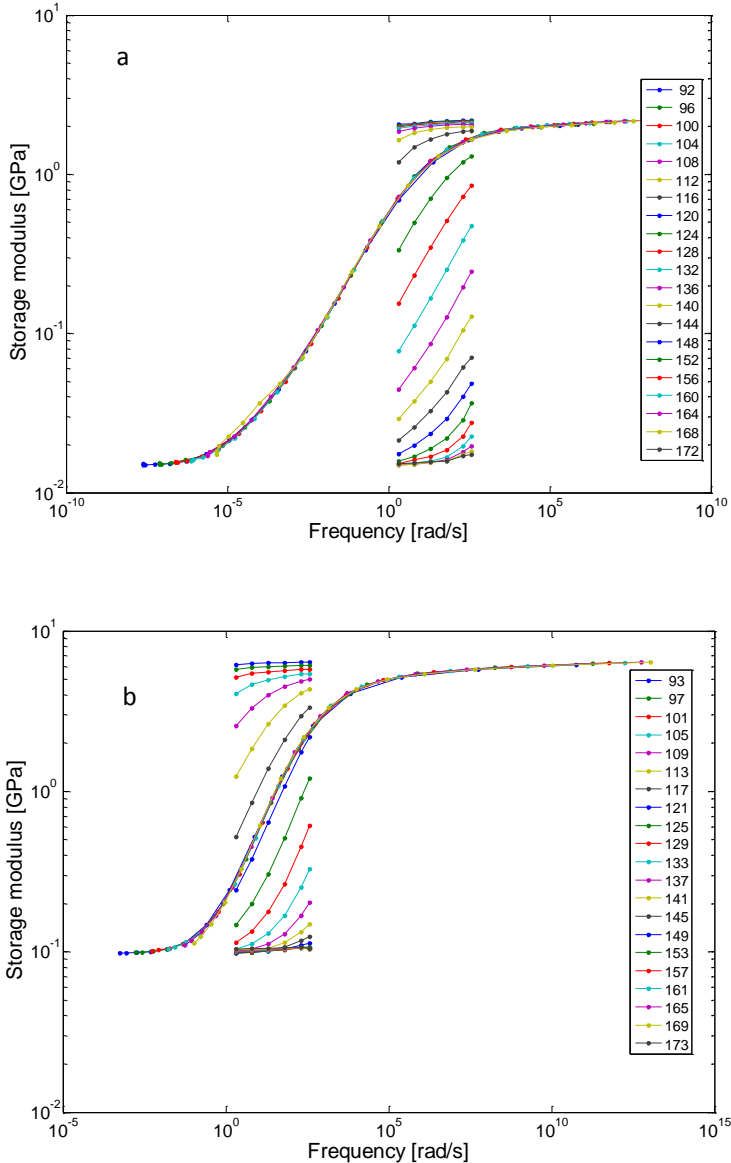


Figure 3-5 Storage modulus (E') and viscoelastic tensile modulus master curve of DU and DF samples as a function of frequency. Data extracted by analyzing the DMA tensile measurements. $T_{ref} = 120^\circ\text{C}$, a): DU sample, b): DF sample.

Material	Properties			
	Glassy Modulus (MPa)	Rubbery Modulus (MPa)	$T_g^{E'}$	$T_g^{\tan \delta}$
DU	2253	16.3	121.3 °C	128 °C
DF	7239	108.3	112.5 °C	121 °C

Table 3-2 Glassy, Rubbery modulus and T_g , according to DMA test, T_g values at 1 Hz.

Table 3-1 and Figure 3-4 show that there are some differences comparing the T_g values obtained from DMA measurement to PVT. Such differences are because the glass transition is a kinetic process which takes place in a certain temperature and time range. It therefore depends on both the measurement method and the data evaluation procedure.

Table 3-2 shows that, due to the usage of filler, the E_g and E_r of the filled DF materials are almost 3.2 and 6.4 times more than those of the unfilled DU materials, respectively.

The storage modulus can be interpolated and plotted as a function of frequency and temperature, see Figure 3-5. Time–temperature superposition appears to be valid for the fully cured filled and unfilled material. The shift factors a_T are determined from the storage modulus curve and are plotted in Figure 3-6, using $T = 120^\circ\text{C}$ as the reference temperature. A marked change in slope of the a_T close to the glass transition temperature is observed in this figure which is attributed to a change in relaxation mechanism. Below the switching temperature, T_c , the shift factor follows the Arrhenius behavior [19] (activation energy driven), equation 3-12, whereas above this temperature it follows the WLF behavior [20,21] (free volume mechanism), equation 3-13. The corresponding parameters related to shift factor are summarized in Table 3-3. The models with the estimated parameters were also plotted in the Figure 3-6 and a good fit in the measured domain was observed.

$$\log a_T^{Arrh} = \frac{-H}{2.30R} \left(\frac{1}{T} - \frac{1}{T_0} \right) \quad T \leq T_c \quad 3-12$$

$$\log a_T^{WLF} = \frac{C_1(T - T_{ref})}{C_2 + T - T_{ref}} \quad T \geq T_c \quad 3-13$$

Material	C_1	C_2	H [kJ/mol]	T_0 [°C]	T_c [°C]
DU	12.6	31	331	140	114
DF	11.1	56.6	401	200.5	90

Table 3-3 WLF and Arrhenius fit parameters for temperature shift factors, $T_{ref} = 120$ °C.

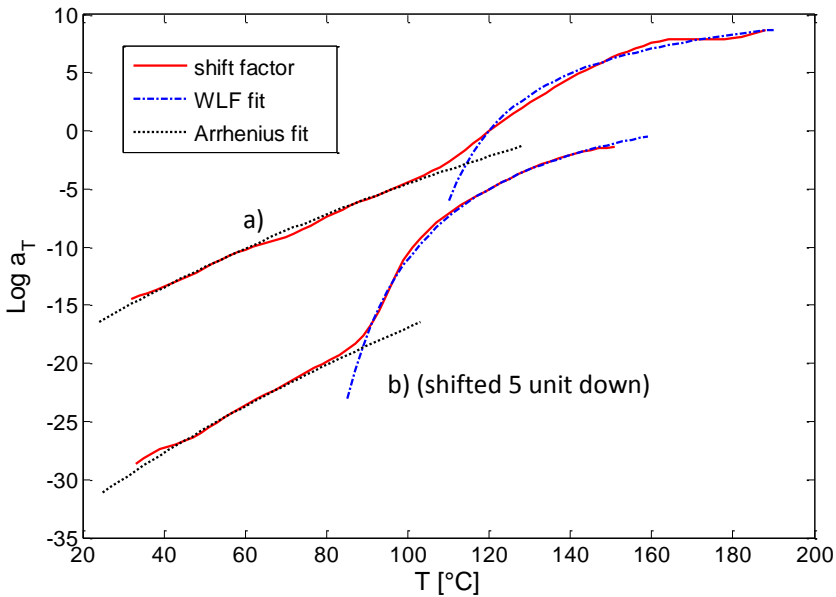


Figure 3-6 Shift factors related to the tensile master curve, Details of Arrhenius and WLF fit to the fully cured shift factor curve, a): DU, b): DF, $T_{ref} = 120$ °C. The DF sample curve was shifted 5 units down for clarity.

3.3 Conclusions

In this Chapter an extensive study on the thermo-mechanical properties of a series of fully cured epoxy resins with and without filler was carried out. Using the GNOMIX high pressure dilatometer the coefficient of thermal expansion and bulk modulus were measured. In addition using a Dynamic Mechanical Analyzer the storage modulus was measured and applying the Time–Temperature Superposition principle, the master curves were extracted. The effect of the filler was also investigated on these thermo-mechanical properties and resulted shows that the filler decreases the thermal contraction of epoxy resins but increase the modulus below and above the glass transition temperature.

References

- [1] E. Suhir, Y.C. Lee, C.P. Wang, *Micro- and opto-Electronic materials and structures: physics, mechanics, design, reliability, packaging*, Springer, New York, 2007.
- [2] D. Lu, C.P. Wang, *Materials for advanced packaging*, Springer, New York, 2009.
- [3] G.Q. Zhang, W.D. van Driel, X.J. Fan, *Mechanics of Microelectronics*, Springer, Dordrecht, 2006.
- [4] J. de Vreugd, K.M.B. Jansen, L.J. Ernst, C. Bohm, A. Kessler, H. Preu, *IEEE 10th Electronic Packaging Conference (Singapore, December 2008)*, pp. 675-682.
- [5] M.Y. Tsai, C.T. Wang, C.H. Hsu, the effect of epoxy molding compounds on thermal/residual deformations, and stresses in IC packaging during manufacturing process, *IEEE transactions on components and packaging technologies*, 29(3) (2006) 625–635.
- [6] J. de Vreugd, *The effect of aging on molding compound properties*, PhD thesis, Delft, 2011.
- [7] J. de Vreugd, K.M.B. Jansen, L.J. Ernst, C. Bohm, Prediction of cure induced warpage of micro-electronic products, *J. Microelectron. Reliab.* 50(7) (2010) 910–916.
- [8] D.G. Yang, *Cure-dependent viscoelastic behavior of electronic packaging polymers*, PhD thesis, Delft, 2007.
- [9] D.G. Yang, K.M.B. Jansen, L.J. Ernst, G.Q. Zhang, H.J.L. Bressers, J.H.J. Janssen, Effect of filler concentration of rubbery shear and bulk modulus of molding compounds, *J. Microelectron. Reliab.* 47 (2007) 233–239.
- [10] K.M.B. Jansen, C. Qian, L.J. Ernst, C. Bohm, A. Kessler, H. Preu, M. Stecher, Modeling and characterization of molding compound properties during cure, *J. Microelectron. Reliab.* 49 (2009) 872–876.
- [11] F. Lapique, K. Redford, Curing effects on viscosity and mechanical properties of a commercial epoxy resin adhesive, *Int. J. Adhes. Adhes.* 22 (2002) 337–346.
- [12] H. Preu, M. Mengel, Experimental and theoretical study of a fast curing adhesive, *Int. J. Adhes. Adhes.* 27 (2007) 330-337.

- [13] D. Lu, C.P. Wong, Effects of shrinkage on conductivity of isotropic conductive adhesives, *Int. J. Adhes. Adhes.* 20 (2000) 189-193.
- [14] R.S. Chambers, R.R. Lagasse, T.R. Guess, D.J. Plazek, C. Bero, A rubbery cure shrinkage model for analyzing encapsulated assemblies, *J. Electron. Packag.* 117(3) (1995) 249–254.
- [15] L.F.M. Da Silva, R.D. Adams, A rubbery cure shrinkage model for analyzing encapsulated assemblies, *J. Adhes. Sci. Technol.* 20 (2006) 1705–1726.
- [16] J. Lange, S. Toll, J.E. Manson, A. Hult, Residual stress build-up in thermoset films cured above their ultimate glass transition temperature, *J. Polym.* 36(16) (1995) 3135–3141.
- [17] R. Simha, P.S. Wilson, O. Olabisi, Pressure–volume–temperature properties of amorphous polymers – empirical and theoretical predictions, *Kolloid- Z. und Z. für polym.* 251(6) (1973) 402–408.
- [18] I.M. Ward, J. Sweeney, an introduction to the mechanical properties of solid polymers, Second edition, John Wiley & Sons, Chichester, West Sussex, 2004.
- [19] A.D. McNaught, A. Wilkinson, *Compendium of Chemical Terminology*, second ed., IUPAC Blackwell Scientific, Oxford, 1997.
- [20] M.L. Williams, R.F. Landel, J.D. Ferry, The temperature dependence of relaxation mechanisms in amorphous polymers and other glass-forming liquids, *J. Am. Chem. Soc.* 77 (1955) 3701–3707.
- [21] J.D. Ferry, *Viscoelastic properties of polymers*, 3rd edition, Wiley, New York, 1980.

Chapter 4

Cure dependent parameters of an epoxy molding compound

4.1 Introduction

Integrated circuits are protected against shocks, vibrations and environmental conditions like moisture by encapsulating them with an epoxy resin, i.e. the so-called molding compound. Molding compounds are designed to possess adequate mechanical strength, excellent adhesion to package components and matched coefficient of thermal expansion. During the encapsulation process the molding compound pellets are melted and injected into a preheated mold which contains the die(s) and lead frame. After the injection the epoxy starts to crosslink (cure) and eventually forms a rubbery substance.

The thermo-mechanical characteristics of the epoxy resin change dramatically during cure [1-4]. A transition occurs from the behavior of a viscoelastic liquid with low shear stiffness, in the uncured state, to the behavior of a viscoelastic solid with relatively high stiffness, in the fully cured state. The evaluation of the viscoelastic behavior during the curing process has been modeled in multiple studies [5-9].

During cure, a 3-dimensional crosslinked network is formed. As a consequence of the curing reaction, the resin network shrinks in volume. Residual stresses develop due to

Based on:

M. Sadeghinia, K.M.B. Jansen and L.J. Ernst. Characterization the viscoelastic properties of an epoxy molding compound during cure. Journal of Microelectronics Reliability. 52:1711-1718, 2012.

the simultaneous increase in material stiffness and volumetric shrinkage if the molding compound is subjected to constraints [11]. Furthermore, warpage may occur in the microelectronic packages [12-14].

In Chapter 3, the thermo-mechanical properties of the fully cured DF and DU EMCs are studied in details. In Chapter 4, the changes in the viscoelastic behavior of the DF and DU samples, during the curing process will be investigated. The characterization methods were earlier developed in [5-9].

As the 1st step, the cure dependent properties of the samples, likewise, the cure kinetics and cure shrinkage were measured using a Differential Scanning Calorimeter (DSC) and a GNOMIX high pressure dilatometer. Then, using the shear setup of a Dynamic Mechanical Analyzer DMA- Q800, the cure dependent viscoelastic behavior of the DF material is determined during heating scans of an intermittent cure experiment.

The governed cure dependent parameters of DU and DF EMCs were initially considered in NanoInterface project for adding in the interfacial FEM model in Chapter 6. However, since the interface samples were replaced by a commercial highly filled IF EMC-Cu, the effect of curing is neglected in the interface model of Chapter 6, see section 6-4.

4.2 Experimental

Different aspects of the cure dependent mechanical and thermal properties of the DF and DU samples were measured using a DSC, a PVT and a DMA Apparatus. Generally the DSC test reveals the T_{g0} which is the T_g of the uncured materials, the T_g of the cured materials, the released heat due to the curing and the reaction kinetics which provides the relation between conversion (degree of cure) and the cure time. The PVT test is also applied measuring the shrinkages of the materials during the curing period. Using the DMA, the cure dependent viscoelastic shear modulus of the DF EMC during an intermittent cure experiment is obtained.

4.2.1 DSC Experiment

4.2.1.1 CURE KINETICS

Differential Scanning Calorimeter (DSC) was used to obtain the curing process parameters, such as the degree and rate of chemical conversion and the glass transition temperature. The experiments were performed with a calorimeter of TA-instruments DSC2920 on samples of approximately 5-10 mg in weight. With this device the reaction heat can be detected and related to the degree of conversion (α) [5]. The degree of conversion was modeled with the autocatalytic Kamal–Sourour Equation [15].

$$\frac{d\alpha}{dt} = k_0 \exp\left[\frac{-E_a}{RT}\right] \alpha^m (1-\alpha)^n \quad 4-1$$

in which α is the degree of conversion, R the universal gas constant 8.314 J/ (mol K), T the temperature in Kelvin and E_a is the activation energy. The unknown parameters m and n as well as k_0 and E_a were determined by analyzing temperature scans on non-reacted materials from 0 to 200°C at heating rates of 5, 10 and 15 °C/min [16].

Figure 4-1 shows the measured heat flow with respect to the time in different heating rates for DU and DF materials. The area below the graphs at each time is related to the released heat. The total amount of the released heat i.e. H_{tot} is calculated and indicated in Table 4-1. As it shows the H_{tot} in different heating rates is almost constant for DF and DU materials, separately. However the peak of the released heat increases with increasing heating rates. This is because for a faster heating, less time is available to reach a certain temperature and so less time for reaction, resulting in a lower conversion.

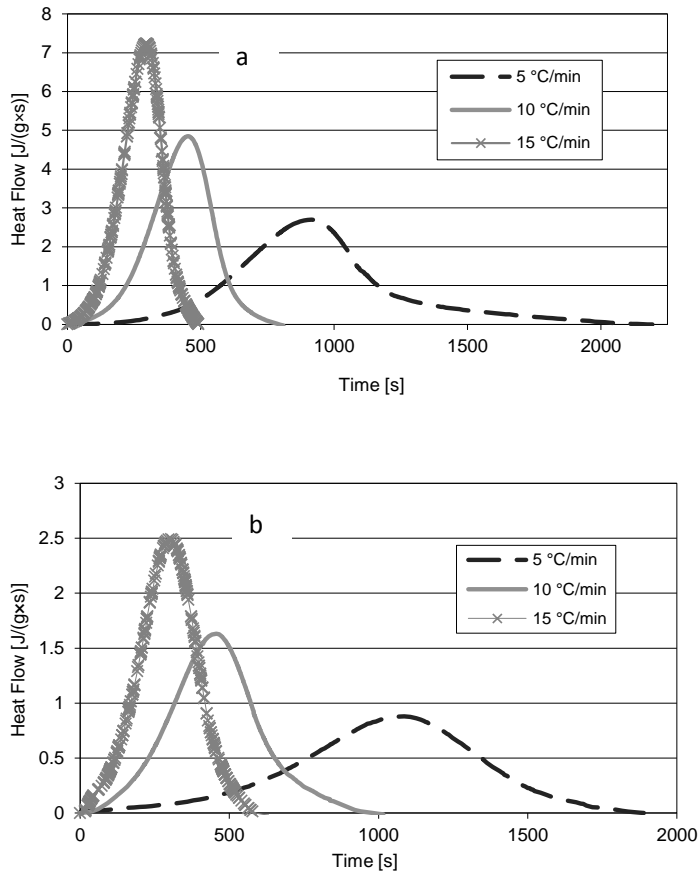


Figure 4-1 DSC scanning of uncured material with different heating rates. The heating rate did not affect the total released heat (see Table 4-1). a): DU sample, b): DF sample.

As an additional check we estimated the reaction heat for the DF sample, based on that of DU samples and the known filler content (64.5 wt%), assuming that the filler is inert and does not contribute to the released heat. The last row of Table 4-1 shows that this assumption is indeed justified.

Properties	Rate of heating		
	5 °C/min	10 °C/min	15 °C/min
Released heat, H_{tot} , (J/g), DU sample	187	187.1	181.6
Released heat, H_{tot} , (J/g), DF sample	67.8	68	63.3
Calculated H_{tot} (DF sample) based on the H_{tot} of DU sample and filler content (J/g)	66.4	66.4	64.5

Table 4-1 H_{tot} of the samples cured with different heating rate.

The predicted results for the reaction kinetics based on equation 4-1 and the scan rate experiments discussed above are shown in Figure 4-2 as the full lines. Results show that the reaction is much slower in DF materials. It takes about 23 minutes at 120°C, for the DU material, to reach 60% conversion whereas for the filled material it takes about 117 minutes to reach this conversion level. This effect can be interpreted as a partial deactivation of the catalyst by the silica filler.

Material	E_a [J/mol]	k_0 [s ⁻¹]	m [-]	n [-]
DU	77.5E3	1.84E7	0.158	1.26
DF	76.1E3	2.48E6	0.163	1.365

Table 4-2 Kinetic parameters of model epoxy system.

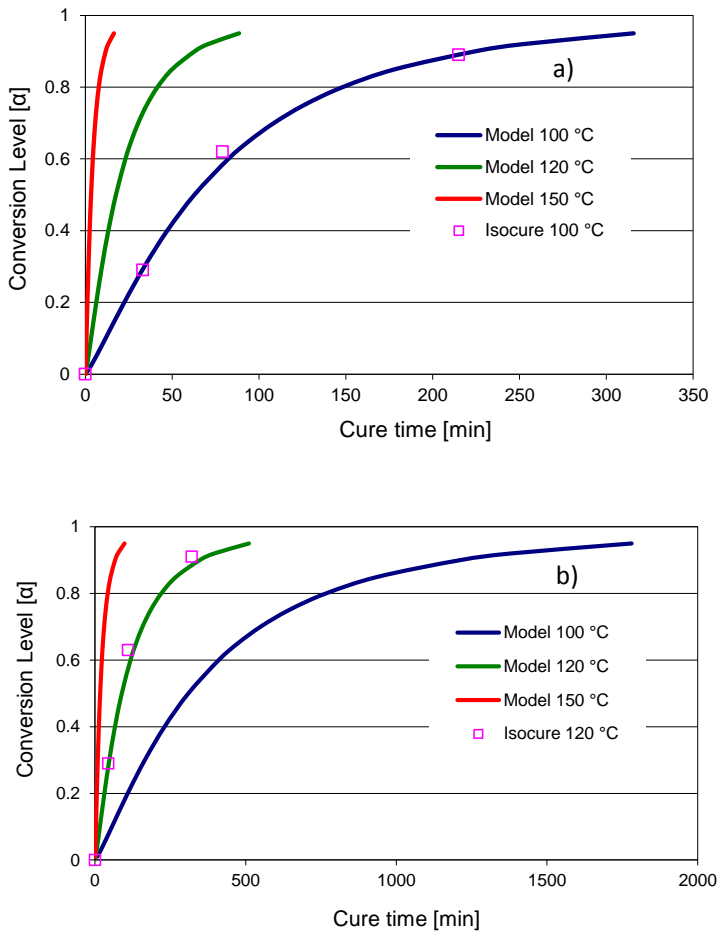


Figure 4-2 Conversion versus curing time at different temperature. Full lines: prediction for the reaction kinetics. Symbols: Independent data from isothermal cure experiments. a): DU, b): DF.

In order to verify the validity of the reaction kinetics predictions a second independent method was used. For this purpose we partly cured the materials in the DSC by heating them for a specific time and temperature (100 °C and 120 °C in this case). These partly cured samples were quickly cooled and subjected to a rescan from -30 to 200 °C at a rate of 10 °C/min (see Figure 4-3). From this rescan the shifted glass transition as well as the remaining heat of reaction could be determined. Based on the latter

quantity the conversion could be calculated using equation 4-2. These values, as well as the used curing time and temperature were added to the kinetics predictions in Figure 4-2. This shows that there is a good agreement between the conversion predictions and the experimental values from the isothermal cure tests.

$$\alpha = 1 - \frac{\Delta H_{residual}}{\Delta H_{total}} \quad 4-2$$

where α is the degree of cure. ΔH_{total} and $\Delta H_{residual}$ are the total reaction heat of uncured and remaining heat of reaction of partly cured samples, respectively [5].

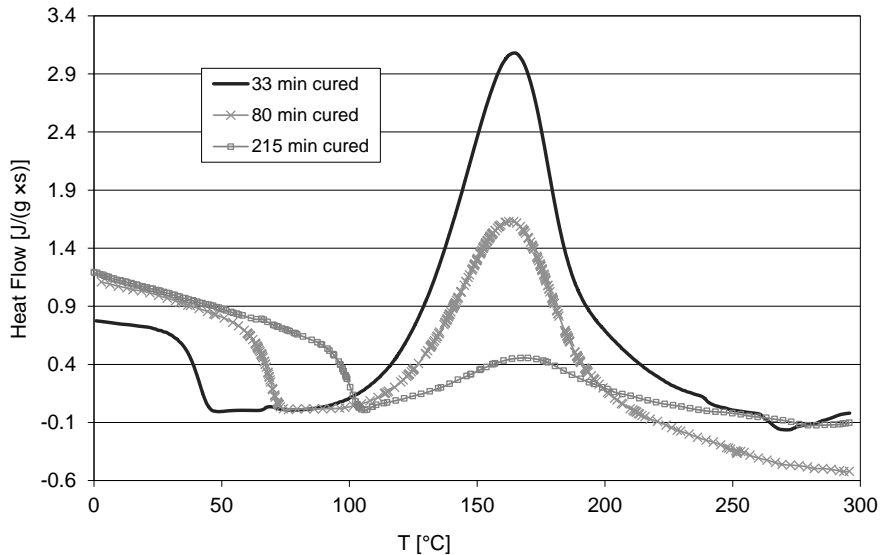


Figure 4-3 DSC heat scans of DU material partly cured at 100 °C. Increasing the conversion level leads to an increase in T_g and a decrease of the released heat.

4.2.1.2 GLASS TRANSITION

The glass transition temperature, indicated as T_g , marks the transition from the glassy (solid) state to the liquid or rubbery state. For polymers this glass transition is not a single temperature but covers a range of about 20-50°C. There are two T_g values related to each thermoset polymer. T_{g0} which is related to the uncured material and T_{g1} which is

related to the fully cured polymer. The T_g values can be obtained from DSC data as the change in the slope of the heat flow vs. temperature curve.

The results of the isothermal cure experiments discussed above were used to generate a plot of the glass transition temperature as a function of the conversion level (see Figure 4-4).

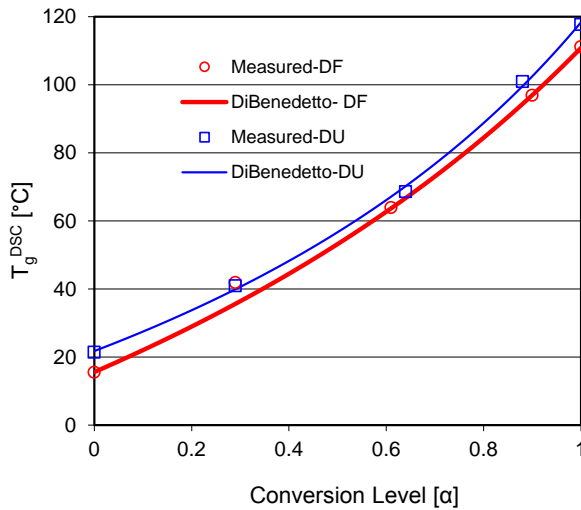


Figure 4-4 T_g of partly cured samples measured in DSC experiment, i.e. T_g^{DSC} . Full lines: fits to equation 4-3, symbols: extracted from the heat scan of partially cured samples.

The glass transition temperature of a thermosetting polymer depends on the crosslink density, the number of free chain ends and the rigidity of the polymeric segments. It was shown that the glass transition temperature in the crosslinked system increases linearly with the concentration of the crosslinks which restricts the free volume and free chain ends [17]. Figure 4-4 also shows a gradual increase of the T_g^{DSC} (T_g of the samples measured by DSC apparatus) by increasing the conversion level from about 21 to 118°C for the unfilled material, i.e. DU. The curve for the filled material (DF) appears to be about 5°C lower over the whole trajectory.

The glass transition temperature curves were fitted to the empirical DiBenedetto model [18]:

$$T_g(\alpha) = T_{g0} + \frac{(T_{g1} - T_{g0})\lambda\alpha}{1 - (1 - \lambda)\alpha} \quad 4-3$$

where α denotes the degree of cure and λ is a fitting parameter. T_{g0} , T_{g1} , and $T_g(\alpha)$ are the glass transition temperature of uncured, fully cured and partly cured sample respectively. The parameters obtained from this fit are summarized in Table 4-3.

	T_{g0} [°C]	T_{g1} [°C]	λ
DU (Unfilled)	21.4	117.7	0.567
DF (Filled)	15.5	111.2	0.652

Table 4-3 Parameters for equation 4-3.

The T_g value of uncured sample at 29% conversion is slightly higher than the DiBenedetto fit. However since the determination of a T_g value is typically with 2-5°C accuracy, the deviation is not considered to be significant.

Note that the DiBenedetto equation reduces to the equation proposed by Pascault and Williams if the fit parameter λ is set to the $\frac{\Delta C_{p1}}{\Delta C_{p0}}$ ratio, used in their publication [18].

4.2.2 PVT Experiment (cure shrinkage)

During cure, the EMC transforms from the liquid state into a viscoelastic solid. The formation of chemical crosslinks leads to a volumetric shrinkage. This shrinkage contributes for some extent to the residual stresses in electronic packages. The GNOMIX high pressure dilatometer (PVT Apparatus) was used to determine the amount of volumetric decrease due to the curing.

The experimental cure shrinkage plots for DF and DU materials are shown in Figure 4-5. The graph is divided in three major parts: increase in volume during heating, subsequent isothermal cure shrinkage and cooling down to room temperature. During heating the material is still un-reacted and is in the liquid state so the thermal expansion

is large. After cure, the glass transition temperature is much higher and the material is mostly cooling down in the solid state where the thermal expansion is low.

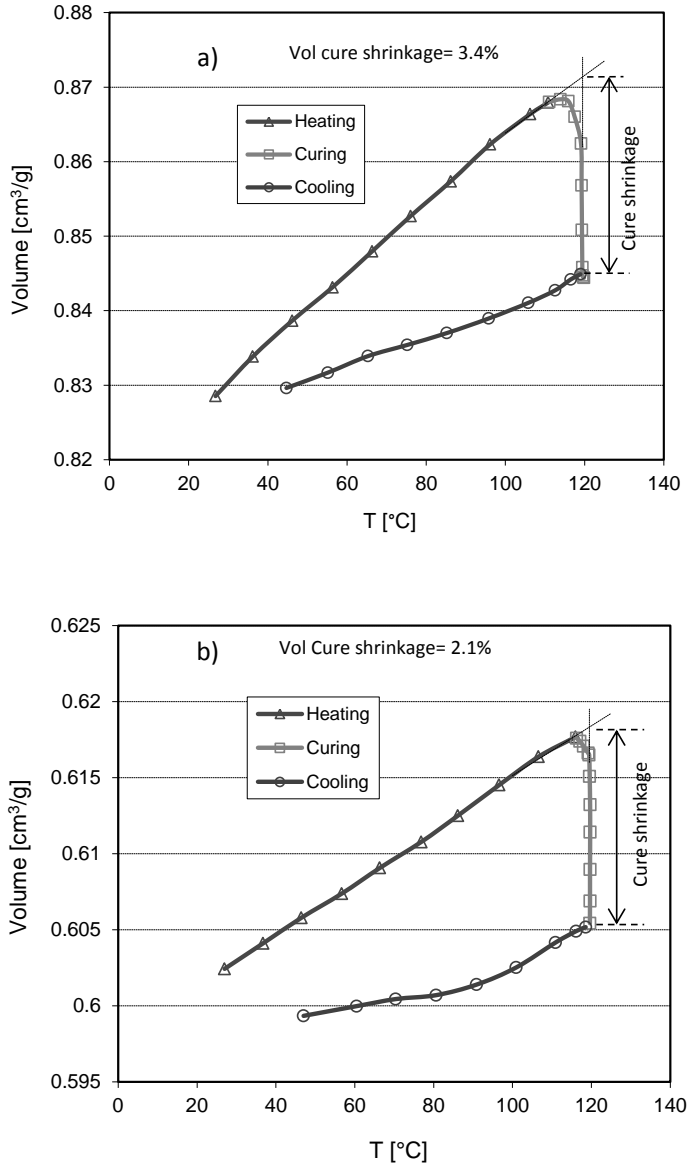


Figure 4-5 Volume changes during heating (5°C/min), cooling and shrinkage during isothermal cure. a): DU, b): DF.

Although molding of microelectronic products is performed at 175°C, in this experiment, a much lower curing temperature (120°C) is applied in order to slow down the reaction. The kinetic study shows that still 100% conversion is obtained for long enough curing at 120°C.

During the heating up stage, the sample already starts to cure in the apparatus before reaching the curing temperature. Therefore the volume changes are then caused by both changes in temperature and actual cure shrinkage. To correct for this, the thermal contribution is estimated by extrapolating the heating curve (full lines in Figure 4-5). The real cure shrinkage is defined as the measured total volume changes minus the thermal expansion contribution.

The total cure shrinkage can be calculated from the difference of the values at the end and starting time of the cure. Due to the filler, the cure shrinkage of the filled material (DF) is less than the unfilled one, DU (2.1 vs. 3.4 vol%).

The cure shrinkage of the DF material can also be calculated assuming the filler as an inert material and that the shrinkage is only caused by the matrix. The calculated value is 1.7 vol% which is reasonably close to the measured one i.e. 2.1 vol%.

Replacing the curing time with conversion (using equation 4-1 and Figure 4-2), the cure shrinkage can be extracted with respect to the conversion, see Figure 4-6. Similar results are observed for the DU sample. Since on a molecular level, the cure shrinkage emerges from the reduction in free volume of monomer units which react to the network, this reduction can be expected to be constant for all reacting units. It is therefore expected that the cure shrinkage is proportional to the conversion. Indeed, Figure 4-6 shows that the cure shrinkage's curves are approximately linear. Deviation at low and high conversion levels emerge because in these regimes the kinetic fits are less accurate.

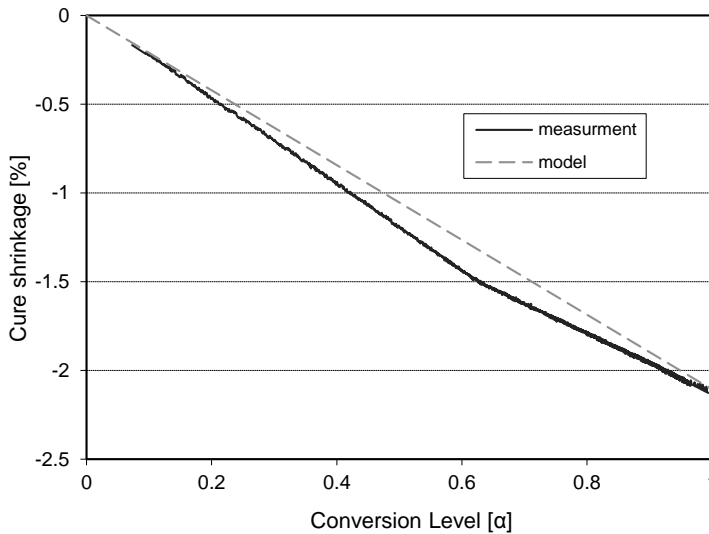


Figure 4-6 Cure shrinkage vs. conversion level for the DF sample. Full lines: PVT measurement, dashed line: linear approximation to equation 4-4.

Since the cure dependent model is not necessary in the interface model of Chapter 6, we neglect these deviations and approximate the cure shrinkage as being linear with conversion, equation 4-4. The result of the model is also shown in Figure 4-6.

$$\varepsilon_v^{cure} = \alpha \gamma_c \quad 4-4$$

Where ε_v^{cure} is the volumetric cure shrinkage and γ_c is the volumetric shrinkage at 100% conversion.

4.2.3 DMA Experiment

4.2.3.1 TEST SETUP

The mechanical properties of the DF material during the curing process were measured with a specially made shear set up [4]. The setup consists of 3mm diameter circular surfaces between which the uncured sample is positioned. The filled samples were gently preheated until they became soft and sticky. Care was taken to avoid

preliminary reaction. The size of the shear surfaces were chosen such that the test was performed in a Dynamic Mechanical Analyzer DMA Q800-TA Instrument. The experiment covers the frequency and temperature range of 0.32-60 Hertz and 20-160°C. Figure 4-7 shows a schematic diagram of the shear tool.

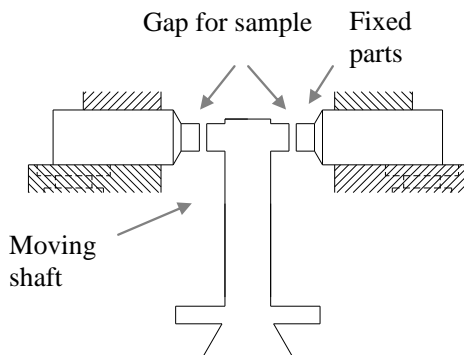


Figure 4-7 Schematic diagram of the shear clamps.

The cure dependent viscoelastic behavior was determined during heating scans of an intermittent cure experiment. As Figure 4-8 shows, in such an experiment the isothermal curing process is interrupted by a quick temperature drop, followed by a heating scan at 2°C/min. The iso-cure heating is done at a temperature where the reaction is still slow. After a short isothermal period the sequence of cooling and reheating is repeated and viscoelastic data is recorded. The reheating scan from below to above $T_g^{tan\delta}$ (after each iso-curing part) is used to determine the glassy and rubbery modulus values as well as the glass transition temperature for each heating ramp. This $T_g^{tan\delta}$ is a measure for the actual cure state after each period of iso-curing. During this heating scan continuous frequency sweeps were performed (0.32-60 Hz, 10 μm amplitude).

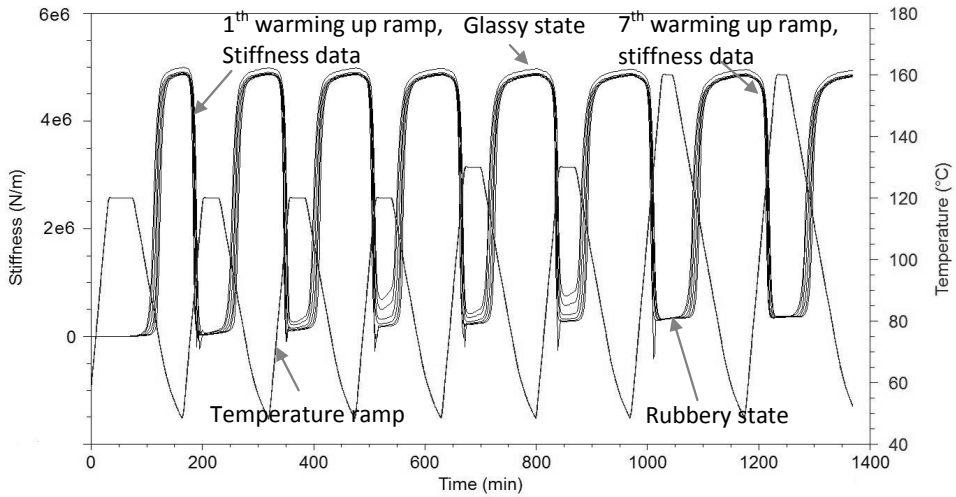


Figure 4-8 Stiffness and temperature profile of the DF sample during the intermittent cure test. The stiffness data is shown for different frequencies ranging from 0.32 to 60HZ. The stiffness curves increase if the temperature drops and decrease during a heating ramp. Each next heating curve is at a higher conversion level.

4.2.3.2 DERIVING THE MODULUS

Deriving the mechanical properties of the curing material through the usage of the shear test set up is not simple, since cured molding compounds are about as stiff as the mechanical frame of most tensile testers which complicates the exact determination of modulus values for the molding compounds. As a result, the apparent measured storage modulus may deviate from the real one. We therefore correct the storage modulus by assuming that the measured deformation consists of the sample plus the frame deformation (Figure 4-9 and equation 4-5).

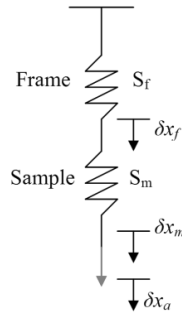


Figure 4-9 Schematic diagram of the frame and sample stiffness.

$$\delta x_a = \delta x_m + \delta x_f \quad 4-5$$

The stiffness was derived by dividing equation 4-5 through the force F . ($1/S = \delta x/F$)

$$\frac{1}{S_a} = \frac{1}{S_m} + \frac{1}{S_f} \quad 4-6$$

Where S_a , S_m , S_f are the apparent, sample and frame stiffnesses respectively. Equation 4-6 can be rearranged for extracting the sample stiffness:

$$S_m = \frac{S_a}{1 - S_a/S_f} \quad 4-7$$

The yet unknown frame stiffness, S_f , is obtained by comparing the measured glassy and rubbery stiffness with separately determined glassy and rubbery shear modulus values. The latter is done by measuring the tensile and the bulk modulus. In glassy and rubbery region the material is elastic and therefore the following relation exists between bulk (K), shear (G) and elongation modulus (E) [6].

$$G = \frac{3KE}{9K - E} \quad 4-8$$

Furthermore, the relation between the measured sample's shear stiffness and the shear storage modulus is:

$$G_m = \frac{S_m}{b_{geo}} \quad 4-9$$

Where, G_m and S_m are the measured sample's shear storage modulus and the sample's shear stiffness respectively. b_{geo} is a geometry factor.

Applying the glassy and rubbery bulk and tensile modulus for the fully cured DF material (Figure 3-3 and Figure 3-4 in Chapter 3) to the equation 4-8, the glassy and rubbery shear modulus were calculated for the fully cured DF material (Table 4-4).

Property	Glassy state	Rubbery state
	50°C	150°C
E [MPa]	7200	102
G [MPa]	2520	37.7
K [GPa]	15.2	4.9

Table 4-4 Elastic moduli at 50°C (glassy values) and 150°C (rubbery), fully cured DF material.

Deriving the sample's stiffness in different heating scans from the apparent one consists of three steps.

- 1- For the last heating scan, the rubbery stiffness of the material is low compared to the frame stiffness. Therefore, the frame stiffness correction (S_f) is small and the b_{geo} is calculated assuming $S_m=S_a$ via equation 4-9 and Table 4-4.
- 2- Using the derived b_{geo} , S_f will be calculated through using Table 4-4, equation 4-7 and equation 4-9, for the fully cured material i.e. the last heating scan.
- 3- Finally the full range of S_m is calculated applying the calculated values of S_a and S_f in equation 4-7.

If the frame stiffness is not corrected, the apparent measured storage modulus will be almost half of the true value in the glassy region. However its effect is small in the rubbery state. Therefore, if the uncorrected values are used to calculate the glassy bulk modulus or Poisson ratio, significant errors may occur.

4.2.3.3 CONSTRUCTION OF TIME-CURE MASTER CURVE

For each heating scan a master curve, related shift factor and glass transition temperature can be derived via the Time-Temperature Superposition principle (TTS). The frequency continuously cycles between 0.32- 60 Hz and the temperature increases at 2°C/min such that each frequency scan takes about one minute. The next step of the analysis process consists of deriving the conversion level at each heating scan. This could be done by applying the $T_g^{tan\delta}$ values of different heating scans (Table 4-5) to the DiBenedetto model, Figure 4-4. Please note that in this Chapter, the maximum in $\tan \delta$ is taken as the criterion for the DMA mechanical glass transition.

Heating ramp	1	2	3	4	5	6	7
$T_g^{tan\delta}$ (°C)	96	107	113	118	124	127	132
Conversion level (α)	0.71	0.81	0.86	0.9	0.94	0.96	1

Table 4-5 $T_g^{tan\delta}$ and conversion level for all heating scans of DF material. DMA intermittent cure test.

Figure 4-4 and Table 4-5 show that there is a difference between the T_g values for the fully cured DF samples in different test methods: 111.2°C for DSC and 132°C for DMA. Such differences are because the glass transition is a kinetic process which takes place in a certain temperature and time range. It therefore depends on both the measurement method and the data evaluation procedure. Therefore, the $T_g^{tan\delta}$ turned out to be about 21°C higher than the T_g^{DSC} used to establish the relation with the conversion. After compensating the difference, the determination of the conversion is done using Figure 4-4.

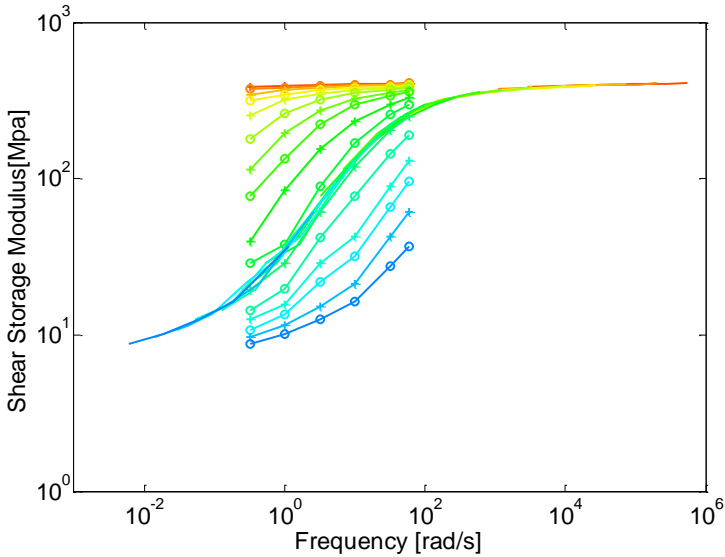


Figure 4-10 Shear storage modulus master curve as a function of frequency for 81% cured material (2th heating scan). Data extracted by analyzing the DMA measurement, $T_{ref} = 110^{\circ}\text{C}$.

Figure 4-10 shows the shear storage modulus vs. frequency for an 81% cured DF material (second heating ramp). The individual lines correspond to the modulus vs. frequency curves at a single temperature. Applying the TTS principle, these curves can be shifted along the frequency axis to form a single master curve. The master curve in the frequency domain can be converted to relaxation modulus in the time domain using appropriate prony series [4, 19-21]. Using the same procedure, different master curves are made for the all heating scans, considering 110°C as the reference temperature. These curves show the typical development of the relaxation modulus with cure (Figure 4-11).

Figure 4-11 shows that in different heating steps the glassy plateaus are identical. However the rubbery plateaus move upwards as cure proceeds. In addition, the curves shift to the right side, i.e. longer time scales, during cure which can be attributed to the

increase of T_g . Therefore we decide to use the T_g as the reference temperature. Figure 4-12 shows that now the master curves almost coincide.

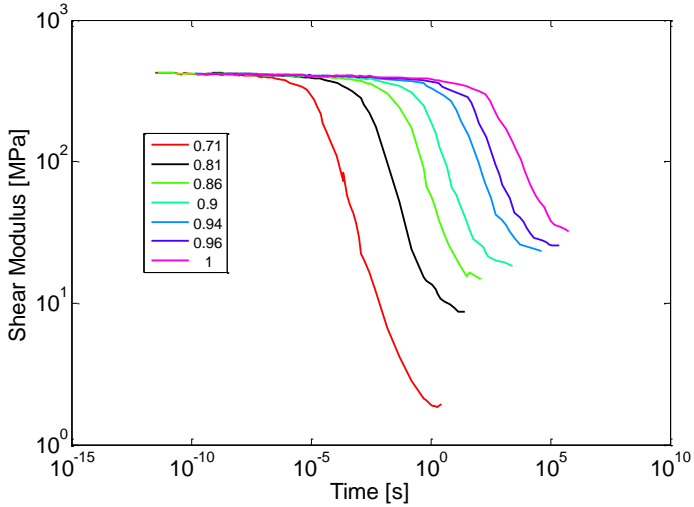


Figure 4-11 Shear relaxation master curve for different heating scan, $T_{ref} = 110^\circ\text{C}$.

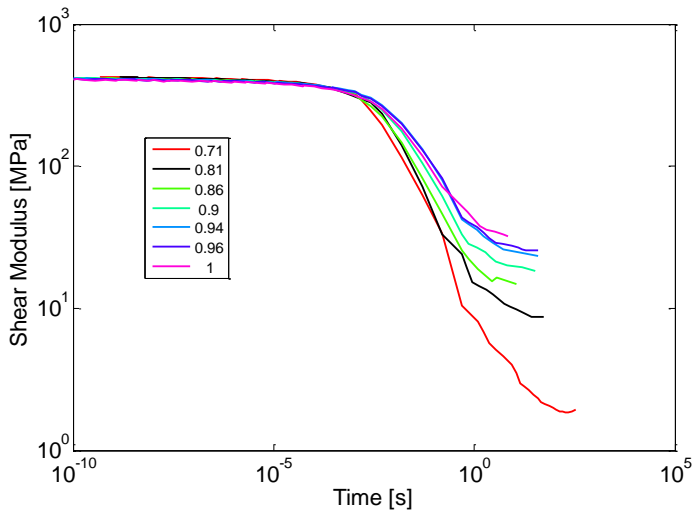


Figure 4-12 Shear relaxation master curves for different heating scans with $T_{ref} = T_g^{\tan\delta}$.

As a next step of data analysis we subtract the rubbery modulus and normalized the master curves as equation 4-10:

$$G_n(t, T) = \frac{G(t, T, \alpha) - G_r(\alpha)}{G_g - G_r(\alpha)} \quad 4-10$$

Here G_n denotes the normalized shear curve, G_g and G_r are the glassy and rubbery shear modulus respectively.

Without further need for adjustments all relaxation curves collapse to a single master curve, Figure 4-13. This temperature- conversion master curve is therefore sufficient to describe all cure dependent viscoelastic behavior.

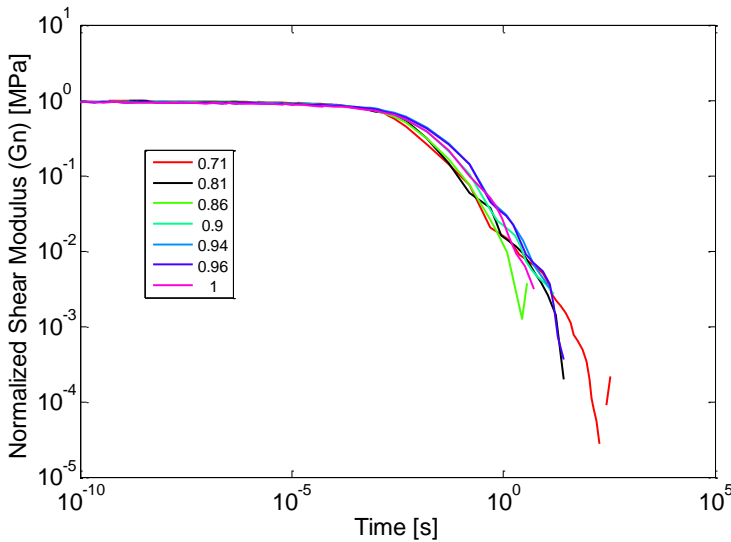


Figure 4-13 Normalized shear modulus master curve with $T_{ref} = T_g^{\tan\delta}$. All relaxation curves collapse to a single master curve.

For each of the intermittent shear master curves in Figure 4-12, there is a corresponding temperature-shift factor, Figure 4-14. It can be seen that the shift factor curves shifted to the right side with increasing the conversion level. Furthermore, close to the glass transition temperature of each of these curves there is a marked change in

slope, which is attributed to a change in relaxation mechanism. Below the switching temperature, T_c , the shift factor follows the Arrhenius behavior (activation energy driven), whereas above this temperature it follows the WLF behavior [22] (free volume mechanism). The first linear parts in Figure 4-14 correspond to the shift factors in the glassy state of each heating scan. Since the modulus variation in this region is not much (Figure 4-10), care should be taken for finding the right shift factor data in this region.

$$\log a_T^{Arrh} = \frac{-H}{2.30R} \left(\frac{1}{T} - \frac{1}{T_0} \right) \quad T \leq T_c \quad 4-11$$

$$\log a_T^{WLF} = \frac{C_1(T - T_{ref})}{C_2 + T - T_{ref}} \quad T \geq T_c \quad 4-12$$

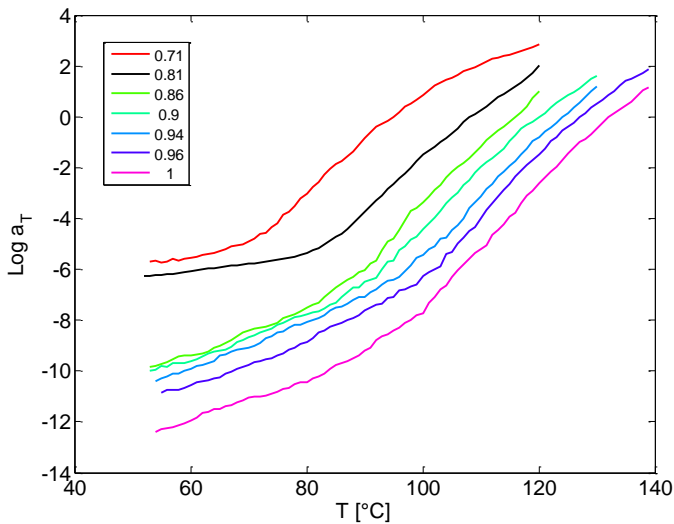


Figure 4-14 Shift factor related to the shear modulus for different heating scans, $T_{ref} = T_g^{tan\delta}$.

If the shift factors were plotted versus $T - T_g^{tan\delta}$, the glass transition regions of all curves collapse onto a single shift factor curve, Figure 4-15.

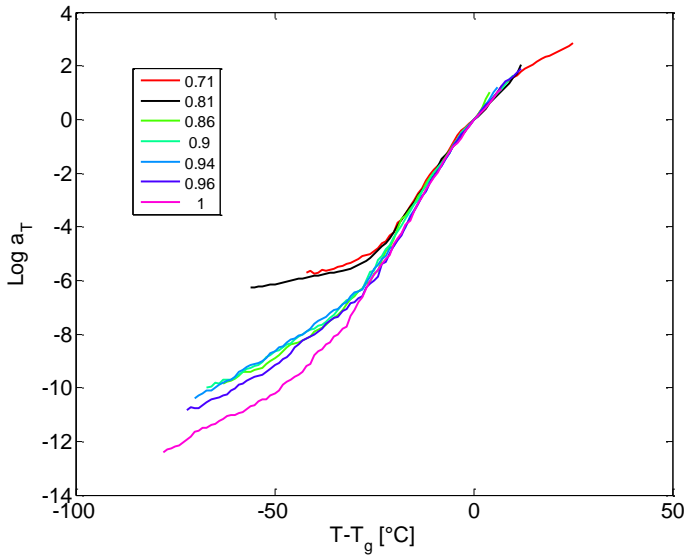


Figure 4-15 Shift factor related to the shear master curves in different heating scans vs.

$$T - T_g^{\tan\delta}, T_{ref} = T_g^{\tan\delta}.$$

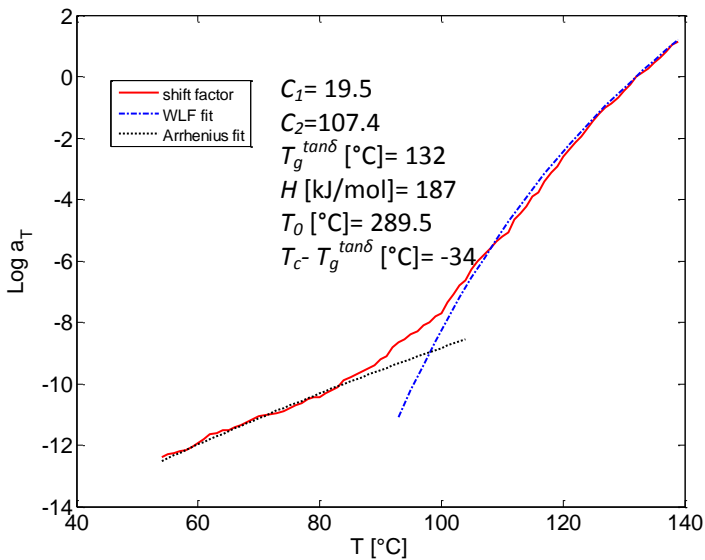


Figure 4-16 Details of Arrhenius and WLF fit to the fully cured shift factor curve, $T_{ref} =$

$$T_g^{\tan\delta}.$$

For the last heating scan, the Arrhenius and WLF models fitted to the shift factor's curve and the corresponding parameters are summarized in Figure 4-16.

4.2.3.4 CURE DEPENDENCY OF ELASTIC PARTS

Figure 4-8 and Figure 4-11 clearly shows that the dependency of the glassy modulus on cure is small and will be neglected here. However the rubbery elastic modulus increases from zero to about 33.2 MPa, starting at the point of gelation. This increase is modeled by Martin & Adolf's scaling law [23], equation 4-13. Figure 4-17 shows that there is good agreement between the experimental data and the model.

$$G_r(\alpha) = G_r^f \left(\frac{\alpha^2 - \alpha_g^2}{\alpha_f^2 - \alpha_g^2} \right)^{8/3} \quad 4-13$$

Here α_f denotes the final conversion (usually 1.0), α_g is the gelpoint and G_r^f is the rubbery modulus at $\alpha = \alpha_f$. Below the gelation point i.e. for $\alpha < \alpha_g$, the rubbery shear modulus vanishes.

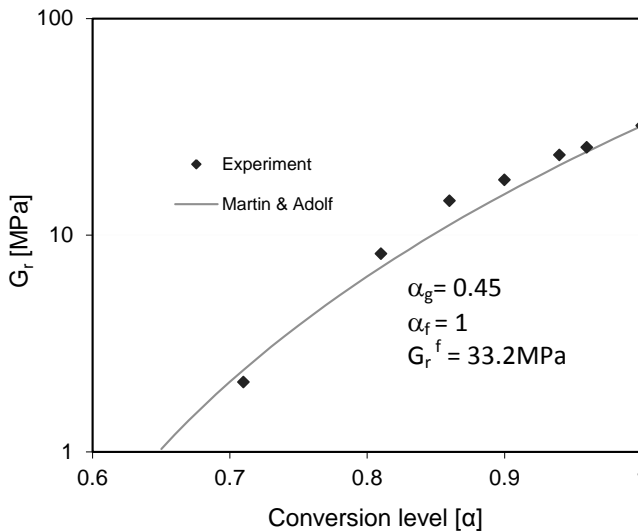


Figure 4-17 Cure dependency of rubbery shear plateau. Full lines are according to the Martin & Adolf theory, equation 4-13.

4.3 Conclusions

In this Chapter the viscoelastic properties of an epoxy molding compound are investigated during the curing period. Using the Differential Scanning Calorimeter and GNOMIX high pressure dilatometer the cure kinetics and cure shrinkage were measured for the DU and DF sample.

Furthermore, the changes in the shear modulus of the DF EMC are investigated during an intermittent cure test with a DMA apparatus. The Time- Temperature superposition principle was applied to all heating steps, the master curves and the related shift factors are extracted. Using these master curves, the $T_g^{tan\delta}$ in all heating scans are measured and the conversion level is calculated. It is shown that partial curing increases the glass transition temperature at each heating scan. This phenomena shifts the master curves to the longer time domain. In addition partial curing increased the rubbery modulus. However the glassy shear modulus turns out to be almost independent of the conversion level. Considering the $T_g^{tan\delta}$ as the reference temperature, the master curves and shift factors (for temperatures above T_c) collapse to a single curve. The normalized form of the master curves which is suitable as the input for the finite element programs is extracted from this curve. Finally, the growth of the rubbery modulus in different conversion level is measured and fitted to the model.

The governed techniques and procedures for material characterization during cure can not only be used for molding compounds but are also well suited to characterize epoxy adhesives and other thermoset materials.

References

- [1] J.S. Nakka, K.M.B. Jansen, L.J. Ernst, effect of epoxy resin chemistry on the viscoelasticity of its cure product, *J. appli. Polym. Scien.*, 108(3) (2008) 1414–1420.
- [2] K.M.B. Jansen, L. Wang, C. van't Hof, L.J. Ernst, H.J.L. Bressers, G.Q. Zhang, Cure temperature and time dependent constitutive modeling of molding compounds, *IEEE 5th EuroSime conference (Brussels, May 2004)*, pp. 581-585.
- [3] K.M.B. Jansen, L. Wang, D.G. Yang, C. van't Hof, L.J. Ernst, H.J.L. Bressers, G.Q. Zhang, Constitutive modeling of molding compounds, *IEEE 54th ECTC conference (Las Vegas, June 2004)*, pp. 890-894.
- [4] J. de Vreugd, The effect of aging on molding compound properties, PhD thesis, Delft, 2011.
- [5] J.S. Nakka, Tailoring of epoxy material properties, PhD thesis, Delft, 2010.
- [6] K.M.B. Jansen, C. Qian, L.J. Ernst, C. Bohm, A. Kessler, H. Preu, M. Stecher, Modelling and characterization of molding compound properties during cure, *J. Microelectron. Reliab.* 49 (2009) 872–876.
- [7] D.G. Yang, L.J. Ernst, C. van't Hof, M.S. Kiasat, J. Bisschop, J. Janssen, F. Kuper, Z.N. Liang, R. Schravendeel, G.Q. Zhang, Vertical die crack stresses of Flip Chip induced in major package assembly processes, *J. Microelectron. Reliab.* 40 (2000) 1533-1538.
- [8] L.J. Ernst, et al, Time- and temperature dependent thermo-mechanical modeling of a packaging molding compound and its effect on packaging process stresses, *J. Electron. Packag.* 125 (2003) 539- 548.
- [9] W.D. van Driel J.H.J. Janssen, G.Q. Zhang, D.G. Yang, L.J. Ernst, Packaging induced die stresses- Effect of chip anisotropy and time-dependent behavior of molding compound, *J. Electron. Packag.* 125 (2003) 520-525
- [10] L.J. Ernst, C. van't Hof, D.G. Yang, M.S. Kiasat, G.Q. Zhang, H.J.L. Bressers, J.F.J. Caers, A.W.J. den Boer, J. Janssen, Mechanical modeling and characterization of the curing process of underfill materials, *J. Electron. Packag.* 124 (2002) 97-105.
- [11] M.S. Kiasat, curing shrinkage and residual stresses in viscoelastic thermosetting resins and composites, PhD thesis, Delft, 2000.

- [12] D.G. Yang, K.M.B. Jansen, L.J. Ernst, G.Q. Zhang, W.D. van Driel, H.J.L. Bressers, J.H.J. Janssen, Numerical modelling of warpage induced in QFN array modelling process, *J. Microelectron. Reliab.* 47(2007) 310-318.
- [13] J. de Vreugd, K.M.B. Jansen, L.J. Ernst, C. Bohm, prediction of cure induced warped of micro-electronic products, *J. Microelectron. Reliab.* 50 (2010) 910-916.
- [14] G. Hu, J.E. Luan, S. Chew, Characterization of chemical cure shrinkage of epoxy molding compound with application to warpage analysis, *J. Electron. Packag.* 131 (2009) 1-6.
- [15] S. Sourour, M.R. Kamal, Differential scanning calorimetry of epoxy cure: isothermal cure kinetics, *Thermochim. Acta.* 14(1) (1976) 41-59.
- [16] A. Turi, Thermal characterization of polymeric materials, second ed., Academic Press, San Diego, 1997.
- [17] T.G. Fox, S. Loshaek, Influence of molecular weight and degree of crosslinking on the specific volume and glass temperature of polymers, *J. Polym. Sci.* 15 (1955) 371-390.
- [18] S.Z.D. Cheng, Handbook of thermal analysis and calorimetry, Vol 3: application to polymers and plastics, Elsevier Science, Amsterdam, 2002.
- [19] S.W. Park, R.A. Schapery, Methods of interconversion between linear viscoelastic material functions. Part I-a numerical method based on Prony series, *Int. J. Solids Struct.* 36(1999) 1653-1675.
- [20] R.A. Schapery, S.W. Park, Methods of interconversion between linear viscoelastic material functions. Part II-an approximate analytical method, *Int. J. Solids Struct.* 36(1999) 1677-1699.
- [21] Y. He, Thermomechanical and Viscoelastic Behavior of a No-Flow Underfill Material for Flip-Chip Applications, *Thermochim. Acta.* 439(2005) 127-134.
- [22] M.L. Williams, R.F. Landel, J.D. Ferry, The temperature dependence of relaxation mechanisms in amorphous polymers and other glass-forming liquids, *J. Am. Chem. Soc.* 77 (1955) 3701-3707.
- [23] D.B. Adolf, J.E. Martin, calculation of stresses in crosslinking polymers, *J. Compos. Mater.* 30(1996) 13-34.

Chapter 5

Developing the harsh environment testing setup

5.1 Introduction

Microelectronic devices consist of a combination of highly dissimilar materials. The devices are fabricated and cured at high temperature and subsequently cooled down to room temperature. Due to the differences in thermo-mechanical properties of the components, interfacial delamination related failures are among the major reliability issues [1-4]. Delamination will decrease the reliability of microelectronic packages. Therefore establishing the critical fracture properties of the interfaces is desired.

The interface properties are highly dependent to the temperature and moisture. The interface strength of electronic chips is also affected by the generated steam during the soldering reflow in the microelectronic assembly process. Here the temperature reaches above 200°C for a short period of time which generates the pressurized steam in the EMC and interfaces due to the trapped water, see Figure 5-1. The generated steam had two major effects on the delamination properties which are summarized as:

1. Effect of temperature and moisture on the interfacial bonding
2. Additional crack driving force in the interface

Based on:

M. Sadeghinia, K.M.B. Jansen, L.J. Ernst and H. Pape. Mechanical characterization of epoxy molding compound in pressurized steam. International Journal of Adhesion and Adhesives. 40: 103-107, 2013.

In the soldering reflow process, the effects of above two factors are coupled together. However applying a hydrostatic pressurized steam around the sample will fully compensate the additional steam pressure effect due to the trapped water, see Figure 5-2. As a result, the effect of temperature and steam on the interfacial bonding will only be considered. This emerges the principle idea of designing a Pressure Vessel (PV) testing setup.

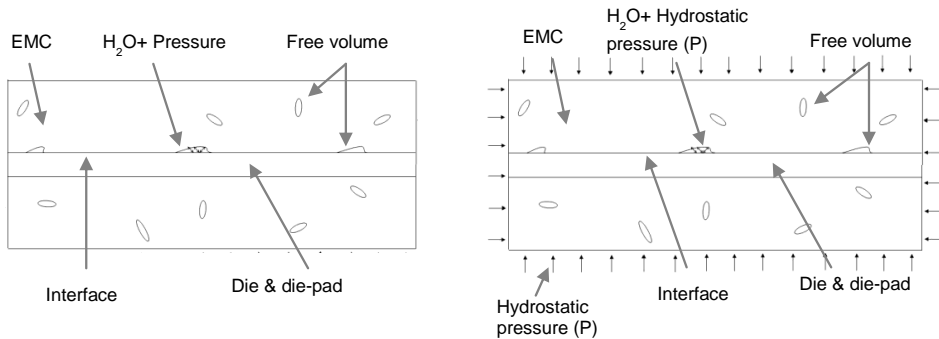


Figure 5-1 Effect of high temperature and moisture on the interfacial bonding **Figure 5-2** Effect of hydrostatic pressurized steam on the interfacial bonding

This Chapter focuses on the development of a pressurized steam chamber (Pressure Vessel) with a highly accurate tensile setup. The designed and developed chamber accompanied with its mixed mode bending setup will be used in Chapter 6 for establishing the critical interfacial fracture properties of copper- molding compound interfaces in pressurized steam condition.

The developed instrument is also capable for establishing the steam effect on the thermo-mechanical properties of the molding compounds. Therefore, in this Chapter, the functionality and performance of the setup is assessed measuring the viscoelastic creep compliance of an EMC in dry condition and comparing that with creep measurements using a commercial Dynamic Mechanical Analyzer. Applying the Time–Temperature Superposition principle, the viscoelastic creep compliance master curves and related shift factors are extracted and compared. As the next step, the mechanical

properties of the EMC (creep compliance, T_g and corresponding shift factor) are determined for the pressurized steam environment and the effect of the moisture is quantified.

5.2 Design of the setup

A special steam chamber is developed in order to investigate the interfacial delamination of microelectronic packages in pressurized steam. This property will be considered in Chapter 6. The instrument is also useful for measuring the viscoelastic properties of the EMC in steam at elevated pressure. The simplified schematic diagram of this setup is shown in Figure 5-3. The steam chamber with tensile setup initially contains 0.5 liter water. This water partly converts to steam while heating up the setup. The initial air in the system is removed by a pressure release valve in top of the vessel (X in Figure 5-3) such that the chamber always contains water vapor at 100% humidity. For temperatures above 100°C this corresponds to a higher pressure, a relation which is known from standard thermodynamics [5].

The designed and developed pressure vessel consists of a thick walled steel housing and a loading section. The loading section includes a 3 point bending set up (I, J), force transducer (N) and displacement measurement part. (B, U in Figure 5-3). 3 point bending has been selected in this experiment since the load transducer (N) is designed for relatively low forces, up to 2N.

The moving setup consists of a controllable micrometer (B), a step motor with holding fixture (A) and a shaft (W). The controllable micrometer is positioned on top (=outside) of the vessel in the relatively cool area and is driven by a programmable stepping motor. The movable shaft enters the upper flange plate through a hole with appropriate pressure seal. The upper side of the shaft is clamped by the guiding fixture, moving the shaft vertically. The movement of the shaft is captured by the displacement transducer (Laser sensor, 2820 KEYENCE Co.) mounted outside of the vessel.

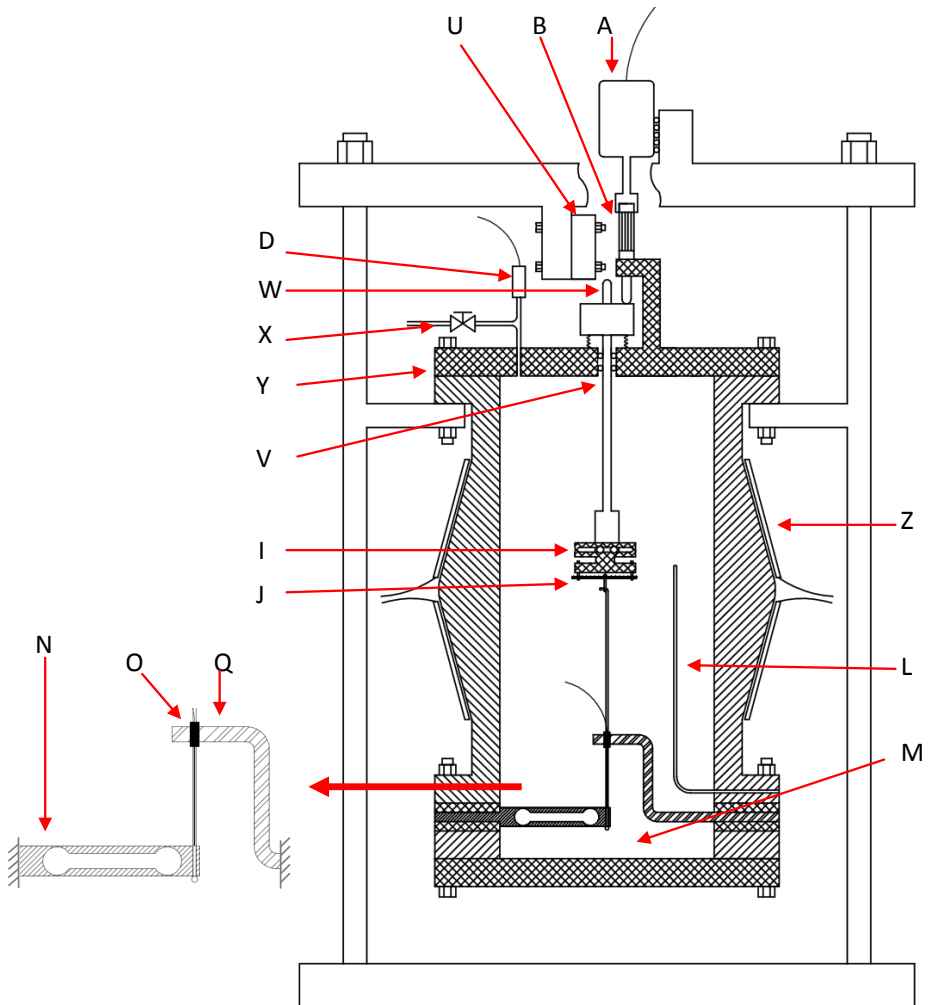


Figure 5-3 Schematic drawing of Pressure Vessel apparatus (not to scale). A: programmable stepping motor with guiding fixture, B: controllable micrometer, U: displacement transducer (laser sensor), D: pressure transducer, W: shaft, X: pressure release valve, Y: top flange, V: pressure seal, I and J: 3 Point Bending setup (3PB) with sample, Z: heating elements, L: thermocouple, M: water reservoir, N: force transducer (load cell), O: DVRT, Q: DVRT holding fixture.

As Figure 5-3 shows, the 3PB setup along with the sample is positioned at the lower part of the movable shaft. The 3PB setup can be used for specimen with various

dimensions. It is also possible to replace it with a Mixed Mode Bending setup for doing delamination measurements [6, 7].

A rigid rod connects the sample to the load cell positioned on the lower flange plate inside the vessel. The load cell consists of a hollow beam (N) of which the deflection is measured using a Differential Variable Reluctance Transducer (O in Figure 5-3, type: M-DVRT-1.5 mm, high resolution, Microstrain Co.). This DVRT is especially chosen for this application as it can operate at temperatures up to 170°C in humid environments, while strain gauges are unreliable under these extreme conditions.

For a 3PB experiment the sample is loaded by moving the shaft upwards. The applied load and displacement of the load cell are monitored by recording the voltage differences of the DVRT. These voltages are converted to load and displacement of the DVRT using a calibration curve. The calibration data is obtained by applying known loads and displacements to the load cell at different temperatures, ranging from 100-180°C. An example of such a calibration curve is given in Figure 5-4. The force and displacement calibration factors turn out to be 1.13 N/Volt and 0.406 mm/Volt (at 130°C) and are slightly temperature depended (Figure 5-5). Calibration curves in wet conditions were also performed at two temperatures (120°C and 135°C). The results are included in Figure 5-5 as the open circles and show that the calibration constants are not affected by moisture.

The load cell is designed for relatively low forces (up to 2 newton). Therefore the beam of the load cell has a non-negligible displacement which must be accounted for. The displacement of the sample is defined as the difference between the shaft and load cell displacement.

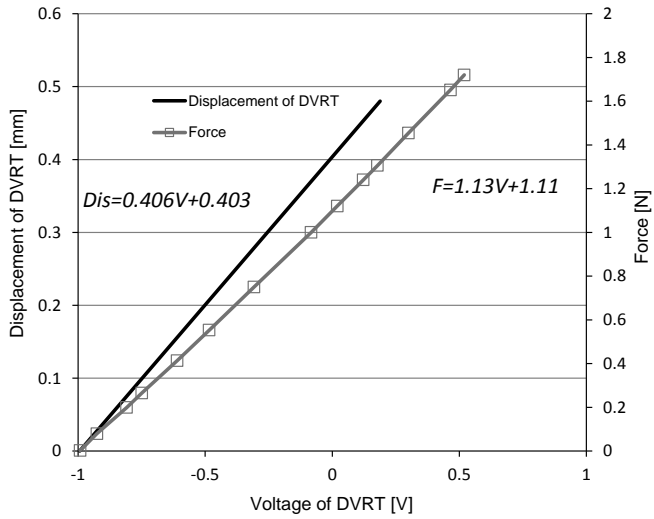


Figure 5-4 Force and displacement calibration data for the load cell at 130°C, dry condition. Symbols: measured data, full line: linear approximation. The full scopes of temperature and testing environment are plotted in Figure 5-5.

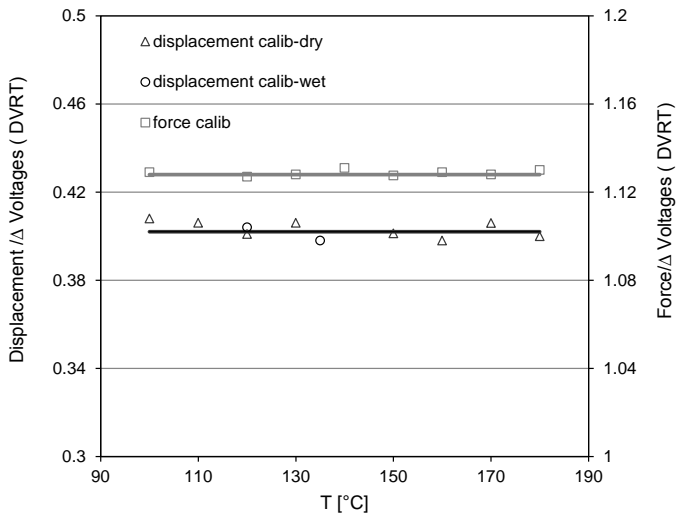


Figure 5-5 Force and displacement calibration data for the load cell at different temperatures in dry and wet environment. Symbols: measured data, full line: linear approximation.

The chamber of the pressure vessel includes three parts: top, middle and bottom. The lower section contains the water reservoir and is made from a bolted flange with flange plate. This section also comprises the load cell and DVRT. The middle section has two removable glass windows for sample mounting and observation. Condensation of steam on the glass windows is effectively prevented by a thin coating (Rain-x, Anti-rain, Shell Car Care International Ltd.) and by external heating of the windows using a hot air blower. Furthermore, this section is equipped with heating elements (6000W, WATLOW Co.) and thermocouple (Z and L in Figure 5-3). The top part is made up from a bolted flange with flange plate on which the motion part with laser sensor is installed. This section also entails the pressure transducer (0-10 bar, WIKA Co.) measuring the inside steam pressure. All signals are analyzed using a dedicated Lab View program.

5.3 Experiments

5.3.1 Material

A commercial epoxy molding compound (MP8000, Nitto Co.) is studied in this Chapter, labeled here as NX. This material was selected such that it remains in its viscoelastic range under the pressurized steam conditions, studied here. It was molded into strips of $38 \times 5 \times 2 \text{ mm}^3$ by NXP Semiconductor Co., Nijmegen. It contains about 75% silica filler particles and has a glass transition temperature of about 160°C .

The thermo-mechanical properties of the IF sample in pressurized steam condition will also be extracted in the same procedure. Since the interface samples are fabricated by the IF EMC on copper lead frames, the thermo-mechanical properties of this molding compound is required for the input of FEM model and will be discussed in details in Chapter 6.

5.3.2 Mechanical properties in dry environment

As a start, the newly constructed apparatus was tested by doing creep measurements in dry condition. The extracted mechanical properties are then compared to the creep data obtained from a commercial apparatus (Dynamic Mechanical Analyzer, DMA Q800,

TA Instruments Co.) in 3 point bending mode with a sample of size $20 \times 2 \times 0.5 \text{ mm}^3$. The experiments cover the temperature range of $100\text{--}190^\circ\text{C}$. The compliance versus time graphs of both measurements are plotted in Figure 5-6 and Figure 5-7.

Time–temperature superposition (TTS) [8] was applied for both sets of measurements. The creep compliance master curves were constructed by horizontal shifting of the compliance curves on the logarithmic time scale by a shift factor a_T , using $T = 160^\circ\text{C}$ as the reference temperature. The reduced time is defined as the creep time multiplied by a shift factor a_T , i.e. $t_{red} = a_T t$. The respective values for the shift functions are shown in Figure 5-8. At higher temperatures the curves could be fitted to the so-called WLF-equation [9], equation 3-13, whereas below the so-called switching temperature, T_C , an Arrhenius model was used [10], equation 3-12. The extracted fitting parameters are shown in Figure 5-8.

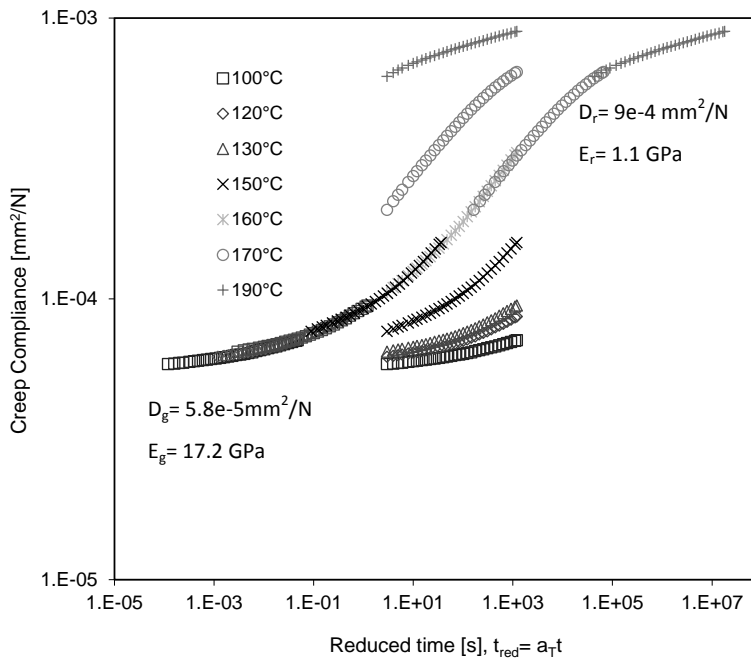


Figure 5-6 DMA measurement of the 3PB creep compliance of the EMC sample along with the corresponding master curve at dry environment. Symbols: measured data at different temperatures. $T_{ref} = 160^\circ\text{C}$.

Figure 5-6 (DMA) and Figure 5-7 (PV) show there is a relatively small difference in glassy and rubbery elastic modulus values. In the viscoelastic region the compliance continuously increased. The obtained master curves appear to be almost identical in the viscoelastic region. The deviation in the glassy and rubbery regions are 1.1 and 0.3 GPa respectively which are relatively small and can be considered as the measurement errors.

Due to the compliance deviation in the glassy state, small differences in the corresponding shift factors are also observed. However above the switching temperature, the shift factor curves are almost identical. (Figure 5-8)

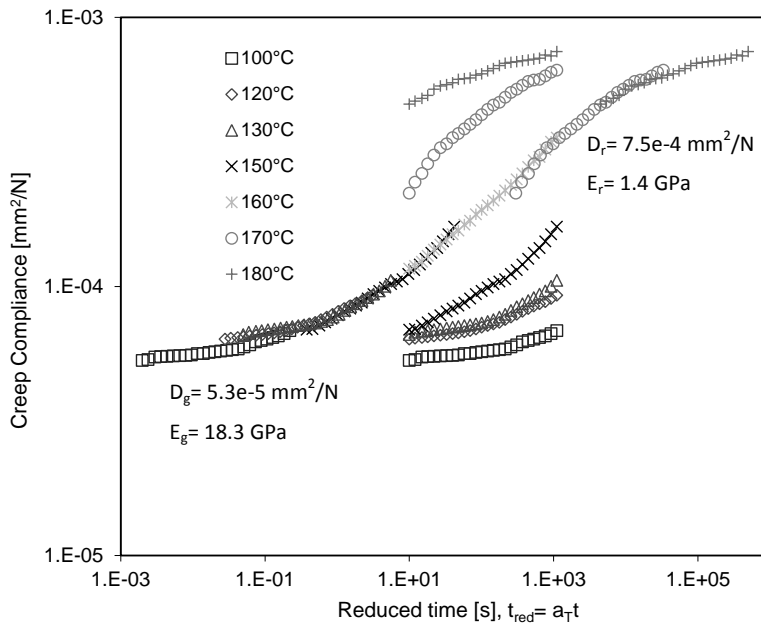


Figure 5-7 Pressure vessel measurement of the 3PB creep compliance of the EMC sample along with the corresponding master curve at dry environment. Symbols: measured data at different temperatures. $T_{ref} = 160^\circ\text{C}$.

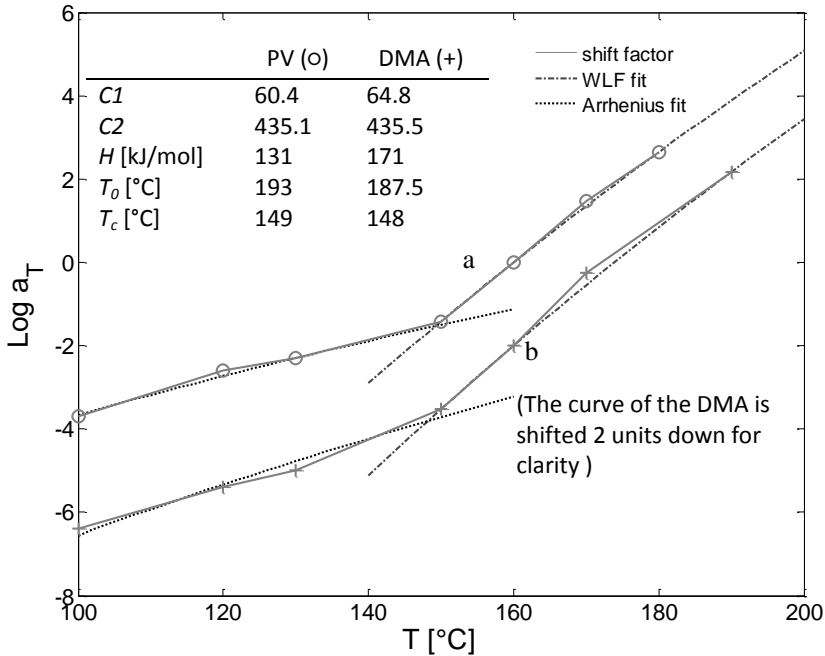


Figure 5-8 Full line: shift factors corresponding to the master curves of Figure 5-6 and Figure 5-7. Dash lines: WLF and Arrhenius model along with fitting parameter. Symbols: measurement data, $T_{ref} = 160^{\circ}\text{C}$. Curve a and b refer to the pressure vessel and DMA results, respectively. The curve of the DMA is shifted two units down for clarity.

A separate independent heating scan (not shown) was performed on the DMA at 1 Hz on an EMC sample (size of $22.6 \times 2 \times 0.5 \text{ mm}^3$) to have a better access to the glassy and rubbery plateaus values and to establish the glass transition temperature. This resulted in an tensile glassy modulus of 18 GPa and a rubbery modulus of 1 GPa. The T_g^E was also determined as 162°C .

5.3.3 Creep under high pressure steam condition

The viscoelastic creep compliance of the EMC in wet condition was measured using the 3PB set up in the pressure vessel. The sample is placed in the setup and connected

to the load cell via the lower shaft. The glass window is closed and securely tightened. The temperature of the test section (and water/ steam mixture) is set to the required value.

During the heating up procedure the air/steam mixture was vented through the pressure release valve in top of the vessel. After some hold time at the set temperature the remaining air can be neglected and the release valve is closed. It takes about 1 hour to reach the required temperature with steam inside the chamber. Afterwards, a hold time of 3 hours is programmed for the moisture to diffuse in the EMC.

The measured creep compliances are plotted in Figure 5-9. Applying the time-temperature superposing principle, the related master curve and shift factors are also extracted assuming $T_{ref}= 120^{\circ}\text{C}$, Figure 5-9 and Figure 5-10.

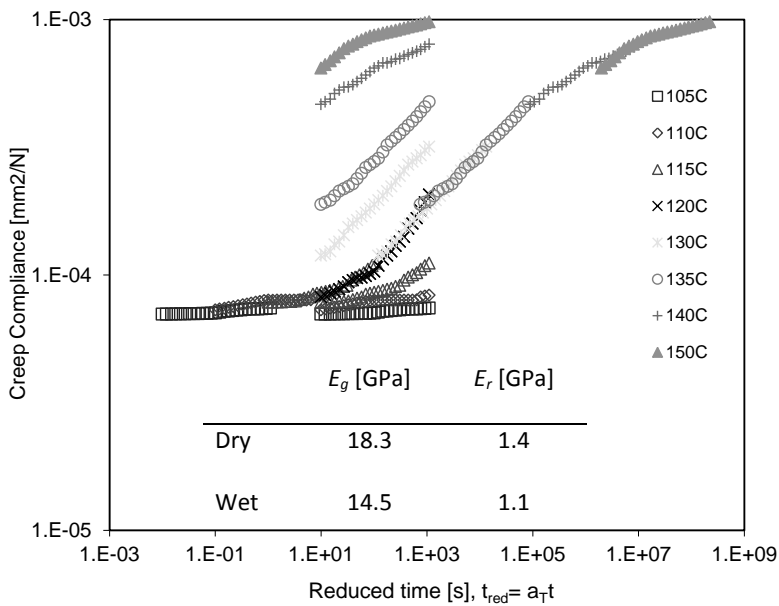


Figure 5-9 EMC creep compliance in wet environment, master curve via TTS principle, $T_{ref}= 120^{\circ}\text{C}$.

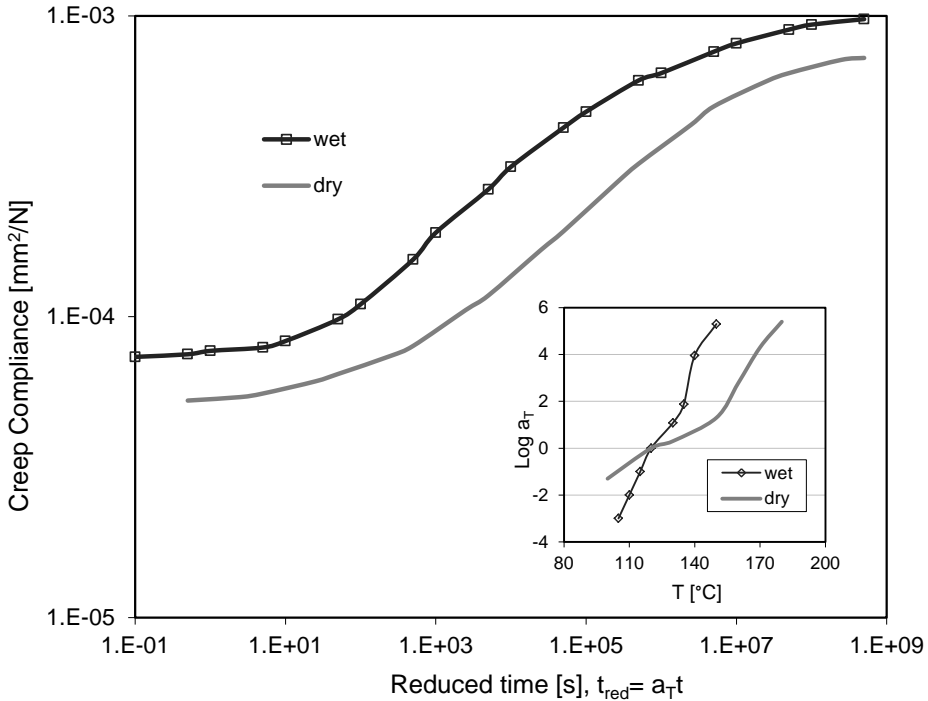


Figure 5-10 Creep compliance master curve in dry and wet environment along with the corresponding shift factor, $T_{ref}=120^{\circ}\text{C}$.

It is known that the process of moisture absorption in polymers is accompanied by swelling which is always associated with changes in the mechanical properties.

As Figure 5-10 shows the absorbed water decreases the glassy and rubbery elastic moduli by almost 20%. In addition water absorption speeded up the relaxation process. The shapes of the master curves seem to be almost identical in both environments. However the creep occurred almost 40 times faster in moisturized condition and the master curve shifted to a shorter time scale. This phenomenon can be attributed to the T_g decrease in wet conditions.

The T_g in the creep measurement can be estimated assuming a cross plot of creep compliance vs. temperature (based on Figure 5-7 and Figure 5-9). To avoid the measurement starting effect, 100 seconds was chosen for cross plotting. This time was

selected such that the material is almost in the middle of its viscoelastic range in different temperatures.

The extracted compliances are plotted in Figure 5-11. The glass transition temperature for the creep measurements ($T_g^{creep, 100s}$) is defined here as the temperature with the threshold value of the glassy compliance being increased by a factor 3. The obtained values for T_g are then 158°C and 130°C for dry and wet condition, respectively. The dry value is close to that obtained from the DMA measurement (162°C, section 5.2.2 of Chapter 5), whereas the wet glass transition is found to be about 30°C lower.

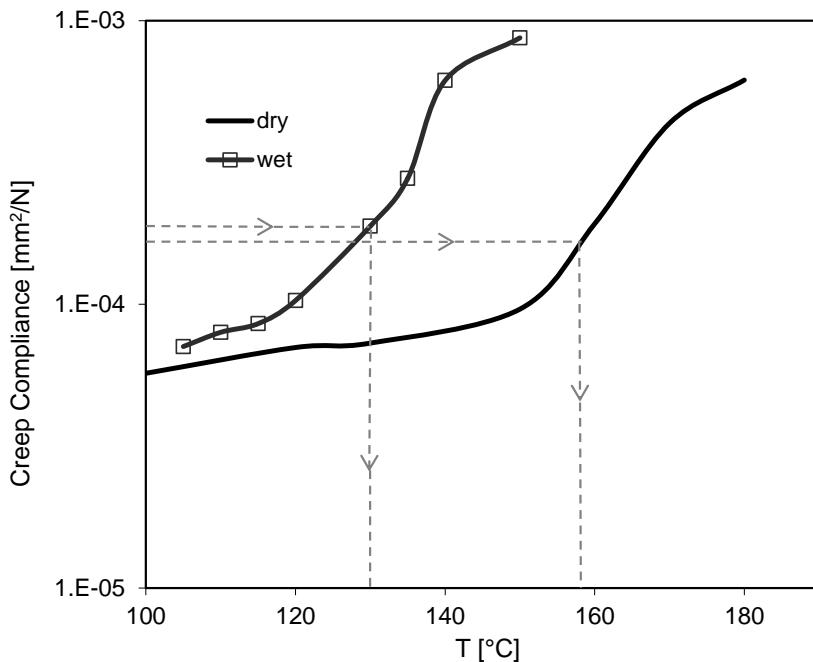


Figure 5-11 Pressure vessel measurements for the creep compliance vs. temperature. Data is extracted from the cross plot of creep compliance vs. temperature at 100 seconds, based on Figure 5-7 and Figure 5-9. The obtained dry and wet glass transition temperatures are 158°C and 130°C, respectively.

The creep compliance master curves are reproduced assuming the $T_g^{creep, 100s}$ as the reference temperature. Firstly, the wet measured compliance data moved with a constant vertically shift factor of 0.82. Afterwards the Time-Temperature Superposition principle is applied for the dry and wet data and the new master curves are extracted using $T_{ref} = T_g^{creep, 100s}$. Figure 5-12 illustrates that now the master curves overlap each other very well.

For each of the compliance master curves in Figure 5-12 there is a corresponding temperature-shift factor graph. If the shift factors are plotted versus $T - T_g^{creep, 100s}$, it turns out that the horizontal shift factor values are similar in the viscoelastic temperature range ($T - T_g^{creep, 100s}$ of $-15\text{ }^\circ\text{C}$ to $5\text{ }^\circ\text{C}$) but deviate in both the rubbery and glassy range.

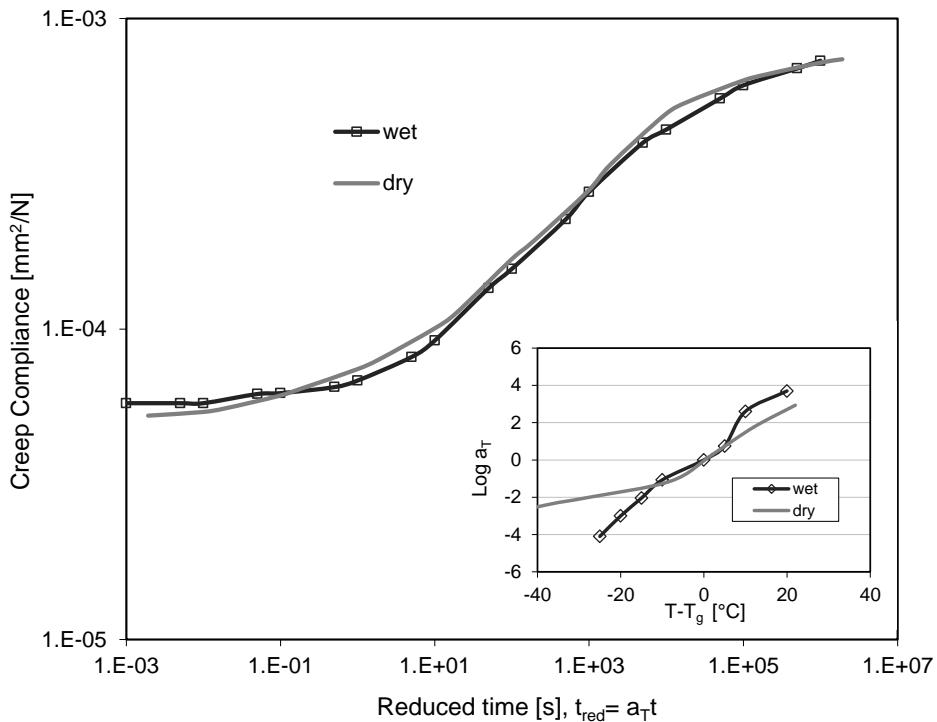


Figure 5-12 Creep compliance master curves for $T_{ref} = T_g^{creep, 100s}$ along with the shift factor. Full lines: dry, line with symbols: wet.

5.4 Conclusions

In this Chapter the thermo-mechanical properties of an Epoxy molding compound in harsh environment is investigated. A special steam chamber with a highly accurate tensile setup is designed. The performance of the set up in dry condition is verified measuring the creep compliance of the EMC sample. Furthermore, the viscoelastic creep compliance of the EMC in wet environment was extracted and it was observed that steam considerably changes the EMC's mechanical properties. Moisture decreased the elastic glassy and rubbery modulus by almost 20%. In addition the glass transition temperature is decreased by almost 30°C. Applying the time–temperature superposition principle, the master curves were extracted for dry and wet environment and it is shown that moisture shifts the compliance master curve to the shorter time domain. The dry and wet master curves coincide if the glass transition temperature is taken as the reference temperature.

References

- [1] G.Q. Zhang, W.D. van Driel, X.J. Fan, *Mechanics of Microelectronics*, Springer, Dordrecht, Netherlands, 2006.
- [2] O. van der Sluis, R.A.B. Engelen, R.B.R. van Silfhout, W.D. van Driel, M.A.J. van Gils, Vertical die crack stresses of Flip Chip induced in major package assembly processes, *J. Microelectron. Reliab.* 47 (2007) 1975-1982.
- [3] W.D. van Driel, M.A.J. van Gils, R.B.R. van Silfhout, G.Q. Zhang, Prediction of delamination related IC and packaging reliability problems, *J. Microelectron. Reliab.* 45 (2005) 1633-1638.
- [4] L.J. Ernst, C. van't Hof, D.G. Yang, M.S. Kiasat, G.Q. Zhang, H.J.L. Bressers, J.F.J. Caers, A.W.J. den Boer, J. Janssen, Mechanical modeling and characterization of the curing process of underfill materials, *J. Electron. Packag.* 124 (2002) 97-105.
- [5] S. Doty, W.C. Turner, *Energy Management Handbook*, seventh ed., Fairmont Press, Lilburn, GA, 2009.
- [6] J.R. Reeder, J.R. Crews, Mixed Mode Bending method for delamination testing, *J. AIAA*, 28: No.7 (1990) 1270-1276.
- [7] ASTM D 6671-01, Standard Test Method for Mixed Mode I—Mode II Interlaminar Fracture Toughness of Unidirectional Fiber Reinforced Polymer Matrix Composites, Annual Book of ASTM Standards, Vol. 15.03, American Society for Testing and Materials, West Conshohocken, PA, 2001.
- [8] J.D. Ferry, *Viscoelastic Properties of Polymers*, 3rd ed., Wiley, New York, 1980.
- [9] M.L. Williams, R.F. Landel, J.D. Ferry, The temperature dependence of relaxation mechanisms in amorphous polymers and other glass-forming liquids, *J. Am. Chem. Soc.* 77 (1955) 3701–3707.
- [10] A.D. McNaught, A. Wilkinson, *Compendium of Chemical Terminology*, second ed., IUPAC Blackwell Scientific, Oxford, 1997.

Chapter 6

Interfacial fracture properties in pressurized steam condition

6.1 Introduction

Due to the fact that microelectronics is made up from various materials with highly dissimilar thermo-mechanical properties, generally the interface between two adjacent materials is the place where delamination related failure most likely would occur. Failure of these interfaces induces decreased reliability and performance of microelectronic components [1-4]. Therefore, adequate knowledge of delamination prediction is desirable.

The interface properties are dependent on various factors. The temperature and stress state effects have been subjected by some studies [5-8]. Furthermore, several research projects have recently been conducted for establishing the critical interfacial fracture properties of electronic packages in the Mechanics of Materials Group at Delft University of Technology. Xiao [9] developed a test method for establishing the delamination toughness of interfaces between epoxy molding compound and copper

Based on:

M. Sadeghinia, K.M.B. Jansen, L.J. Ernst, H. Pape, I. Maus, W.D. van Driel and G.Q. Zhang. Interfacial Fracture Properties of Cu-EMC interfaces in pressurized steam, Submitted.

lead frame. Moreover, Schlottig [10] designed a modified mixed mode Chisel setup and described the interfacial delamination in silicon die from molding compound.

In the cases that moisture sensitivity was included in these studies the highest temperature was always limited below 85°C. However in the soldering reflow process, steam will be generated in microelectronic devices (due to the trapped water in EMC and in interface voids) which will initiate pop-corning and damage in the interfaces.

Therefore in the present Chapter the critical fracture properties of the EMC-Copper lead frame interfaces at pressure cooker conditions, temperature above 100°C and 100%RH, will be investigated. The experimental setup, i.e. the pressure vessel, as designed for this purpose was previously reported in Chapter 5 and [11-13]. In the present work the critical fracture properties are obtained by interpreting the experimental results through dedicated finite element modeling.

The interface samples studied in this Chapter consists of the IF molding compound on copper lead frames. The interfacial crack length is required for the interpretation of the measurement results through FEM-fracture mechanics simulation. Therefore during testing the crack length is captured using a CCD camera. In order to establish the interfacial toughness accurately, the influence of the residual stress in the sample is considered. Furthermore, the effect of the mode mixity and temperature level will also be investigated.

6.2 Material characterization

The interface samples used in this study are a combination of the IF commercial epoxy molding compound (EMC) on a standard copper lead frame, fabricated by Infineon Technologies AG. It is well known that the successful prediction of delamination highly depends on the reliability of the material model used in the calculations. Furthermore, an accurate material model is necessary to calculate the initial stresses and warpage in a package during the cooling down procedure from the molding temperature.

6.2.1 Dry condition

6.2.1.1 CTE AND BULK MODULUS

The procedure of characterization the thermo-mechanical properties of the EMC in dry condition were the subject of our previous studies and discussed in details in Chapter 3. For the present IF EMC, the coefficient of thermal expansion and bulk modulus have been measured using a high pressure dilatometer- PVT apparatus. For these measurements, the sample pressure and temperature were stepwise increased and the corresponding volume changes were recorded. The extracted CTE and bulk modulus are shown in Figure 6-1.

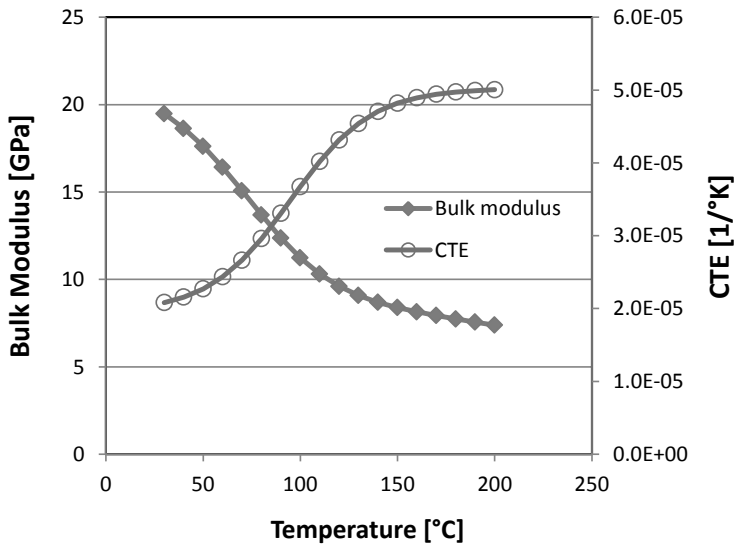


Figure 6-1 CTE and bulk modulus of the dried IF EMC in different temperatures. Data are measured by PVT apparatus.

Figure 6-1 shows that the calculated CTE increases by temperature with a clear change around T_g , while the bulk modulus decreases from 19.5 GPa at 30°C to 7.5 GPa at 200°C. The CTE data is implemented in ABAQUS by making use of user-subroutines, while the temperature dependent bulk modulus is directly added to the model. Here it

should be noted that as a realistic approximation the time dependency of the bulk modulus is assumed to be negligible [14-16].

6.2.1.2 RELAXATION TENSILE AND SHEAR MODULUS

The relaxation tensile modulus of the IF sample has been measured by the Dynamic Mechanical Analyzer, TA instrument Q800, in 3 Point Bending Mode. In relaxation experiment, a constant displacement is applied to the sample and the corresponding force is measured during the time period [17]. The sample had the dimension of $24.2 \times 4.6 \times 0.5 \text{ mm}^3$. The experiments covered the temperature range of 80-180°C. The scan results are presented in Figure 6-2. It turns out that the glassy and rubbery tensile modulus are around 21.5 and 0.5 GPa respectively.

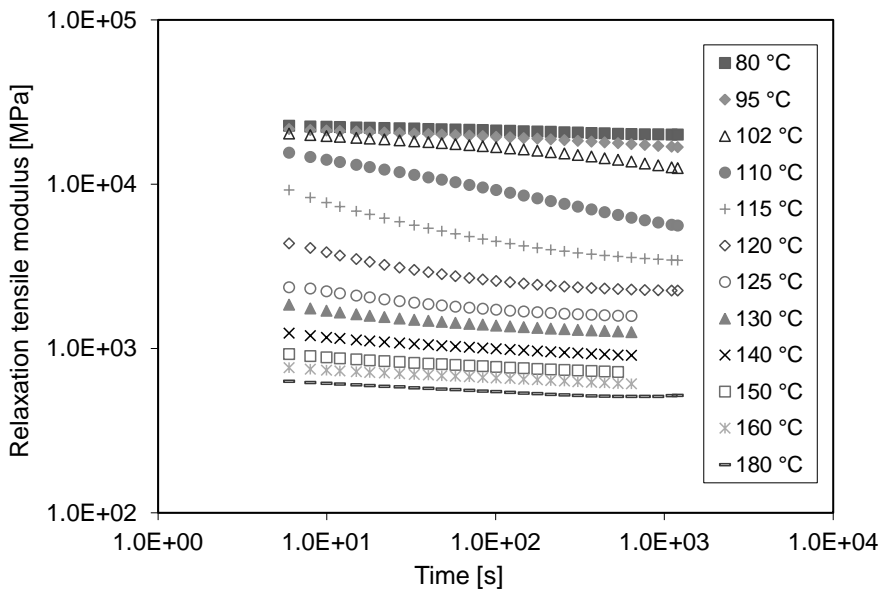


Figure 6-2 Relaxation tensile modulus of the IF sample at different temperatures. The modulus is continuously decreasing by time at different temperatures.

The viscoelastic properties are implemented in FEM-ABAQUS via the relaxation shear modulus master curve. This property is calculated from the bulk and tensile modulus using the following approximation formula [18], equation 6-1:

$$G(T, t) \approx \frac{3.K(T).E(T, t)}{9.K(T) - E(T, t)} \quad 6-1$$

Where $K(T)$ is the temperature dependent bulk modulus. $G(T, t)$ and $E(T, t)$ are the time and temperature dependent shear and tensile modulus respectively. The relaxation shear modulus master curve and corresponding shift factors are also constructed by applying the time–temperature superposition (TTS) principle, considering $T = 110^\circ\text{C}$ as the reference temperature, see Figure 6-3. As discussed in Chapter 3, below the switching temperature, T_c , the shift factor follows the Arrhenius behavior, whereas above this temperature it follows the WLF function. The corresponding parameters related to the established shift factor are summarized in Table 6-1. The shift factor data is implemented in ABAQUS by making use of user-subroutines.

Material	C_1	C_2	H [kJ/mol]	T_0 [°C]	T_c [°C]
IF	24.1	72.9	187	135	104.6

Table 6-1 WLF and Arrhenius fit parameters for temperature shift factors, corresponding to IF sample. $T_{ref} = 110^\circ\text{C}$.

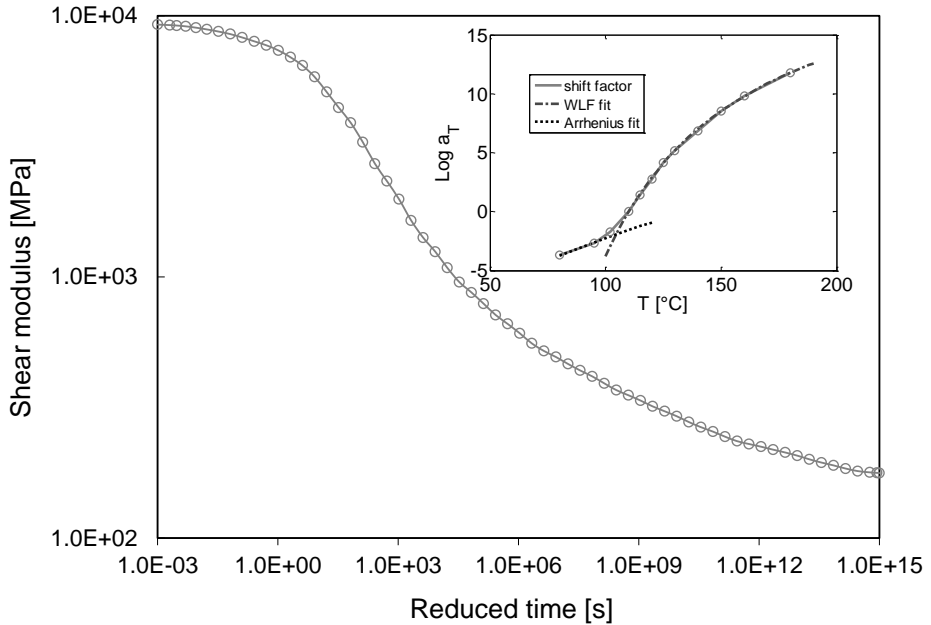


Figure 6-3 Master curve of the relaxation shear modulus of IF sample vs. reduced time along with the corresponding shift factors, $T_{ref} = 110^{\circ}\text{C}$. Results are extracted via implementing Figure 6-2 in equation 6-1.

A separate independent heating scan (Figure 6-4) was also performed on the DMA at 1 Hz on an IF EMC (size of $21.1 \times 2.1 \times 0.45 \text{ mm}^3$) to have a better access to the glassy and rubbery plateaus values and to establish the glass transition temperature. This resulted in a longitudinal storage glassy and rubbery modulus of 22 and 0.5 GPa respectively. The T_g was determined as 118.5°C based on the temperature with the maximum value in tan delta.

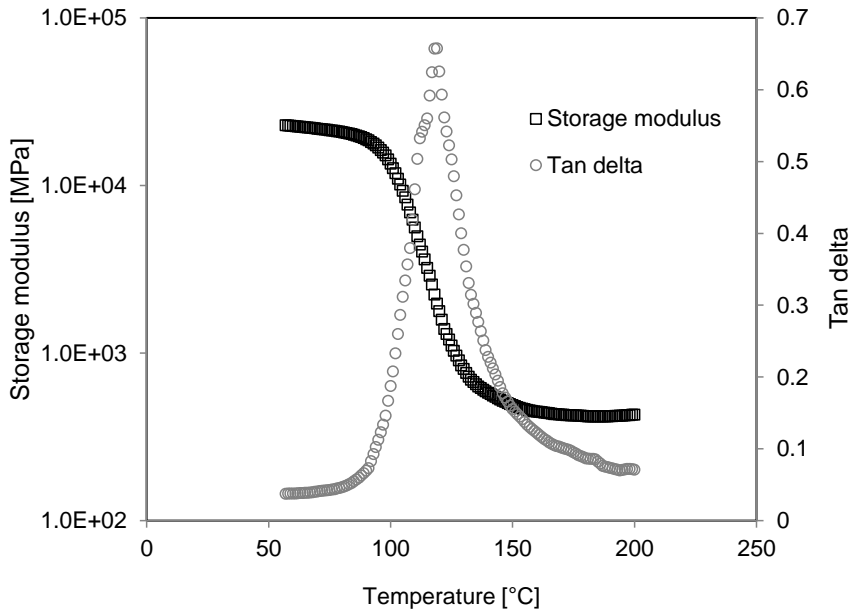


Figure 6-4 Storage modulus and tan delta of the IF EMC in different temperature, frequency= 1Hz. T_g is chosen as the temperature with the maximum tan delta value.

Material	Properties			
	Glassy Modulus (MPa)	Rubbery Modulus (MPa)	$T_g^{E'}$	$T_g^{tan \delta}$
IF	22160	500	107.7 °C	118.5 °C

Table 6-2 Glassy, Rubbery modulus and T_g , according to DMA test, T_g values at 1 Hz.

6.2.2 Creep under high pressure steam condition

The viscoelastic creep compliance of the EMC in pressurized steam condition was measured via the newly developed pressure vessel in 3 point bending mode. The EMC

sample had the dimension of $24.3 \times 2.1 \times 0.5 \text{ mm}^3$. The instrument and testing procedure have been discussed in details in Chapter 5.

It is known that the process of moisture absorption in polymers is accompanied by swelling which is always associated with changes in the mechanical properties. At temperatures above 100°C with 100%RH, i.e. pressure cooker condition, the relaxation occurs very fast and T_g of the materials drop by almost 30°C [13]. Therefore for the corresponding EMC with the dry T_g of about 118°C , the estimated wet T_g will be below 100°C and the behavior above 110°C can be considered as rubbery elastic at pressure cooker conditions. This assumption is assessed and supported by the tensile modulus measurement of the EMC in pressure cooker environment and a good agreement is achieved, Figure 6-5. Consequently, the EMC is considered as rubbery elastic in the FE simulations for the pressure cooker condition.

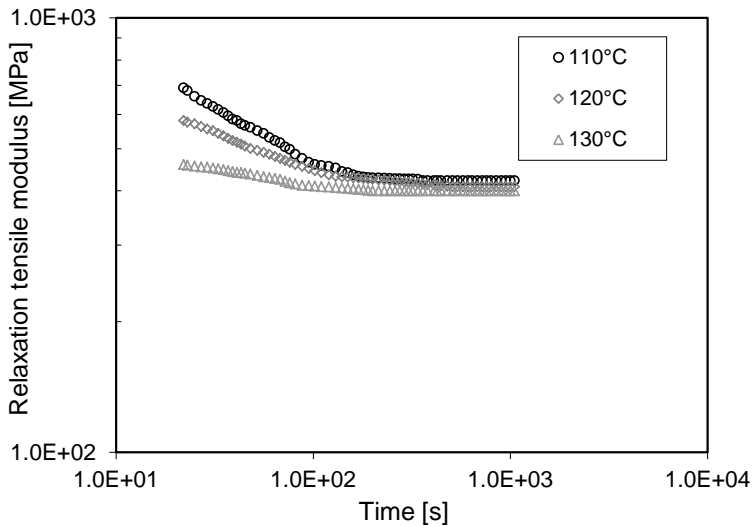


Figure 6-5 Relaxation tensile modulus of the IF EMC as calculated from the creep experiments under wet condition. Since the EMC is almost in rubbery state under pressure cooker conditions, the relaxation modulus is assumed to be as the reverse of the creep compliance.

6.3 Delamination in interfaces

6.3.1 Sample Preparation

The interface samples used in this study had the dimension of $34.8(l) \times 1.1(w) \times 1.4(t)$ mm³ and consists of the IF EMC on a layer of copper lead frame with the thickness of 0.22 mm. To establish a smooth interfacial delamination, a sharp initial pre-crack was made in the samples, which the procedure as previously developed by Xiao [9], Figure 6-6.

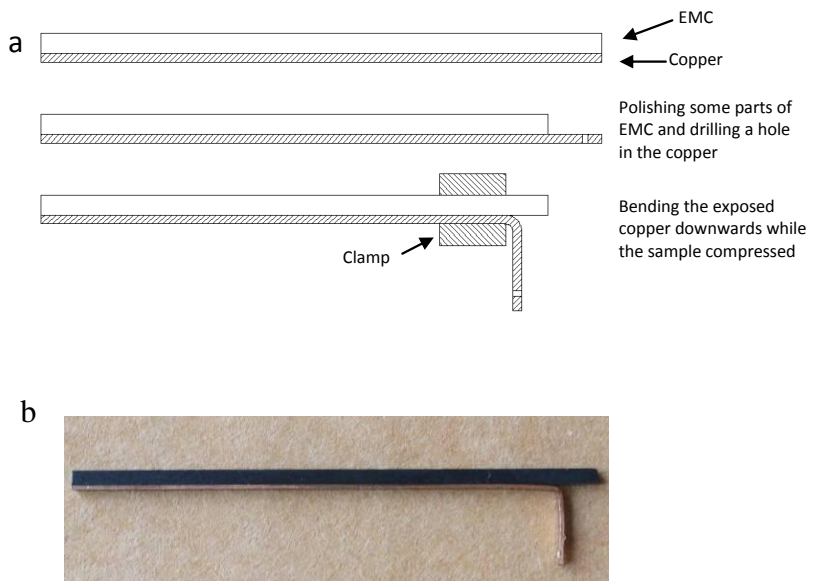


Figure 6-6 a: Procedure of making a sharp initial crack in the EMC-Cu interface, b: example of an interface sample.

6.3.2 Mixed Mode Bending Setup

The mixed mode bending (MMB) test setup, which will be used here, was previously developed by Xiao [9]. The MMB test can be regarded as a superposition of the double cantilever beam test, with mode I loading, and the three point bending test, with mode II loading. It provides steady crack growth over the full range of mode angles. The setup

is modified for the application in the pressure vessel, schematically shown in Figure 6-7. It allows transferring two separated loads on a single specimen and consists of a shaft, a slider, four frames, a lever, two screws and one hook.

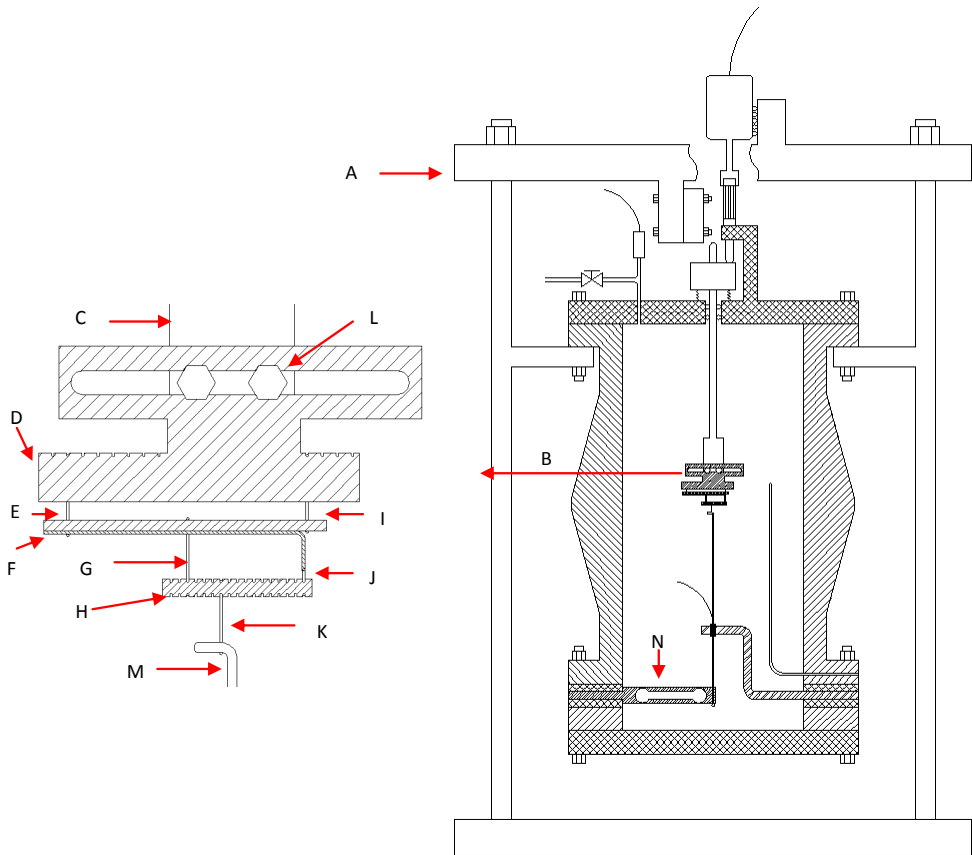


Figure 6-7 Schematic drawing of the pressure vessel apparatus (not to scale) along with the mixed mode bending setup. A: pressure vessel setup, B: detail of the mixed mode bending setup, C: shaft, D: slider, E: left frame, F: sample, G: mid frame, H: lever, I: right frame, J: hook, K: loading frame, L: two tighten screws, M: rigid rod connecting to the load cell, N: load cell.

Firstly the left and right frames (upper frames) are positioned on the grooves of the slider. The sample is then installed in the upper frames, while the mid frame is on the

middle of it. The hook is crossed through the hole in the copper. Then the hook and the mid frame are connected with the lever, on which the loading frame is already positioned.

Changing the position of the loading frame makes it possible to apply various loading mode mixities on the samples. The double cantilever bending (DCB) test occurs when removing the lever, and connecting the hook to the loading frame. The three point bending (TPB) test occurs if the lever is not used and directly connecting the middle of the sample to the loading frame. The grooves in the slider and lever are used to provide the test abilities for different sample length and also preventing frame sliding along the horizontal direction during the experiment.

6.3.3 Delamination Experiment

The delamination experiments in pressurized steam condition have been performed at 120°C, 135°C and 150°C. The T_g of the wet EMC was assumed to be lower than 100°C (section 6.1.2). Therefore, the samples can then be considered as rubbery elastic at 120°C, 135°C and 150°C.

The interfacial delamination tests in dry environment have been performed at 135°C and 150°C. The T_g of the dry sample was measured as 118°C, see section 6.1.1. Therefore, the molding compound is considered as rubbery elastic during the crack propagation at 135°C and 150°C for dry samples. At 120°C and dry conditions the delamination would occur under viscoelastic conditions. Due to the lack of time, it was decided to omit the dry delamination measurement at 120°C, as a more complicated and time consuming procedure would be required. This procedure was clearly documented in [9].

The following procedure was used for all measurements:

- 1) The samples are placed in the MMB setup. The glassy window of the pressure vessel is then completely locked.

- 2a) Dry measurement: samples were pre-heated in the test setup at the test temperature for one hour.

2b) Wet measurement: water was introduced and the vessel was heated until the required temperature and steam pressure are reached. The samples were kept in the pressurized steam environment for almost 4.5 hours for moisture diffusion and stabilization. As shown in [19], above 100°C the estimated coefficient of moisture diffusion for these materials is about $2 \times 10^{-11} \text{ m}^2/\text{s}$ in atmospheric pressure. Therefore, for a sample thickness of 1.18 mm a saturation of 95% is reached after 4.4 hours. It is expected that under pressure the saturation will be reached even quicker.

3) Loading was performed at different mode mixities in the displacement controlled mode.

The experiments were done at different temperatures, in dry and wet environments. Three loading mode mixities were performed at each temperature and testing condition. The loading mode mixity was adjusted by anchoring the loading frame along the lever at different positions. The loading positions were named by the assigned notch number on the lever. The type of loading in the results is indicated by the "P + digit". The first notch on the lever counting from the right was marked as P1 (position 1), the second as P2, and so on. Generally, a higher P number represents a higher shear force component and thus a higher load mode mixity. The loading on the samples was at a constant displacement rate of 30 $\mu\text{m}/\text{min}$. The load was recorded by the load cell.

Figure 6-8 shows an example of the delamination force/displacement curve. The first linear part in this curve is related to the opening of the pre-crack. Interfacial delamination will propagate along the interface after the ultimate load level is reached. As a result the force is slowly decreasing in this region. This part of the loading-displacement curve is used to obtain the interface strength parameters.

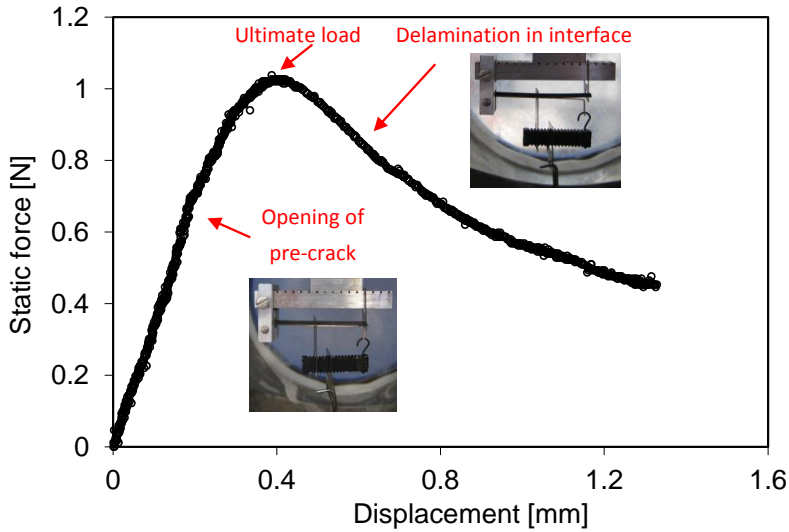


Figure 6-8 Force/displacement delamination curve in 135°C/dry condition, P11 loading. Opening of the pre-cracked and delamination in the interface.

Force/displacement interfacial delamination graphs in dry and wet environment are shown in Figure 6-9-Figure 6-11. Since the pre-crack length was different the initial linear slope of the curve may differ. The results clearly show the effect of the loading mode, temperature and moisture on the delamination force levels. Since the materials are softer at higher temperatures, increasing the temperature would decrease the force level in all loading modes and testing environment. Furthermore, the force levels are significantly affected by the applied loading mode mixity. The loads were found higher with a higher shear component, and lower with higher tensile component. The lowest range of the loads was found with samples measured with mode I loading. Steam is also affecting the delamination loads and significantly decreasing the force levels at different temperature and mode mixities. As Figure 6-10 shows, the interfacial loads are decreased by almost a factor 5 with the presence of steam.

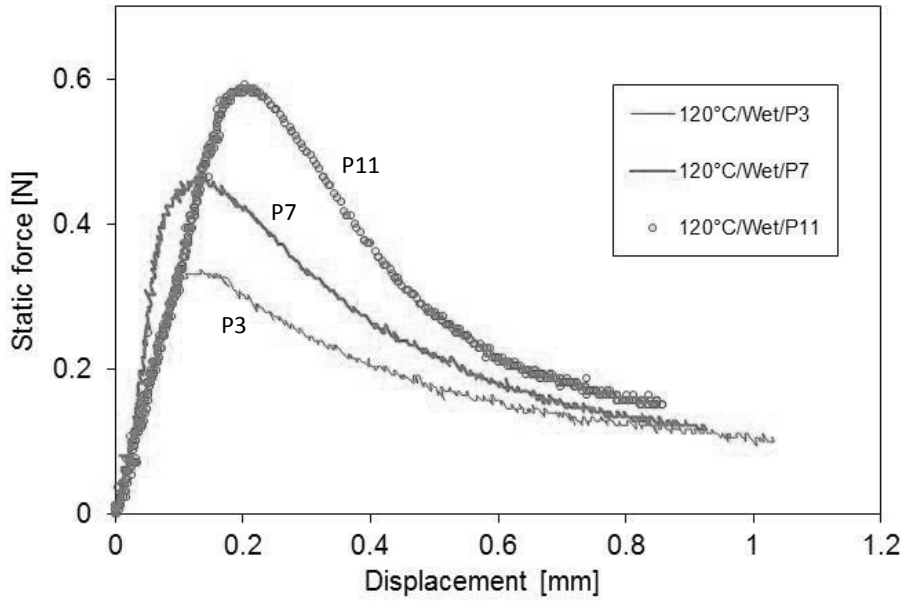


Figure 6-9 Interfacial delamination force levels vs. displacement at different loading modes, pressure cooker environment with $T=120^{\circ}\text{C}$.

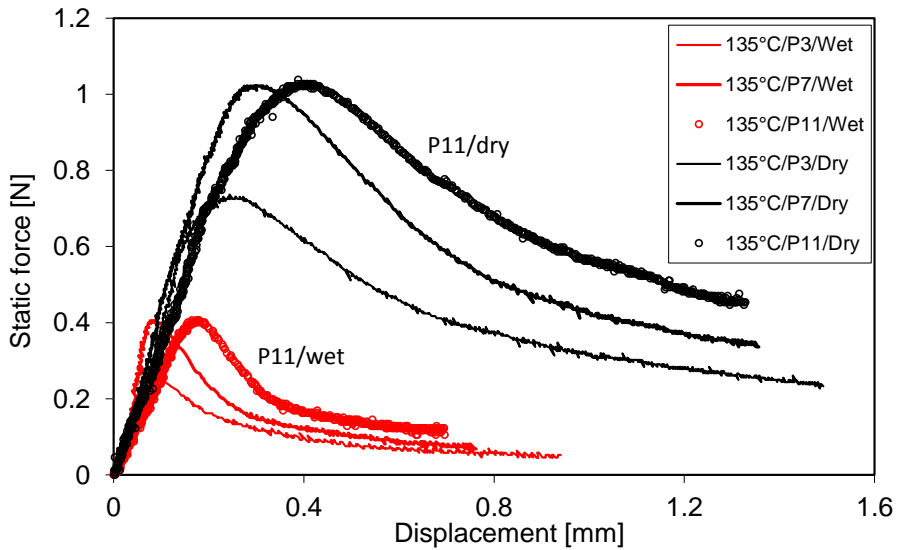


Figure 6-10 Effect of mode mixity and steam on delamination forces, $T=135^{\circ}\text{C}$. The force levels decreased by almost 5 times in presence of steam.

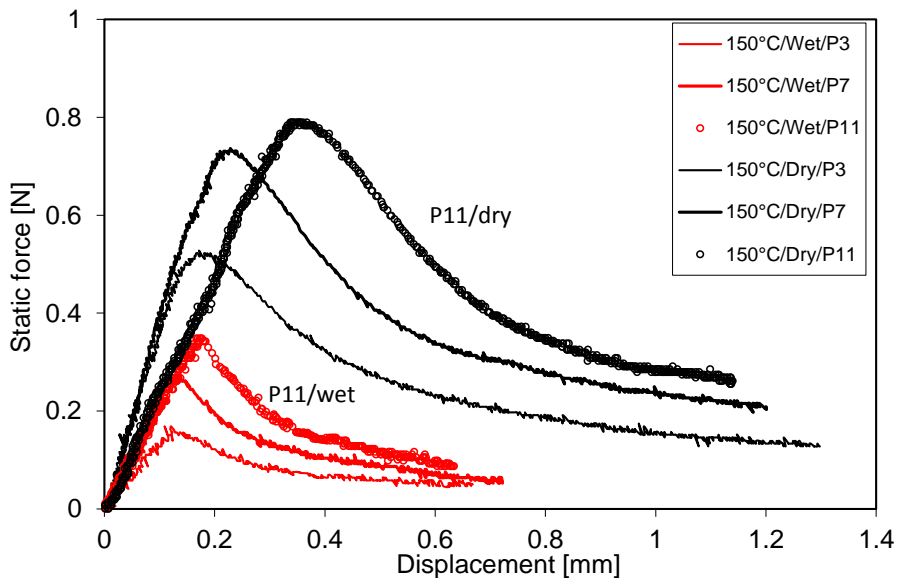


Figure 6-11 Effect of mode mixity and steam on delamination forces, $T=150^{\circ}\text{C}$. Moisture decreasing the delamination force levels significantly.

6.4 Finite Element Model for energy release rate calculation

Establishing the critical energy release rate and mode mixity is performed by using the FEM- ABAQUS code. In the FEM model the crack length corresponding to the measurement and the matching delamination loads are applied. Since the width of the samples is small, a plane stress assumption was imposed. A Crack tip mesh with quarter-point elements around the crack tip was used to capture the singular stress profile close to the crack tip. In order to establish the G_c and matching mode mixity, the residual stress state should be appropriately introduced in a 1st simulation step. The residual stress is generated in the sample due to cure and cooling down of the EMC from the molding temperature. Since the EMC used is highly filled and thus the influence of cure shrinkage is expected to be low, the influence of cure was neglected here. The validity of this assumption will be assessed and supported later in this section by measuring the sample's warpage.

The residual stress from the fabrication process is considered by accounting for the cooling down phase only. For the dry condition, this was done by implementing the viscoelastic properties of the EMC in FEM simulated model. The established residual stress in dry condition is verified by the warpage calculation due to the cooling down procedure from molding to room temperature in a 2D FE model. Figure 6-12 shows that there is a small difference comparing the simulation results with the separately measured warpage of the sample (about 6%). It illustrates that the cure effect is minor compared to the cooling down effect.

For the pressurized steam condition, the material is in the rubbery state at the 120°C, 135°C and 150°C and a viscoelastic model for the EMC in moisturized condition is not needed. Therefore, a 2D elastic model is implemented considering the rubbery modulus of the molding compound as shown in Figure 6-5. For the present highly filled EMC, it is assumed that the hydro-swelling effect can also be neglected. This assumption is verified by capturing two photos of a dry and moisturized sample at 135°C and comparing their curvature. It is found that hardly any difference could be observed, see

Figure 6-13. Therefore, for the wet condition, the residual stress is also considered by accounting for the cooling down phase from the molding to the test temperature.

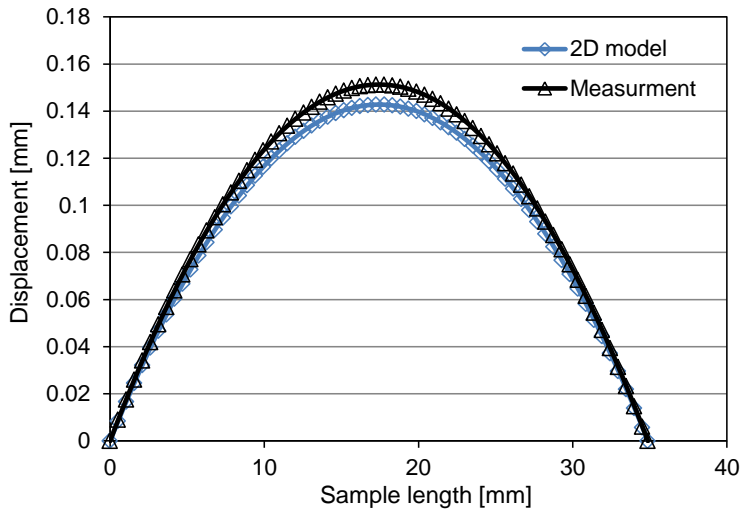


Figure 6-12 Result of the sample warpage in dry condition. The warpage measurement has been performed by the surface profiler instrument, Taylor Hobson, along the length of an un-cracked sample.

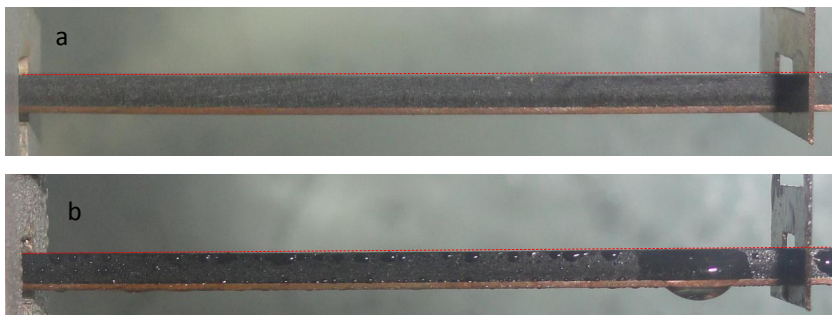


Figure 6-13 Effect of steam on the interface sample warpage. a: dry sample at 135°C, b: sample at 135°C with pressurized steam. For the present highly filled IF samples the swelling effect on the sample warpage and corresponding residual interfacial stresses is assumed to be minor compared to the temperature variation effect and neglected in this study.

The actual loading procedure (crack propagation) is performed in the 2nd step. Since the EMC behaves rubbery elastic in all testing temperatures during the crack propagation, a simplified procedure for establishing the critical energy release rate and mode mixity for a chosen crack tip position can be used. In this simplified procedure, the actual propagation of the crack during loading was not simulated. Instead, for a chosen crack tip position, the previously discussed 1st steps were performed for dry and wet conditions to approximately establish the residual stress state, due to the cooling down. In the next elastic step the external loading was added to the already cracked sample.

There are various approaches proposed for calculation of the mode mixity. Here we calculate the mode mixity based on the crack surface displacements at the crack flanges. The procedure discussed in details in section 2.2.2.

The calculations of the strain energy release rate were performed using a *J*-integral function in ABAQUS for the 2D model, Figure 6-14. Since, the crack length is also required as an input for the model, the experimental setup is equipped with a CCD camera for crack front tracing. The calculated G_c values vs. the established mode mixity are shown in Figure 6-15. The G_c and mode mixity are calculated for 3 different crack lengths in each experiment, Figure 6-16.

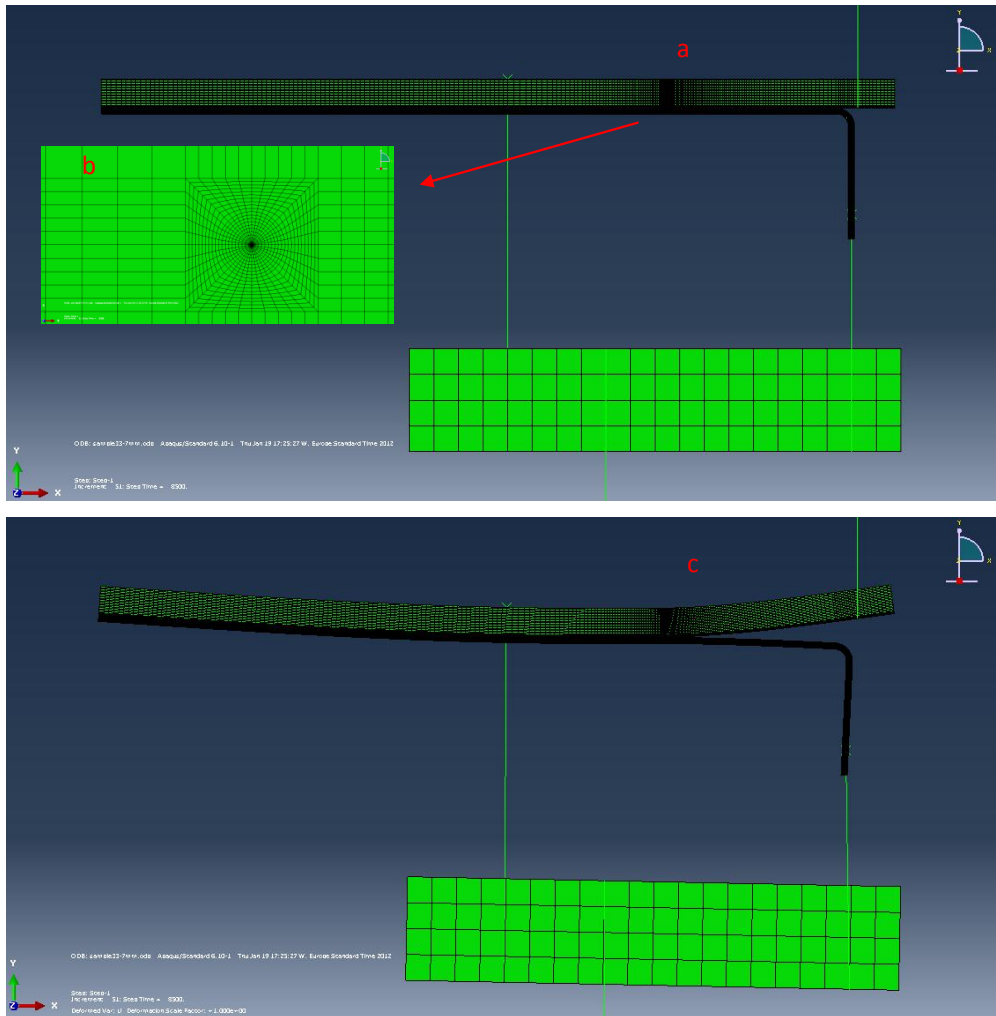


Figure 6-14 a: FEM ABAQUS model in P11 loading mode before applying the load. All parts are added in the simulation. b: details of the crack tip meshing. c: deformed model. The mesh convergence study was performed in the previous PhD work [9].

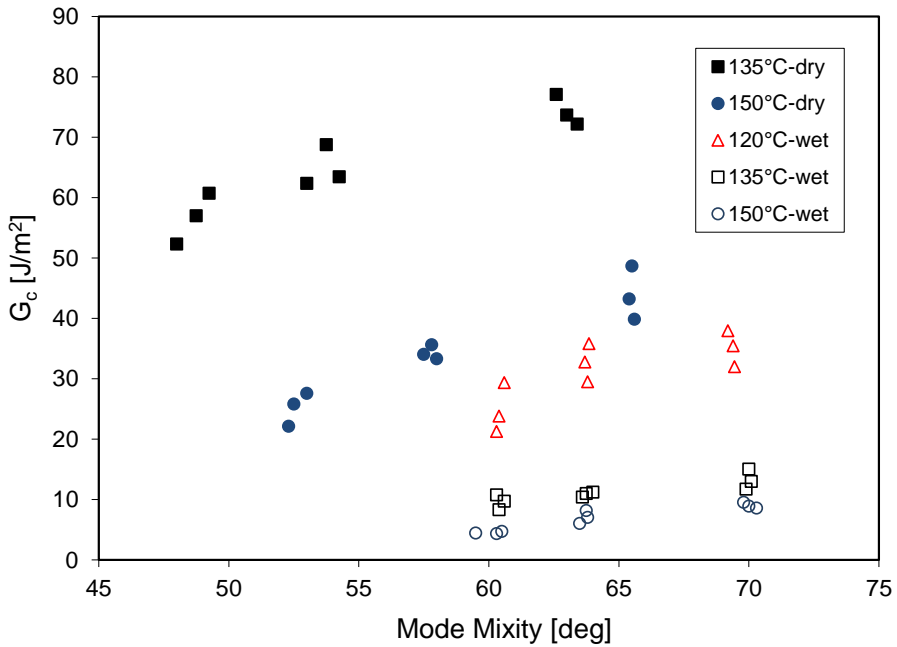


Figure 6-15 critical energy release rate of the Cu-EMC interface in dry and pressurized steam condition. Increasing the temperature and steam decreases the G_c values significantly. The reference length $2a$ in the present work is chosen equal to the current crack length (see section 2.2.2). Establishing the mode mixity values are shown in detail in Figure 6-16.

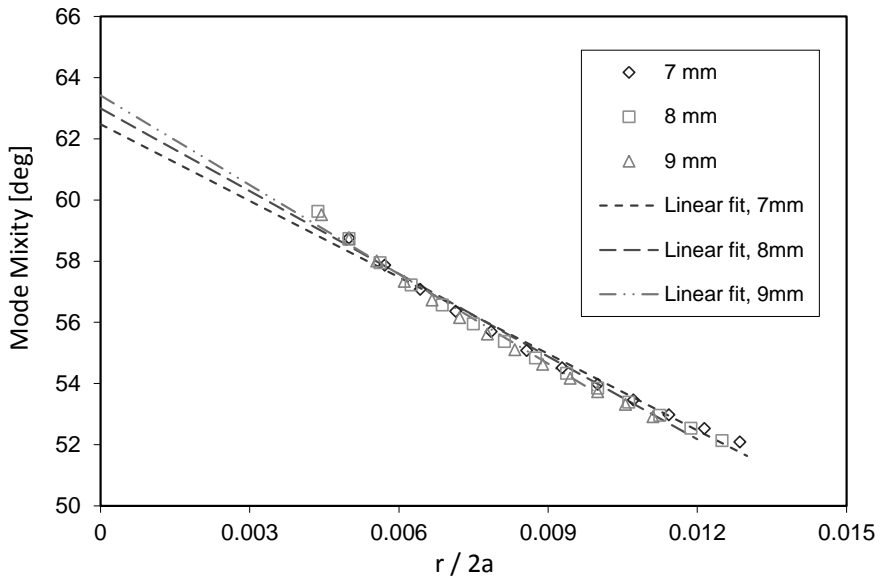


Figure 6-16 Symbols: Mode mixity vs. displacement from the crack tip/crack length, Testing condition: 135°C/P11/dry. Dash line: linear fit.

Figure 6-15 shows that for all studied conditions, the critical energy release rate increases with increasing mode mixity. For instance, at 135°C, the established G_c increased by almost 30% in P11 loading compared to P3. In addition, the G_c decreased considerably as the temperature increases. Temperature increase of 135°C to 150°C in P11 loading decreases the average G_c values by a factor 1.7 in dry condition, while the reduction is a factor 1.5 in wet environment. Furthermore, adding the moisture significantly decreases the simulated critical energy release rate. At 135°C the G_c decreased by almost 7 times in the presence of the moisture, while the reduction is a factor 5 at 150°C.

6.5 Conclusions

In this Chapter, the interfacial fracture toughness of EMC/Cu interfaces was studied for dry and pressure cooker condition. The stress relaxation properties of the EMC were first measured independently and used as an input in the FEM model. The effects of loading mode, temperature and moisture on the interfacial force level and G_c values are investigated. It was shown that P11 loading mode (more shear) establishes higher interfacial force levels and G_c values than in P3 and P7 loading. Moreover, steam had a significant effect on the reduction of G_c values at temperatures above the T_g of the EMC. Increasing the temperature also decreased the critical energy release rate and interfacial force levels in dry and wet conditions.

References

- [1] G.Q. Zhang, W.D. van Driel, X.J. Fan, *Mechanics of Microelectronics*, Springer, Dordrecht, Netherlands, 2006.
- [2] O. van der Sluis, R.A.B. Engelen, R.B.R. van Silfhout, W.D. van Driel, M.A.J. van Gils, Vertical die crack stresses of Flip Chip induced in major package assembly processes, *J. Microelectron. Reliab.* 47 (2007) 1975-1982.
- [3] W.D. van Driel, M.A.J. van Gils, R.B.R. van Silfhout, G.Q. Zhang, Prediction of delamination related IC and packaging reliability problems, *J. Microelectron. Reliab.* 45 (2005) 1633-1638.
- [4] L.J. Ernst, C. van't Hof, D.G. Yang, M.S. Kiasat, G.Q. Zhang, H.J.L. Bressers, J.F.J. Caers, A.W.J. den Boer, J. Janssen, Mechanical modeling and characterization of the curing process of underfill materials, *J. Electron. Packag.* 124 (2002) 97-105.
- [5] N.V.V.R. Murthy Kolluri, M.H.L. Thissen, J.P.M. Hoefnagels, J.A.W. van Dommelen, M.G.D. Geers, In-situ characterization of interface delamination by a new miniature mixed mode bending setup, *Int. J. Fractu.* 158(2) (2009) 183-195.
- [6] N.V.V.R. Murthy Kolluri, J.P.M. Hoefnagels, J.A.W. van Dommelen, M.G.D. Geers, An Improved Miniature Mixed-Mode Delamination Setup for In-Situ Microscopic Interface Failure Analyses, *J. Phys.D: Appl. Phys.*, 44(2011) 034005-1/13.
- [7] J. Thijsse, O. van der Sluis, J.A.W. van Dommelen, W.D. van Driel, M.G.D. Geers, Characterization of semiconductor interfaces using a modified mixed mode bending apparatus, *J. Microelectron. Reliab.*, 48(3) (2008) 401-407.
- [8] J. Thijsse, O. van der Sluis, J.A.W. van Dommelen, W.D. van Driel, M.G.D. Geers, Characterization of semiconductor interfaces using a modified mixed mode bending apparatus, *J. Microelectron. Reliab.*, 49(3) (2008) 401-407.
- [9] A. Xiao, Interface characterization and failure modelling for semiconductor application, PhD thesis, Delft, 2012.
- [10] G. Schlottig, Reliability at chip interfaces: Delaminating the silicon die from molding compound, PhD thesis, Delft, 2012.

- [11] M. Sadeghinia, K.M.B. Jansen, L.J. Ernst, H. Pape, IEEE 13th EuroSime conference (Lisbon, April 2012), pp. 1/4-4/4.
- [12] M. Sadeghinia, K.M.B. Jansen, L.J. Ernst, H. Pape, IEEE 62th ECTC conference (San Diego, May 2012), pp. 1/5-5/5.
- [13] M. Sadeghinia, K.M.B. Jansen, L.J. Ernst, H. Pape, Mechanical characterization of molding compound in pressurized steam, *Int. J. Adhes. Adhes.* 32 (2012) 82–88.
- [14] M.K. Saraswat, K.M.B. Jansen, M.D. Patel, IEEE 9th EuroSime conference (Freiburg im Breisgau, April 2008), pp. 463-466.
- [15] B. Boehme, K.M.B. Jansen, S. Rzepka, K.J. Wolter, IEEE 10th EuroSime conference (Delft, April 2009), pp. 289-296.
- [16] K.M.B. Jansen, M. Patel, M.K. Saraswat, L.J. Ernst, 24th annual meeting of the Polymer Processing Society-PPS conference (Salerno, June 2008), pp. 467-468.
- [17] I.M. Ward, J. Sweeney, an introduction to the mechanical properties of solid polymers, Second edition, John Wiley & Sons, Chichester, West Sussex, 2004.
- [18] J.D. Ferry, *Viscoelastic properties of polymers*, 3rd edition, Wiley, New York, 1980.
- [19] Y. de Vreugd, The effect of aging on molding compound properties, PhD thesis, Delft, 2011.

Conclusion

This thesis has presented the research results in four main aspects:

- 1) Characterization the thermo-mechanical properties of fully cured EMCs
- 2) Cure-dependent characterization of viscoelastic properties of EMCs
- 3) Developing a pressure vessel along with a mixed mode bending setup for material characterization and interface delamination testing
- 4) Establishing the critical fracture properties of the EMC-Cu interfaces and investigating the effect of temperature, moisture and mode mixity on the interfacial toughness, in particular under pressurized steam conditions

The general conclusions from the work are summarized as follows:

7.1 Conclusion concerning the establishment of fully cured material model

Chapter 3 discussed the mechanical properties of the fully cured epoxy molding compounds. The coefficient of thermal expansion, bulk and storage modulus of the EMCs are measured through various experiments. The experiments are carried out in temperature and pressure ranges of 40-200°C and 10 to 100 MPa. The main conclusions from these experiments are:

- The bulk modulus and coefficient of thermal expansion of molding compounds varies with temperature and filler content. A modified Tait-equation is used to model the bulk modulus and CTE as function of temperature. It is shown that the filler decreases the thermal contraction of epoxy resins but increases the modulus below as well as above the glass transition temperature. The temperature dependency of CTE can be implemented in finite element code by user-subroutines.
- The viscoelastic storage modulus is determined by performing dynamic mechanical analysis. The obtained tensile glassy and rubbery modulus are almost independent of the frequency. However in the glass transition regime clear frequency dependent effects can be seen.

7.2 Conclusion concerning the characterization of the cure dependent material properties

In this thesis the characterization of the cure-dependent material properties includes three parts: DSC analysis for the cure kinetics and T_g - α relationship, PVT measurements for establishing the cure shrinkage and DMA experiment for cure-dependent viscoelastic behavior. In addition, the effect of the filler on the major material properties is investigated. From this part of the research, following conclusions can be drawn:

- DSC analysis shows that the glass transition temperature of the epoxy molding compounds will increase by the degree of cure. According to [1] a model describing the rate of the reaction during cure is presented. The Kamal-Sourour equation is used here. Unknown parameters are found through DSC studies.
- The cure shrinkage is measured by dilatometric experiments. The cure shrinkage turns out to scale linearly with the degree of conversion, as earlier shown by de Vreugd [2].
- The changes in the shear modulus of the EMC are investigated during an intermittent cure test with a DMA apparatus. The procedure is earlier developed by Jansen et al. [3,4]. The time- temperature superposition principle was applied to all

heating steps, the master curves and the related shift factors are extracted. It is shown that partial curing increases the glass transition temperature at each heating scan. This phenomenon shifts the master curves to the longer time domain. Considering the $T_g^{\tan\delta}$ as the reference temperature, the master curves and shift factors (for temperatures above T_c) collapse to a single curve [4].

- The cure-dependent shear rubbery modulus is modeled with the equation of Martin and Adolf, for the intermittent cure test. As earlier shown [4], partial curing increases the rubbery modulus. However the glassy shear modulus turns out to be almost independent of the conversion level.

7.3 Conclusion concerning the development of the pressure vessel apparatus

Due to the fact that microelectronics is made up from various materials with highly dissimilar thermo-mechanical properties, generally the interface between two adjacent materials is the place where delamination related failure often occurs. Failure of these interfaces induces decreased reliability and performance of microelectronic components. Therefore, adequate knowledge of delamination prediction is desirable.

The interface properties of the packages are highly dependent of the temperature and moisture. The interface strength of electronic chips is also affected by the generated steam during the soldering reflow, part of the assembly process.

For various microelectronic packages the interfacial strength of EMC-Cu interfaces was explored in different temperatures and humidity levels [5-8]. However the characterization of humidity influences was restricted to temperature below 100°C.

The present work, separately investigate the effect of temperature and moisture on the interfacial properties of EMC-Cu interfaces for $T > 100^\circ\text{C}$ and 100%RH environmental condition, while removing the effect of additional crack driving force due to the trapped steam in the interfaces, a special steam chamber was designed and developed. The setup is also applicable for thermo-mechanical characterization of the molding

compounds in pressurized steam condition. Therefore the functionality of the setup is assessed measuring the viscoelastic creep compliance of an EMC in dry condition and comparing that with creep measurements using a commercial instrument.

The main conclusions from this part of the work are:

- From the study of the viscoelastic creep compliance of the EMC in pressurized steam environment, it was observed that steam considerably changes the EMC's thermo- mechanical properties. The elastic glassy and rubbery modulus decreased by almost 20% in the presence of the moisture. In addition the glass transition temperature is decreased by almost 30°C.
- From the determination of the creep compliance master curves of the EMC in dry and wet environment, it was concluded that moisture shifts the compliance master curve to the shorter time domain. The dry and wet master curves coincide if the actual glass transition temperature is taken as the reference temperature.

7.4 Conclusion concerning the interfacial fracture properties

The present study deals with the establishment of the interfacial fracture toughness of EMC-Cu lead frame interfaces for temperatures above the T_g of EMC in dry and in pressure cooker condition, i.e. temperature larger than 100°C and 100% RH. The main conclusions regarding the interfacial delamination are:

- The critical energy release rate increases with increasing the mode mixity. At 150°C, the established critical energy release rate increased by almost 75% in P11 loading compared to P3 loading for dry conditions. In the steam condition the increase is about 100%.
- The G_c values decreases with increasing the temperature. At P3 loading, the G_c values decreased almost a factor 2.2, due to temperature increase of 135°C to 150°C in dry environment. Almost similar G_c reduction was observed for wet condition.

-
- The critical energy release rate reduces significantly in the presence of moisture. Due to the steam, at 135°C the G_c decreased by almost 7 times, while the reduction is about a factor 5 at 150°C.

Reference

- [1] M.G. Lu, H.K. Choi, H.K. Lee, M.J. Shim, S. W. Kim, Thermal reaction characterization of an epoxy molding compound, *J. Polym.* 33(1) (2001) 49–53.
- [2] J. de Vreugd, The effect of aging on molding compound properties, PhD thesis, Delft, 2011.
- [3] K.M.B. Jansen, L. Wang, C. van't Hof, L.J. Ernst, H.J.L. Bressers, G.Q. Zhang, Cure temperature and time dependent constitutive modeling of molding compounds, IEEE 5th EuroSime conference (Brussels, May 2004), pp. 581-585.
- [4] K.M.B. Jansen, L. Wang, D.G. Yang, C. van't Hof, L.J. Ernst, H.J.L. Bressers, G.Q. Zhang, Constitutive modeling of molding compounds, IEEE 54th ECTC conference (Las Vegas, June 2004), pp. 890-894.
- [5] A.A.O. Tay, T.Y. Lin, Influence of temperature, humidity and defect location on delamination in plastic IC packages, *IEEE Transaction on components and packaging technologies*, 22(4) (1994) 512-518.
- [6] A. Xiao, H. Pape, B. Wunderle, K.M.B. Jansen, J. de Vreugd, L.J. Ernst, Interfacial fracture properties and failure modeling for microelectronics, IEEE 58th ECTC conference (Lake Buena Vista, May 2008), pp. 1724-1730.
- [7] G. Schlottig, H. Pape, B. Wunderle, L.J. Ernst, Establishing the critical fracture properties of the die backside to molding compound interface, IEEE 61st ECTC conference (Lake Buena Vista, June 2011), pp. 1090-1096.
- [8] G. Hu, A.A.O. Tay, Y. Zhang, W. Zhu, S. Chew, Experimental and numerical study of the effect of viscoelasticity on delamination in a plastic IC package, IEEE 57th ECTC conference (Reno, May 2007), pp. 1062-1068.

Summary

Thin layers of dissimilar materials are used in most microelectronic components in order to achieve special functional requirements. Generally, the interface between two adjacent materials forms a weak link, not only because of the relatively low delamination strength, but also because of the existing mismatch in thermo-mechanical properties, such as Young's modulus, coefficient of thermal expansion, hygro-swelling, and vapor pressure induced expansion. Residual stresses from the production processes and initial strains due to the changing thermal and humidity conditions together with acting mechanical loading form the crack driving factors for interface delamination. Failure of interface induces decreased reliability of microelectronic components. Nowadays, interfacial delamination forms one of the key reliability issues in the microelectronic industry and therefore is getting more and more attention. The analysis of a laminate structure with a crack along the interface is central to the characterization of the delamination toughness. The delamination toughness is highly dependent to temperature, moisture and mode mixity.

In recent years, several studies were directed at the determination of the delamination behavior of Cu-EMC interfaces. In the event that moisture sensitivity was included in these studies, the temperature had to be limited to below 100°C. This limitation reduces the applicability of the toughness data obtained in a number of reliability studies of micro-electronic components. This is due to the fact that, in preconditioned (humid) micro-electronic components the interface delamination often occurs above this temperature limit. In many cases the damage is initiated during heating up in subsequent production steps, where temperatures can reach far above 100°C. Therefore the present research focuses on interface delamination measurements, especially interested in harsh environment (humidity combined with temperatures above the 100°C limit).

In this thesis the thermal-mechanical properties of epoxy molding compounds in dry conditions are first investigated. The coefficient of thermal expansion and bulk modulus

were measured via a dilatometer (PVT apparatus). DMA experiments in relaxation mode as well as in multi frequency mode were employed for obtaining the viscoelastic master curve and corresponding shift factors. Secondly, the thermo-mechanical properties of EMC during cure were studied. The volumetric contraction of the material during the curing period was measured via a PVT test. Furthermore the increasing shear modulus of the EMC because of the progressing cure was established through DMA experiments.

For the dry state, the previous two-material characterization steps are sufficient to be able to interpret the measurement results of delamination tests via FEM simulation. For the humid state with $T > 100\text{ }^{\circ}\text{C}$, in the delamination measurements the effect of (trapped) steam at the interface should be compensated by performing the measurements in a pressure chamber. Therefore, in a third step a pressure vessel surrounding the delamination test setup is designed and built.

For the sake of simplicity the humid delamination measurements with $T > 100\text{ }^{\circ}\text{C}$ were only performed under full steam pressure (=relative humidity is 100%). The functionality of the setup has been verified by the measurement of the viscoelastic creep compliance of an EMC in dry state and to compare this with the result from measurements obtained from a commercially available measurement instrument. In order to be able to perform delamination measurements a mixed-mode bending setup is installed in the pressure vessel. Interfacial delamination measurements for a EMC-Cu lead frame interface (as obtained from a real production process) are subsequently performed for dry conditions as well as under pressurized steam conditions(= relative humidity 100%). A (I / II) mixed mode mechanical load is applied to the test sample, in which the initial stress state due to the manufacturing and the steam pressure (relative humidity 100%) is already present, in order to initiate and propagate the delamination.

In conclusion: This dissertation shows that the temperature, the mix mode and the humidity under these conditions ($T > 100\text{ }^{\circ}\text{C}$ and 100% relative humidity) results in a significant effect on the delamination properties of interfaces. As far as known to the

author, here for the first time a good insight on the impact of this harsh environment on the delamination properties is presented.

Mahdi Sadeghinia
January 2013

Samenvatting

Dunne lagen van verschillende materialen worden gebruikt in de meeste micro-elektronische componenten ten einde aan speciale functionele eisen te kunnen voldoen. In het algemeen, vormt het raakvlak van twee aangrenzende materialen een zwakke schakel, niet alleen vanwege de relatief lage delaminatie-sterkte, maar ook door de bestaande discontinuïteit in de thermo-mechanische eigenschappen, zoals elasticiteitsmodulus, thermische uitzettingscoëfficiënt, hygro-zwelling en dampdruk geïnduceerde expansie. Restspanningen van de productieprocessen en initiële vervormingen als gevolg van de veranderende thermische en luchtvochtigheids condities vormen tezamen met optredende mechanische belastingen de drijvende factoren voor interface delaminatie. Het falen van interfaces induceert verminderde betrouwbaarheid van micro-elektronische componenten. Tegenwoordig vormt interface delaminatie een van de belangrijkste betrouwbaarheidsproblemen in de micro-elektronische industrie en daarom wordt er steeds meer aandacht aan besteed. De analyse van een laminaatstructuur met een scheur langs de interface staat centraal bij de karakterisering van de delaminatie-taaiheid.

De delaminatie taaiheid is sterk afhankelijk van temperatuur, vochtigheid en mode mix. In de afgelopen jaren waren verschillende onderzoeken gericht op het bepalen van het delaminatie-gedrag van Cu-EMC-interfaces. In het geval dat vocht gevoeligheid werd inbegrepen in deze onderzoeken, moest de temperatuur worden beperkt tot onder de 100°C. Deze beperking reduceert de toepasbaarheid van de verkregen taaiheidsdata op een aantal betrouwbaarheidsstudies van micro-elektronische componenten. Dit is vanwege het feit dat bij geconditioneerde (vochtige) micro-elektronische componenten de interface delaminatie vaak pas optreedt boven deze temperatuurgrens. In veel gevallen wordt de schade geïnitieerd tijdens het opwarmen in opeenvolgende productiestappen, waarbij de temperatuur tot ver boven de 100 °C kan oplopen. Daarom is het onderhavige onderzoek gericht op interface-delaminatie metingen onder

relatief barre omstandigheden (vochtigheid in combinatie met temperaturen boven de 100 °C).

In dit proefschrift worden eerst de thermo-mechanische eigenschappen van epoxy moulding compound in droge staat onderzocht. De thermische uitzetting en bulk modulus werden gemeten met een dilatometer (PVT apparaat). DMA experimenten in relaxatiemodus evenals in frequentiemodus werden gebruikt om de visco-elastische mastercurve en overeenkomstige verschuivingsfactoren te verkrijgen. Ten tweede werden de thermo-mechanische eigenschappen van EMC tijdens het uitharden bestudeerd. De volumetrische krimp van het materiaal tijdens de uitharding werd gemeten via een PVT test. Verder werd de toenemende afschuifmodulus van de EMC als gevolg van de voortschrijdende uitharding vastgesteld door middel van DMA experimenten.

Voor de droge toestand zijn de voorgaande twee materiaal-karakteriseringsstappen voldoende voor het kunnen interpreteren van delaminatie meetresultaten via EEM-simulatie. Voor de vochtige toestand met $T > 100$ °C, moet bij de delaminatie metingen het effect van (afgesloten) stoom op de interface worden gecompenseerd, door het uitvoeren van de metingen in een drukkamer. Derhalve in een 3e stap drukvat rondom de delaminatie testopstelling ontworpen en gebouwd. Voor de eenvoud zijn de vochtige delaminatie metingen met $T > 100$ °C uitsluitend uitgevoerd onder volledige stoomdruk (= relatieve vochtigheid 100%). De functionaliteit van de installatie is geverifieerd door het meten van de viscoelastische kruipcompliantie van een EMC in droge toestand en deze te vergelijken met de resultaten verkregen van metingen met een commercieel beschikbaar meetinstrument. Teneinde delaminatie metingen te kunnen uitvoeren is een mixed-mode buigingsopstelling geïnstalleerd in het drukvat. Interface-delaminatie metingen voor een EMC-Cu leadframe interface (zoals verkregen van een echte productieproces) worden vervolgens uitgevoerd voor droge omstandigheden en onder stoomdruk (= relatieve vochtigheid 100%). A (I / II) mixed mode mechanische belasting wordt aangebracht op het proefstuk, waarin de initiële spanningstoestand als gevolg van de fabricage en de stoomdruk (relatieve vochtigheid 100%) reeds aanwezig is,

teneinde de delaminatie te initiëren en te laten voortschrijden. De “critical energy release rate” en de mode mix werd vastgesteld via geschikt gekozen EEM-simulaties.

Concluderend: Dit proefschrift laat zien dat de temperatuur, de mode mix en de vochtigheid onder deze omstandigheden ($T > 100\text{ °C}$ en 100% relatieve vochtigheid) leiden tot een significant effect op de delaminatie eigenschappen van interfaces. Zover bekend bij de auteur, is hier voor het eerst een goed inzicht verkregen omtrent de impact van deze “harsh environment” op de delaminatie eigenschappen.

Mahdi Sadeghinia

January 2013

Acknowledgement

The work presented in this thesis was hardly possible without direct and indirect contribution of many people. First of all, I would like to thank my promoter Prof. Leo Ernst for his professional support and guidance with which I could keep on being on the right track with an optimistic hard working attitude.

I would also like to express my sincere grateful to my co-promoter Dr. Ir. Kaspar Jansen. Kaspar, I really appreciate your scientific guiding and support during the research work. I found our numerous discussions quite constructive and essential to this work. Accuracy, critical thinking and respecting all small details while having the big picture in mind are among the values I got well aware of in light of your supervision within the past several years.

Furthermore, I want to acknowledge the helps of the TUDelft laboratory staff: Harry Jansen, Patrick van Holst, Jos van Driel and Rob Lutjjeboer. Harry and Patrick, I would like to explicitly express my great appreciation to your attention and helps during these years.

My gratitude goes out to all of my colleagues of the Mechanics of Materials group in Delft: Dr. Jan de Vreugd, Dr. John Suman Nakka, Ali Adli, Muhammad Akram and Dr. Stanley Leung.

Furthermore, I would like to thank Dr. Heinz Pape, Dr. Gerd Schlottig and Ingrid Maus from Infineon Technologies AG for their technical and non-technical supports.

I am also thankful to my friends: Masoud, Abbas, Peyman, Rahim, Mehdi, Ali, Umut, Javad, Arash, Alireza , Hamed and Saber. I will never forget the time being together.

Last but not least, I want to thank my wife and family for their helps and support during these years. I am particularly grateful to my wife, Elaheh, for being incredibly understanding, supportive and patient.

Mahdi Sadeghinia

January 2013